Photocatalytic CO_2 Activation by Water - Catalyst Screening and Mechanistic Evaluation

Chieh-Chao Yang

Photocatalytic CO_2 Activation by Water

- Catalyst Screening and Mechanistic Evaluation

Graduation committee

Chairman:

Prof. dr. G. van der Steenhoven	University of Twente

Secretary:

Prof. dr. G. van der Steenhoven	University of Twente

Promotor:

Prof. dr. G. Mul	University of Twente

Members:

Prof. dr. ir. L. Lefferts	University of Twente
Prof. dr. ir. J. Huskens	University of Twente
Dr. ir. D.W.F. Brilman	University of Twente
Prof. dr. J.A. Moulijn	Delft University of Technology
Prof. dr. ir. K.P. de Jong	Utrecht University
Prof. dr. V. Meynen	University of Antwerp

The research work reported in this dissertation was financially supported by ACTS (NWO, the Netherlands), in the framework of an NSC-NWO project (Project Number NSC-97-2911-I-002-002).

Cover design: Chieh-Chao Yang and Robert French

ISBN: 978-90-365-3214-30
Printed by: *Gildeprint Drukkerijen* - Enschede, the Netherlands

PHOTOCATALYTIC CO_2 ACTIVATION BY WATER - CATALYST SCREENING AND MECHANISTIC EVALUATION

PROEFSCHRIFT

ter verkrijging van de graad van doctor
aan de Universiteit Twente,
op gezag van de rector magnificus,
Prof. dr. H. Brinksma,
volgens besluit van het College van Promoties
in het openbaar te verdedigen
op vrijdag 24 juni 2011 om 12.45 uur

door

Chieh-Chao Yang

geboren op 7 september 1980
te Tainan, Taiwan

Dit proefschrift is goedgekeurd door de promotor

Prof. dr. G. Mul

Dedicated to Mom, Li-Ling and Money

Contents

Chapter 1

General Introduction

Photocatalytic activation of CO_2 in the presence of water can convert this highly thermally stable reagent into hydrocarbons. This is accompanied by the oxidation of water into O_2, and mimics photosynthesis. The mitigation of the green house gas CO_2, and simultaneous production of useful hydrocarbons renders this a technology to close the carbon cycle. Eq. 1-4 show the Gibbs free energy for CO_2 conversion to single carbon (C_1) molecules.[1] To obtain these C_1 hydrocarbons, suitable photocatalysts need to be developed.

$$CO_{2(g)} + 2H_2O_{(l)} \rightarrow HCOOH_{(aq)} + \tfrac{1}{2}O_{2(g)} \qquad \Delta G = 1.428\text{eV} \qquad (1)$$

$$CO_{2(g)} + H_2O_{(l)} \rightarrow HCHO_{(aq)} + O_{2(g)} \qquad \Delta G = 1.350\text{eV} \qquad (2)$$

$$CO_{2(g)} + 2H_2O_{(l)} \rightarrow CH_3OH_{(aq)} + \tfrac{3}{2}O_{2(g)} \qquad \Delta G = 1.119\text{eV} \qquad (3)$$

$$CO_{2(g)} + 2H_2O_{(l)} \rightarrow CH_{4(aq)} + 2O_{2(g)} \qquad \Delta G = 1.037\text{eV} \qquad (4)$$

.

Clearly, to obtain selectivity in CO_2 reduction is an additional challenge as compared to water splitting, with H_2 and O_2 being the only possible final products.

Photocatalytic CO_2 reduction: An overview of results

One of the earliest observations of photoelectrochemical CO_2 reduction was reported by Halmann in 1978.[2] A system consisting of a single crystal of p-type gallium phosphide (Zn-doped GaP) as the working electrode, a carbon rod as the counter electrode, and a saturated calomel electrode as the reference electrode were employed. The carbon rod was chosen as the counter electrode, as it was reported that formic acid and other hydrocarbon compounds were not oxidized on this material.[3] A high pressure mercury arc or halogen lamp was focused on the GaP electrode. CO_2 was continuously bubbled through the electrolyte, containing a buffer solution of K_2HPO_4-KH_2PO_4(aq). The photocurrent density was 6 mA/cm^{-2}, compared to 0.1 mA/cm^{-2} in dark conditions. Analysis of the electrolyte solution showed the presence of formic acid, formaldehyde and methanol. 36 μmol of formic acid, 9.6 μmol formaldehyde and 3.3 μmol methanol were produced after 18 h of illumination. Other results were shown by replacing the counter electrode with n-type crystalline TiO_2 and lithium carbonate solution as electrolyte. 30 μmol of methanol was detected after 16 h of illumination.

Inoue et al. extended the study to various materials that were found active for photocatalytic CO_2 reduction in 1979.[4] CO_2 was bubbled through the solution, in which the catalyst was suspended, and the mixture illuminated by a 500 W Xenon lamp, or high pressure mercury arc lamp, respectively. After 7h illumination, 110 μmol formaldehyde and 23 μmol methanol were found. GaP, CdS and ZnO showed a methanol production rate of 110, 117, and 35 μmol, respectively. The highest methanol production rate was detected for SiC, 535 μmol for 7 h of illumination. The production was correlated to the energy levels between photogenerated carriers (electrons and holes) and the redox agents (H_2CO_3 into reduced compounds, such as formaldehyde and methanol) in solution. This correlation was reflected by the absence of methanol production over WO_3, which possesses a conduction band energy level lower than the level required for H_2CO_3 reduction into methanol.

In 1987, Thampi et al. investigated photo-methanation of CO_2 over Ru-loaded TiO_2 in the gas phase.[5] CO_2 methanation was performed in a pyrex cell with the catalysts spread over the bottom, and filled with 1 mL CO_2 and 12 mL H_2, STP. The initial methane formation rate was found to be 0.17 μmol/h at 25^{o}C, 5.18 μmol/h at 46^{o}C and 10.5 μmol/h at 90^{o}C, illumination under a solar simulator (0.08W/cm^2). In dark conditions, there was only 0.17 μmol/h methane produced at 46^{o}C. As compared to the methane production rate under the illumination condition, 5.18 μmol/h, the effect of light in methane production is significant.

A report in 1992 demonstrated CO_2 reduction by water in a gas-solid photocatalytic system. M. Anpo and his coworkers investigated TiO_2 anchored on porous Vycor glass for photocatalytic CO_2 reduction, leading to the production of methane, ethylene, ethane and methanol.[6] In the presence of CO_2 and H_2O, illumination was carried out by using a 75 W high pressure mercury lamp. By changing the ratio of H_2O/CO_2 from 1 to 15, the overall hydrocarbon production rate was increased. 0.005 μmol/h methane and 0.0003 μmol/h methanol were detected at 2^{o}C after 8 h of illumination. Besides, electron spin resonance (ESR) spectra provided evidence for the presence of C radicals and H atoms formed by conversion of CO_2 and H_2O, which suggests an involvement of these species in the mechanism of CH_4 formation. Though the production of methane and methanol was extremely low, water oxidation to sustain photocatalytic CO_2 reduction was demonstrated to be feasible.

TiO_2 is still one of the leading catalysts for photocatalytic applications, in terms of the acitivity, robustness and cost. Its applicability in CO_2 reduction in immobilized form was also

recently demonstrated. Commercial Degussa P25 TiO_2, consisting of a mixture of 30 % rutile and 70 % anatase phase, was immobilized on quartz wool (50 mg over 200 mg of quartz wool), and placed in a close loop quartz reactor.[7] A 1000 W Xenon short arc lamp was used as the light source, combined with a $CuSO_4$ solution to cut-off radiation above 700 nm. After 25 hours of illumination, 2.7 μmol/h carbon monoxide, 1.4 μmol/h hydrogen and 0.1 μmol/h methane were detected by gas chromatography, using deionized water saturated CO_2. The sequence of production in quantity CO, CH_4 and H_2, resulted in postulation of a tentative mechanism of photocatalytic CO_2 reduction. Partially reduced $TiO_{2-\delta}$ induced by illumination served as an electron pool, which led to the three dark reactions: H_2O into H_2, CO_2 into CO, and the analogue to the Sabatier reaction forming CH_4.[7]

Various authors have focused on improving performance of TiO_2. Hirano et al. reported photocatalytic CO_2 reduction in aqueous phase TiO_2 suspension mixed with copper powder.[8] An increase in methanol and formaldehyde yield was observed during illumination. The addition of co-catalyst to TiO_2 was studied to promote activity in CO_2 reduction. Different metals (Pd, Rh, Pt, Au, Cu and Ru) were deposited on Degussa P25 TiO_2 by photochemical deposition with methanol as reductant. 650 torr of CO_2 was introduced to a catalyst-suspended water solution, prior to illumination. After 5 h irradiation by a 500 W high pressure mercury lamp ($\lambda > 310$ nm), methane, ethane, formic acid and acetic acid were detected. Pd-TiO_2 showed the highest production rate in methane (0.0494 μmol/h) and ethane (0.0028 μmol/h). Cu-TiO_2 exhibited less methane production (0.0038 μmol/h), but was more selective to formic acid (0.0012 μmol/h) and acetic acid production (0.0082 μmol/h). Tseng et al. showed Cu/TiO_2 and Ag/TiO_2 synthesized by a modified sol-gel method was active in methanol production when CO_2 was bubbled through a NaOH solution.[9] 16.7 μmol/g-cat/h methanol was produced over 2 wt% Cu/TiO_2, under irradiation of 254 nm light. Isolated Cu(I), identified to be present by XPS and EXAFS studies, was regarded as the primary active site for photoreduction. The lower methanol production rate (14.3 μmol/g-cat/h) over Ag/TiO_2 than Cu/TiO_2 was correlated to the size of Ag clusters, and photogenerated electrons, enhancing lifetimes of the photo-excited states.

Dispersed TiO_2 within zeolite cavities was prepared by ion exchange and anchoring methods in 1995. Yamashita et al. showed relatively high production in CO over Ti-ZSM-5 materials in photocatalytic CO_2 reduction, whereas Ti-Y-zeolite and anchoring of Ti on porous Vycor glass (PVG) showed higher selectivity to CH_4 and CH_3OH.[10] The photoreaction

was performed in an environment of CO_2 and H_2O at 0-50^oC, and illumination was performed by a 75 W high pressure mercury lamp ($\lambda > 280$ nm). Highly dispersed, isolated tetrahedral titanium oxide was considered to be the active site for photocatalytic CO_2 reduction. XANES and EXAFS spectra displayed a tetrahedral coordination of the isolated Ti-O species over PVG. A strong dependency of the product distribution on the chemical nature of the support was observed. Dispersed titanium oxide in different zeolites (Y-zeolite) and mesoporous (MCM-41 and MCM-48) molecular sieves were applied in photocatalytic CO_2 reduction.[11] The photocatalytic CO_2 reduction was carried out with the catalysts placed on the flat bottom of a quartz cell. After illumination at 55^oC in the presence of 24 μmol CO_2 and 120 μmol H_2O, methane and methanol production was observed in quantities of 3.6 and 1.4 μmol/g-TiO_2/h for Ti-MCM-41; 4.6 and 3 μmol/g-TiO_2/h for Ti-MCM-48. The photoluminescence spectra showed an efficient quenching in photoluminescence, when adding CO_2 and H_2O to the catalyst, which suggested interaction of the reagents with the isolated Ti-sites. Combined with X-ray spectroscopy (XANES), isolated Ti-oxide species were attributed to yield the formation of methane and methanol. The effect of Pt-loading was also investigated, and found to promote the selectivity to CH_4 over CH_3OH, reaching a yield of 13.3 μmol/g-TiO_2/h in CH_4, and 0.2 μmol/g-TiO_2/h in CH_3OH. Pt acts as electron transfer center, preventing the reaction between carbon and hydroxyl radicals, thus leading to methane formation. Ti-SBA-15 prepared by hydrothermal synthesis showed a high yield in methane (106 μmol/g-Ti/h) and methanol (27.7 μmol/g-Ti/h).[12] The influence of acid in the synthesis of Ti-SBA-15 was considered, leading to a better dispersion of Ti-oxide species in the pore wall, as compared to Ti-MCM-41 and Ti-MCM-48 prepared in less acidic conditions. Summarizing, highly dispersed titanium oxide in mesoporous silica materials leads to relatively high yield in CH_4 and CH_3OH. Reasons for this observation are indicated below.

Dispersion of titanium oxide in porous silica scaffolds yields various morphologies, ranging from the nanoparticle range down to isolate titania sites. Minimizing particle size increases the specific surface area, and shortens the pathway for photogenerated charges to reach the surface. Another attempt in minimizing particle size and limiting charge transfer path length was synthesis of nanotubes. Varghese et al. recently reported that nitrogen-doped TiO_2 nanotubes show efficient solar conversion of CO_2 and water vapor into methane and other hydrocarbons.[13] The breakthrough of the study is to directly make use of sunlight driving photocatalytic CO_2 reduction, achieved by nitrogen-doping to increase the sensitivity

of TiO_2 to visible light. TiO_2 nanotube was synthesized by anodizing titanium foil in an electrolyte consisting of ammonium fluoride (NH_4F) and ethylene glycol at 55 V. NH_4F is the source of incorporating nitrogen into TiO_2 nanotubes. Different annealing temperatures (460 or 600^oC) led to different absorptions in the visible light region, 400-500 nm. 600^oC annealed TiO_2 combined with copper as the cocatalysts showed production in methane of 70 ppm/cm^2/h or 3.09 μmol/g-cat/h under AM 1.5 sun light irradiation. H_2, CO and other hydrocarbons – olefins and branched paraffins – were also detected as the final products.

One of the challenges to directly make use of solar light is the light sensitivity for TiO_2, which is limited to the UV. Efforts are focused on the exploration of visible light sensitive materials for photocatalytic applications. Other semiconductors with higher visible light absorption intensity were found active in photocatalytic CO_2 reduction. $InTaO_4$ was tested in the photocatalytic CO_2 reduction by Pan and his coworkers.[14] The intrinsic energy gap, 2.7 eV, allows photo-excitation initiated by visible light. Moreover, the conduction band potential is sufficient for reduction of CO_2 into methanol. For a suspended system, consisting of CO_2 saturated $KHCO_3$ solution, a yield of 1.39 μmol/g-cat/h of methanol was found over 1 % NiO-loaded $InTaO_4$, using a 500 W halogen lamp. The quantum yield was calculated as 2.45 % for photon-into-methanol production. Wang et al. discussed the application of a $NiO/InTaO_4$ optical-fiber reactor for gas phase photocatalytic CO_2 reduction.[15] $NiO/InTaO_4$ was immobilized onto the optical fibers, and it was proposed that better light-harvesting properties, as compared to conventional configurations for the catalytic system, such as a top-illuminated reactor, resulted in improved performance. Under 100W halogen lamp irradiation, 11.1 μmol/g-cat/h methanol was produced over $NiO/InTaO_4$. The corresponding quantum yield was 0.063 % for photon-to-methanol production. A combination of CdSe quantum dots and Pt-loaded TiO_2 was found active in photocatalytic CO_2 reduction under visible light irradiation.[16] Under illumination by a 300 W Xenon lamp, and wavelengths below 420 nm removed, the gas products were analyzed to be 48 ppm/g-cat/h (or 0.6 μmol/g-cat/h) of methane and 3.3 ppm/g-cat/h of methanol (methanol production was not reported in μmoles).

Table 1 summarizes literature reports on photocatalytic CO_2 reduction in the past decades. The chronological compilation shows scientific progress for TiO_2 and other semiconductors, varying from metal incorporated TiO_2 to dispersed TiO_2 over porous silica scaffolds. In summary, major products are methane and methanol for gaseous phase CO_2 reduction, and formaldehyde, formic acid and methanol for liquid phase CO_2 reduction. Current challenges

for CO_2 activation by photocatalysis are the extremely low production of hydrocarbons (mainly in μmol/g-cat/h range), and to improve photo-excitation of most catalysts, which are often limited to the use of UV light.

Photocatalytic H_2O oxidation

As reported in many studies, H_2O oxidation is the limiting factor for photocatalytic CO_2 activation. The $[Ru(bpy)_3]^{2+}$ - catalyst system has often been used to evaluate photocatalytic H_2O oxidation activity, due to its unique combination of chemical stability, redox properties, excited state reactivity and lifetime.[17]

Tris(2,2'-bipyridyl)ruthenium(II) ($[Ru(bpy)_3]^{2+}$) contains two intense absorption bands at 240 and 450 nm, which are assigned to a metal-to-ligand charge transfer of $d \rightarrow \pi^*$ (MLCT).[18] The lowest MLCT excited state of $[Ru(bpy)_3]^{2+}$ lives long enough to encounter other solute molecules (even where these are present at relatively low concentration) and possesses suitable properties as energy donor, electron donor, or electron acceptor.[17] The respective equations are (5) to (7). The energy available to $^*[Ru(bpy)_3]^{2+}$ for energy transfer is 2.12 eV (ca. 584 nm) and its reduction and oxidation potentials are +0.84 and -0.86 V (aqueous solution, vs SCE), respectively.

$$^*[Ru(bpy)_3]^{2+} + Q \rightarrow [Ru(bpy)_3]^{2+} + {}^*Q \qquad \text{energy transfer} \qquad (5)$$

$$^*[Ru(bpy)_3]^{2+} + Q \rightarrow [Ru(bpy)_3]^{3+} + Q^- \qquad \text{oxidative quenching} \qquad (6)$$

$$^*[Ru(bpy)_3]^{2+} + Q \rightarrow [Ru(bpy)_3]^{+} + Q^+ \qquad \text{reductive quenching} \qquad (7)$$

$[Ru(bpy)_3]^{3+}$ and its derivatives are found to be capable of initiation of oxidizing water to O_2 at the surface of colloidal and bulk heterogeneous catalysts.[19-21] Scheme 1 shows the principle of photocatalytic water oxidation, summarized by Hara et al.[22] The photo-excited Ru complex is rapidly oxidized in the presence of an electron acceptor, $S_2O_8^{2-}$. When O_2 is evolved, the catalyst injects electrons in the oxidized Ru complex ($[Ru(bpy)_3]^{3+}$), which is reduced back to the original oxidation state, $[Ru(bpy)_3]^{2+}$, available for a second cycle.

The absence of a O_2 evolution catalyst leads to the hydrolysis of the oxidized Ru complex. Then, eventually the catalytic cycle is stopped. The spontaneous reduction of $[Ru(bpy)_3]^{3+}$ to $[Ru(bpy)_3]^{2+}$ in aqueous solution yields only traces of O_2, accompanied by around 10 %

degradation of the Ru complex.[23] On the other hand, the photo-excited Ru complex is only stable at pH 5. The rate of $[Ru(bpy)_3]^{3+}$ reduction is thus pH dependent. The decreasing pH as a result of proton formation during the photoreaction will stop the catalytic cycle as a consequence.

Scheme 1. Schematic representation of photocatalytic H_2O oxidation in the $[Ru(bpy)_3]^{2+}$-catalyst system.[22]

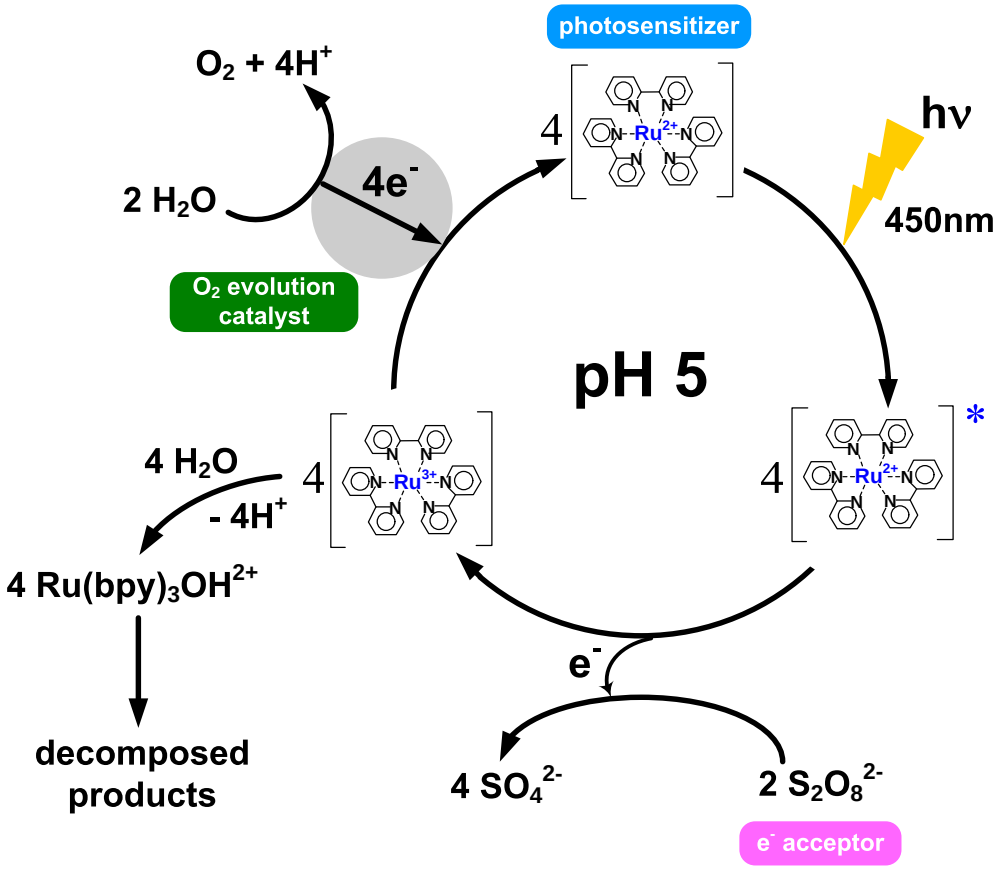

Knowledge from recent progress in photocatalytic water splitting

Photocatalytic water splitting also appears a viable option for photon-into-fuel conversion. As compared to CO_2 reduction, H_2O reduction is thermodynamically easier to achieve, giving H_2 as final product.

TiO_2 is one of the most active photocatalysts for water splitting. Leung and his coworkers indicated four main drawbacks of TiO_2 for photocatalytic H_2 evolution [24]: (1) a large overpotential is required for production of H_2 and O_2, making TiO_2 alone inactive for H_2

generation [25]; (2) a rapid recombination rate of photo-induced e^- and h^+ before migrating to the surface to split water; (3) the fast thermal back reaction to produce H_2O from H_2 and O_2; (4) the inability to make use of visible light. They summarized various strategies to overcome these barriers for hydrogen production over titania-based photocatalysts. First, the incorporation of cocatalysts (such as Pt, Pd, Au, Rh and Ag) decreases the overpotential for H_2 evolution, and suppresses the recombination of photo-induced carriers. Second, increasing the crystallinity of TiO_2 also helps to reduce the recombination rate of photoinduced carriers. Third, incorporating NaOH, Na_2CO_3, or B_2O_3 into TiO_2, and physically separating H_2 and O_2 evolution by using a two-compartment cell prevents thermal back reaction of H_2 and O_2. Forth, doping TiO_2 with cations (such as V, Cr, Fe, Co, Mo, In, La, Ce, and Sm), or anions (such as N, C, S, F, and B) successfully tuned photocatalytic activity of TiO_2 toward the visible-light region, by narrowing the band gap of TiO_2. Fifth, coupling TiO_2 with small-band-gap semiconductors (such as CdS, RuS_2, Bi_2S_3, WS_2 and AgGaS) or organic dyes extends the energy excitation range of TiO_2 further to the visible-light region. The principle of sensitizing TiO_2 is to photo-excite small-band-gap semiconductors or organic dyes in the visible-light region. The photoexcited electrons thus migrate to TiO_2 for H_2 evolution. O_2 production takes place at the valence band sites of TiO_2.

Zhu et al. also categorized literature-reported photocatalysts for H_2 production.[26] Various non-TiO_2 materials, nanocomposites, and so-called Z-scheme systems are alternatives for water splitting. Non-oxide materials include nitrides, sulfides, oxynitrides, and oxysulfides. Different valence band energy levels can be obtained by combination of these materials, shifting the absorption spectrum towards the visible-light region. A nanocomposite usually consists of intercalated nanoparticles (such as TiO_2, CdS, and Fe_2O_3) in layered compounds (such as $H_2Ti_4O_9$, H_4NbO_{17}, $K_2Ti_{3.9}NbO_9$, $HNbWO_6$, $HTiNbO_5$, and $HTiTaO_5$). The photo-excited electrons or holes of these nanoparticles can be quickly transferred to the matrix of the layered compounds. The rapid charge separation is thus achieved, leading to high activity in water splitting. A Z-scheme system consists of an H_2-evolution catalyst, and an O_2-evolution catalyst, and often an electron mediator. The advantage of the Z-scheme system is to employ two photocatalysts, one active in H_2- and one in O_2-evolution, with visible light absorption capacity. H_2 and O_2 evolution take place on largely separated sites, potentially reducing the probability of the back reaction to H_2O. The two catalytic cycles are completed by reduction/oxidation of the electron mediator, such as IO_3^-/I^- and Fe^{3+}/Fe^{2+}. Key factors in the

design of a Z-scheme system are to find a pair of photocatalysts with redox potentials which can meet the requirements of electron donor and acceptor in the respective half reactions.[26]

Scope and outline of this dissertation

Although various studies have shown that photocatalytic CO_2 activation is feasible (Table 1), the mechanism is still not very well understood, and results are usually explained largely based on speculation. The research topic of this dissertation is focused on a mechanistic study of photocatalytic CO_2 activation into hydrocarbons, by using water as reductant. The dissertation is divided into two parts: mechanistic exploration by IR spectroscopy, and reactor design for systematic activity evaluation. The in-situ IR technique provides information on the interaction between the reactants (CO_2 and H_2O) and products (CO in this case). The custom-built parallel photoreactor system is of great advantage for a fair comparison of various samples. The equipment has also been used successfully to study the effect of gas composition on catalysts' performance.

In **Chapter 2**, a study of gas phase photocatalytic CO_2 reduction over dense phase TiO_2 is reported, using in-situ DRIFT spectroscopy. Copper-loaded TiO_2 (Cu/TiO_2) is capable to produce CO, as is evident by enhancement in the spectral signature of CO adsorbed on Cu^+-sites. Isotopic $^{13}CO_2$ introduction is used to clarify the contribution of CO_2 decomposition to the primary product CO. The spectral observations show that an internal carbon source leads to the growth of ^{12}CO. The contribution of the carbon residue - remaining from the synthesis procedure - to the production of CO, can lead to false quantification of production. Especially considering the low photocatalytic conversion of CO_2 into CO, the genuine products from CO_2 reduction requires careful evaluation.

In **Chapter 3**, a DRIFTS investigation is discussed on how carbonates are involved in CO_2 reduction. Carbonate deposition dominates spectral development, when the catalyst, Cu/TiO_2, is contacted with CO_2. Impregnating carbonate onto pure Cu/TiO_2 is the strategy to clarify the role of carbonates in CO_2-to-CO conversion. The carbonate-impregnated sample shows direct carbonate decomposition into CO. The results demonstrate carbonate as an intermediate in CO_2 reduction to CO over crystalline Cu/TiO_2.

Chapter 4 discusses the technical part of catalyst evaluation. It describes the principle of a parallel photoreactor system, designed for catalyst screening in photocatalysis applications. The difficulty of comparing catalysts' performance reported in literature lies in the diversity of the experimental equipment, and applied reaction conditions. The combinatorial photoreactor system offers a good platform for fair comparison among various catalysts. All the reactors are designed to operate under equal reaction conditions with no cross-talk issues for quantification of products. A screening result of the catalysts (especially Ti-based catalysts) active in photocatalytic CO_2 reduction is presented, including further evaluation of reaction parameters, such as catalyst loading and light distribution characteristics of the device.

The most active catalyst, Ti-SBA-15, is used for a mechanistic study, reported in **Chapter 5**. By changing the initial composition of the gas mixture (CO, CO_2, H_2, and H_2O), variations in hydrocarbon production have been observed. The results indicate CO activation by H_2O is the predominant reaction to yield most hydrocarbons. A mechanism for CO_2 reduction is proposed, and compared with propositions in the literature.

The concomitant reaction of CO_2 reduction is H_2O oxidation into O_2. **Chapter 6** discusses a study on photocatalytic H_2O oxidation. The investigation is focused on a suspension of catalyst, containing photosensitizer (Ru complex) and electron acceptor (persulfate). Screening of catalysts active for H_2O oxidation is presented. Dispersed cobalt oxide in porous silica materials (Co_3O_4-SBA-15) shows the highest O_2 production rate for H_2O oxidation. The effect of particle size and silica support on O_2 evolution is addressed. It will also be discussed how process parameters influence evaluation of catalysts' performance. Catalyst loading and absorption of Ru complex on silica sites, as well as reaction pH, are important factors to be considered.

Finally, a summary of the results, recommendations, and concluding remarks are presented in **Chapter 7**.

Table 1 Compilation of literature reports on photocatalytic CO_2 reduction.

year	catalysts	loading	primary products	product yield: methane	product yield: methanol	quantum yield	reactor/sample cell	reactants	temp.	light source	light intensity	reference
1978*	p type-GaP (WE); n type-TiO_2 (CE)		HCHO, HCOOH, CH_3OH	-	1.88 (μmol/h)			CO_2 in $Li_2CO_{3(aq)}$	25°C	Hg lamp	210 mW/cm^2	Halmann et al.[2]
1979*	SiC		HCHO, CH_3OH	-	76.4 (μmol/g-cat/h)	0.45% (CH_3OH)	glass cell,	CO_2 in H_2O	-	500 W Xe/Hg lamp	-	Inoue et al.[4]
	TiO_2			-	4.9 (μmol/g-cat/h)	0.019% (CH_3OH)	quartz window					
	GaP			-	15.7 (μmol/g-cat/h)	-						
	CdS			-	16.7 (μmol/g-cat/h)	-						
	WO_3			-	0	-						
1987	Ru/TiO_2	3.8 wt% Ru	CH_4	1.7 (μmol/g-cat/h)	-		pyrex cell	CO_2, H_2O (1:12)	25°C	solar simulator	80 mW/cm^2	Thampi et al.[5]
				51.8 (μmol/g-cat/h)	-				46°C			
				105 (μmol/g-cat/h)	-				90°C			
				2.7 (μmol/g-cat/h)	-				25°C	150 W Xe lamp+ filter		
	Ru/TiO_2 - no illumination	3.8 wt% Ru		1.7 (μmol/g-cat/h)	-				46°C	(λ < 435 nm)		
1992*	TiO_2 (anatase, Furuuchi) + Cu (Wako)	0.5g TiO_2 + 0.3g Cu	CO, HCHO, HCOOH,	-	0.56 (μmol/g-cat/h)		Cylindrical	CO_2 in H_2O	40°C	500 W Xe lamp	-	Hirano et al.[8]
			CH_3OH	0.05 (μmol/g-cat/h)	1.32 (μmol/g-cat/h)		pyrex cell	CO_2 in $KHCO_{3(aq)}$				
1993*	Degussa P25 TiO_2	-	CH_4, C_2H_6, CH_3OH,	0.9 (μmol/g-cat/h)	trace		quartz cell	CO_2 in H_2O	5°C	500 W Hg lamp	-	Ishitani et al.[27]
	$Pd-TiO_2$	2 wt% Pd	HCOOH, CH_3COOH	32.9 (μmol/g-cat/h)	trace					(λ > 310 nm)		
	$Rh-TiO_2$	2 wt% Rh		13.3 (μmol/g-cat/h)	trace							
	$Pt-TiO_2$	2 wt% Pt		6.7 (μmol/g-cat/h)	trace							
	$Au-TiO_2$	2 wt% Au		4.4 (μmol/g-cat/h)	trace							
	$Cu-TiO_2$	2 wt% Cu		2.5 (μmol/g-cat/h)	trace							
	$Ru-TiO_2$	2 wt% Ru		0.8 (μmol/g-cat/h)	trace							
1995	TiO_2 (100) (rutile single crystal on wafer)	-	CH_4, CH_3OH	3.5 (μmol/g-cat/h)	2.4 (μmol/g-cat/h)		quartz cell	CO_2, H_2O (1:3)	2°C	75 W Hg lamp	-	Anpo et al.[28]
	TiO_2 (110)	-		0	0.8 (μmol/g-cat/h)					(λ > 280 nm)		
	TiO_2 anchored on porous Vycor glass	-		0.02 (μmol/g-cat/h)	-			CO_2, H_2O (1:5)				
1995	Ti-ZSM-5 (ion exchange)	10 wt% Ti	CO, CH_4, CH_3OH	0.03 (μmol/g-cat)	-		-	H_2O/CO_2 = 5	50°C	75 W Hg lamp	-	Yamashita et al.[10]
	Ti-ZSM-5 (anchored)	10 wt% Ti		0.01 (μmol/g-cat)	-					(λ > 280 nm)		
	Ti-Y (ion exchange)	10 wt% Ti		0.20 (μmol/g-cat)	0.13 (μmol/g-cat)							
	Ti-PVG (anchored)	10 wt% Ti		0.17 (μmol/g-cat)	0.03 (μmol/g-cat)							
1995	Degussa P25 TiO_2	-	H_2, CO, CH_4	2 (μmol/g-cat/h)	-		quartz cell	CO_2, H_2O	70°C	1000 W Hg lamp	-	Saladin et al.[7]
										(λ < 700 nm)		
1997	TiO_2 (anatase, 500 m^2/g)	-	H_2, CH_4, C_nH_m	3.75 (μmol/g-cat/h)	-		miniaturized	CO_2, H_2O	100°C	200 W Hg/Xe lamp	-	Saladin et al.[29]
	Degussa P25 TiO_2	-		4.74 (μmol/g-cat/h)	-		photoreactor		25°C	(λ < 900 nm)		
		-		5.68 (μmol/g-cat/h)	-				100°C			
		-		6.42 (μmol/g-cat/h)	-				200°C			
1998*	Degussa P25 TiO_2	-	CH_4, HCOOH	0.43 (μmol/g-Ti/h)			stainless steel vessel	CO_2 in isopropanol	-	4200 W Xe lamp	62 mW/cm^2	Kaneco et al.[30]

* stands for liquid phase photocatalytic CO_2 reduction. The rest is gas phase photocatalytic CO_2 reduction.

year	catalysts	loading	primary products	Product yield methane	methanol	quantum yield	reactor/sample cell	reactants	temp.	light source	light intensity	reference
1998	Pt-Ti/MCM-48	80 (Si/Ti ratio)	CH_4, CH_3OH	12.3 (μmol/g-TiO_2/h)	0.2 (μmol/g-TiO_2/h)		quartz cell	CO_2, H_2O (1:5)	55ºC	Hg lamp (λ > 280nm)	-	Yamashita
	Ti-MCM-48	80 (Si/Ti ratio)		7.6 (μmol/g-TiO_2/h)	3 (μmol/g-TiO_2/h)							et al.[11]
	Ti-MCM-41	100 (Si/Ti ratio)		3.6 (μmol/g-TiO_2/h)	1.4 (μmol/g-TiO_2/h)							
	TS-1	85 (Si/Ti ratio)		2.7 (μmol/g-TiO_2/h)	0.6 (μmol/g-TiO_2/h)							
	Pt-ion-ex-TiOY	1 wt% Pt; 1.1% Ti		12.4 (μmol/g-TiO_2/h)	1.1 (μmol/g-TiO_2/h)							
	ion-ex-TiOY	1.1 wt% Ti		7.2 (μmol/g-TiO_2/h)	4.8 (μmol/g-TiO_2/h)							
	imp-TiO_2/Y (SiO_2/Al_2O_3=5.5)	1 wt% Ti		5 (μmol/g-TiO_2/h)	0.3 (μmol/g-TiO_2/h)							
	imp-TiO_2/Y (SiO_2/Al_2O_3=5.5)	10 wt% Ti		1.2 (μmol/g-TiO_2/h)	-							
	TiO_2 (JRC-TIO-4)	-		0.3 (μmol/g-TiO_2/h)	-							
1999*	TiO_2/Pd/SiO_2	10 wt% TiO_2	CH_4, HCHO,	0.8 (μmol/h)	2.5 (μmol/h)		batch type reactor	CO_2 in $KHCO_{3(aq)}$	-	250 mW Hg lamp	-	Subrahmanyam
	Li-TiO_2/Al2O_3		CH_3OH, C_2H_5OH	2.5 (μmol/h)	0.8 (μmol/h)							et al.[31]
2001	TiO_2/FSM-16 (physical mix)	1 wt% Ti	CH_4, CH_3OH	127 (μmol/g-cat/h)	5.4 (μmol/g-cat/h)		quartz cell	CO_2, H_2O (1:5)	50ºC	100 W Hg lamp	-	Ikeue et al.[32]
	imp-Ti/FSM-16	1 wt% Ti		207 (μmol/g-cat/h)	10.8 (μmol/g-cat/h)					(λ > 250 nm)		
	anc-Ti/FSM-16 (with TPOT)	1 wt% Ti		270 (μmol/g-cat/h)	35 (μmol/g-cat/h)							
	Ti-FSM-16 (direct synthesis)	1 wt% Ti		259 (μmol/g-cat/h)	40.5 (μmol/g-cat/h)							
2001	Ti-Beta(F)	2 wt% Ti	CH_4, CH_3OH	0.70 (μmol/g-Ti/h)	0.47 (μmol/g-Ti/h)		quartz cell	CO_2, H_2O (1:5)	50ºC	75 W Hg lamp	-	Ikeue et al.[33]
	Ti-Beta(OH)	2 wt% Ti		5.76 (μmol/g-Ti/h)	1.35 (μmol/g-Ti/h)					(λ > 250 nm)		
	TS-1	-		1.29 (μmol/g-Ti/h)	0.41 (μmol/g-Ti/h)							
	Degussa P25 TiO_2	-		0.35 (μmol/g-Ti/h)	-							
2002*	Degussa P25 TiO_2	-	CH_3OH	-	6.37 (μmol/g-cat/h)	3.41% (CH_3OH)	inner-irradiated cell	CO_2 in $NaOH_{(aq)}$	50ºC	8 W Hg lamp	0.138 mW/cm^2	Tseng et al.[34]
	TiO_2	-		-	0.78 (μmol/g-cat/h)	0.42% (CH_3OH)				(λ = 254 nm)		
	Cu/P25 TiO_2	2 wt% Cu		-	10 (μmol/g-cat/h)	5.35% (CH_3OH)						
	Cu/TiO_2	2 wt% Cu		-	19.8 (μmol/g-cat/h)	10.02% (CH_3OH)						
2002	Ti-containing nanoporous silica films (Ti-PS)						quartz cell	CO_2, H_2O (1:5)	50ºC	100 W Hg lamp	0.265 mW/cm^2	Ikeue et al.[35]
	Ti-PS film (c,50)	50 (Si/Ti ratio)	CH_4, CH_3OH	1.2 (μmol/g-Ti/h)	1.7 (μmol/g-Ti/h)	0.07% #				(λ > 250 nm)		
	Ti-PS film (h,25)	25 (Si/Ti ratio)		4.2 (μmol/g-Ti/h)	0.2 (μmol/g-Ti/h)	0.17% #						
	Ti-PS film (h,50)	50 (Si/Ti ratio)		7.1 (μmol/g-Ti/h)	1.8 (μmol/g-Ti/h)	0.28% #						
	Ti-PS powder (h,50)	50 (Si/Ti ratio)		3.6 (μmol/g-Ti/h)	0.9 (μmol/g-Ti/h)	-						
	Ti-MCM-41 powder	100 (Si/Ti ratio)		3.0 (μmol/g-Ti/h)	1.3 (μmol/g-Ti/h)	-						
2003	Fe-Cu-K/DAY and Pt/$K_2Ti_6O_{10}$ (1:1)		H_2, HCHO,	0.013 (μmol/g-cat/h)	-		optical quartz cell	CO_2, H_2O	25ºC	300 W Xe arc lamp	-	Guan et al.[36]
			CH_4, CH_3OH,	0.05 (μmol/g-cat/h)	-				25ºC	150 W Hg lamp	-	
			HCOOH,	0.047 (μmol/g-cat/h)	4.83 (μmol/g-cat/h)				317ºC	concentrated sunlight	62 mW/cm^2	
			C_2H_5OH	0.043 (μmol/g-cat/h)	2.3 (μmol/g-cat/h)				289ºC	concentrated sunlight	72 mW/cm^2	
				0.037 (μmol/g-cat/h)	trace				261ºC		101 mW/cm^2	
2004*	TiO_2 (anatase, Aldrich)		CH_4	0.88 (μmol/g-TiO_2/h)	-		Rayonet photoreactor	CO_2 in H_2O	25ºC	350 nm light source	-	Dey et al.[37]
				0.84 (μmol/g-TiO_2/h)	-			CO_2 in 2-propanol				
				2.16 (μmol/g-TiO_2/h)	-			CO_2 in 2-propanol				
2004*	Cu/TiO_2 ($CuCl_2$-0hr)	2 wt% Cu	CH_3OH	-	20 (μmol/g-cat/h)		cylindrical quartz reactor	CO_2 in $NaOH_{(aq)}$	-	UVC (λ = 254 nm)	-	Tseng et al.[38]
	Cu/TiO_2 ($CuCl_2$-8hr)	2 wt% Cu		-	10 (μmol/g-cat/h)					UVC (λ = 254 nm)		
	Cu/TiO_2 ($CuCl_2$-8hr)	2 wt% Cu		-	0.33 (μmol/g-cat/h)					UVA (λ = 365 nm)		

The authors did not mention how the quantum yield was calculated.

year	catalysts	loading	primary products	product yield: methane	product yield: methanol	quantum yield	reactor/sample cell	reactants	temp.	light source	light intensity	reference
2004*	Cu/TiO_2	2 wt% Cu	CH_3OH		16.7 (μmol/g-cat/h)		cylindrical reactor	CO_2 in $NaOH_{(aq)}$	50°C	8 W Hg lamp	-	Tseng et al.[9]
	Ag/TiO_2	2 wt% Ag			14.3 (μmol/g-cat/h)					(λ = 254 nm)		
2004*	TiO_2/Nafion film	10 wt% TiO_2/g-Nafion	HCOOH, CH_3OH,	-	56 (μmol/g-TiO_2/h)		flow system,	liquid CO_2	-	990 W Xe arc lamp		Pathak et al.[39]
	Degussa P25 TiO_2	-	CH_3COOH	-	1.8(μmol/g-TiO_2/h)		quartz window					
2004*	Degussa P-25 TiO_2 (1gTiO_2/L sol.)		CH_4, CH_3OH	-	93.75 (μmol/g-cat/h)		inner-irradiated cell	$NaHCO_{3(aq)}$	-	15 W UV lamp (365 nm)	1.3 mW/cm^2	Ku et al.[40]
2005	Ti-MCM-41	100 (Si/Ti ratio)	CH_4, CH_3OH	2.99 (μmol/g-Ti/h)	1.33 (μmol/g-Ti/h)		quartz cell	CO_2, H_2O (1:5)	50°C	100 W Hg lamp	-	Hwang et al.[12]
	Ti-MCM-48	80 (Si/Ti ratio)		7.57 (μmol/g-Ti/h)	3.06 (μmol/g-Ti/h)					(λ > 250 nm)		
	Ti-SBA-15	270 (Si/Ti ratio)		106 (μmol/g-Ti/h)	27.7 (μmol/g-Ti/h)							
	TS-1	85 (Si/Ti ratio)		2.6 (μmol/g-TiO_2/h)	0.6 (μmol/g-TiO_2/h)							
	Degussa P25 TiO_2	-		0.33 (μmol/g-Ti/h)	0.005 (μmol/g-Ti/h)							
2005	Cu/TiO_2	0.52 wt% Cu	CH_3OH		0.18 (μmol/g-cat/h)		optical fiber reactor	CO_2, H_2O (50:1)	75°C	Hg lamp	13500 mW/cm^2	Wu et al.[41]
		1.2 wt% Cu			0.42 (μmol/g-cat/h)					(λ = 365 nm)		
		2.06 wt% Cu			0.35 (μmol/g-cat/h)							
2006*	Ru/TiO_2	0.5 wt% Ru	CH_4, CH_3OH	205.4 (μmol/g-Ti)	13.8 (μmol/g-Ti)		inner-irradiated cell	CO_2 in H_2O	-	1000 W Hg lamp	-	Sasirekha et al.[42]
	TiO_2/SiO_2	10 wt% Ti		267.7 (μmol/g-Ti)	80.7 (μmol/g-Ti)					(λ = 365 nm)		
	Ru-TiO_2/SiO_2	0.5 wt% Ru; 10 wt% Ti		223.8 (μmol/g-Ti)	43.8 (μmol/g-Ti)							
	TiO_2 (99%, Lancaster)	-		184.6 (μmol/g-Ti)	11.9 (μmol/g-Ti)							
2007	Degussa P25 TiO_2 pellet	-	CH_4	0.001 (μmol/g-TiO_2/h)	-		top-illuminated cell		38°C	4.8 W UVC	-	Tan et al.[43]
										(λ = 253.7 nm)		
2007	multi-walled carbon nanotube	-	CH_4, HCOOH, C_2H_5OH	0.98 (μmol/g-cat/h)	-		samples laid over glass,	CO_2, H_2O (1:5)	25°C	15W UVA	-	Xia et al.[44]
	TiO_2-MWCNTs (0.01g CNT)	-		11.74 (μmol/g-cat/h)	-		stainless steel reactor			(λ = 365 nm)		
	Degussa P25 TiO_2	-		14.67 (μmol/g-cat/h)	-							
	TiO_2-AC (0.01g activated carbon)	-		4.31 (μmol/g-cat/h)	-							
	Activated carbons (AC)	-		0.67 (μmol/g-cat/h)	-							
2007*	titania-supported cobalt phthalocyanine	0.5wt% CoPc	CO, CH_4, HCOOH, HCHO	0.63 (μmol/g-cat/h)	0.21 (μmol/g-cat/h)		pyrex cell	CO_2 in $NaOH_{(aq)}$	-	500 W halogen lamp	-	Liu et al.[45]
2007*	$InTaO_4$	-	CH_3OH	-	1.06 (μmol/g-cat/h)		continuous flow reactor,	CO_2 in $KHCO_{3(aq)}$	-	500 W	-	Pan et al.[14]
	NiO-$InTaO_4$	1 wt% NiO		-	1.39 (μmol/g-cat/h)	2.45% (CH_3OH)	down-window type cell			halogen lamp		
2008*	TiO_2 (anatase 773K)	-	CH_4	33.68 (μmol/g-cat/h)	-		commercial annular	CO_2 in	20 –	450 W Hg lamp	-	Li et al.[46]
	TiO_2 (anatase-rutile 773K)	-		14.03 (μmol/g-cat/h)	-		reactor	$NaHCO_3$/	25°C			
	Degussa P25 TiO_2	-		3.51 (μmol/g-cat/h)	-			isopropanol				
2008	Degussa P25 TiO_2	-	-	trace	-		optical fiber	CO_2, H_2O	75°C	UVA light	225 mW/cm^2	Nguyen et al.[47]
	Cu-Fe/TiO_2	0.5 wt% Cu; 0.5 wt%Fe	CH_4, C_2H_4	0.91 (μmol/g-cat/h)	-	0.025% (CH_4)	photoreactor			(λ = 320-500 nm)		
2009	nitrogen-doped titania nanotube (NT)		H_2, CO, CH_4, alkanes,				stainless steel chamber	CO_2, H_2O	44°C	sun light (AM 1.5)	75-102 mW/cm^2	Varghese et al.[13]
	NT/Pt-460	0.75 at% N	olefin, branched paraffin	1.19 (μmol/g-cat/h)	-							
	NT/Pt-600	0.4 at% N		2.86 (μmol/g-cat/h)	-							
	NT/Cu-600	0.4 at% N		3.09 (μmol/g-cat/h)	-							
	NT/Cu-600	0.4 at% N		0.09 (μmol/g-cat/h)	-					sun light (>400nm)	78.5 mW/cm^2	

* stands for liquid phase photocatalytic CO_2 reduction. The rest is gas phase photocatalytic CO_2 reduction.

year	catalysts	loading	primary products	product yield: methane	product yield: methanol	quantum yield	reactor/sample cell	reactants	temp.	light source	light intensity	reference
2009*	Degussa P25 TiO_2		CH_3OH	-	430 (μmol/g-cat/h)		inner-irradiated quartz cell	CO_2 in $NaOH_{(aq)}$	42°C	400 W halide lamp	-	Yang et al.[48]
	TiO_2/SBA-15	45 wt% TiO_2		-	972 (μmol/g-cat/h)					(λ = 300-600 nm)		
	Cu/TiO_2	2 wt% Cu		-	1250 (μmol/g-cat/h)							
	Cu/TiO_2/SBA-15	45 wt%TiO_2; 2 wt% Cu		-	1444 (μmol/g-cat/h)							
2009	Degussa P25 TiO_2 (TO-NP)	-	CH_4	-	-		quartz plate,	CO_2, H_2O (50:1)	50°C	300 W Hg lamp	-	Zhang et al.[49]
	Pt/TO-NP	0.12 wt% Pt		0.06 (μmol/g-Ti/h)	-		top-irradiated cell					
	TiO_2 nanotube (TO-NT)	-		-	-							
	Pt/TO-NT	0.15 wt% Pt		0.13 (μmol/g-Ti/h)	-							
2010*	$InTaO_4$ (1100°C)	-	CH_3OH	-	0.31 (μmol/g-cat/h)		cylindrical quartz reactor	CO_2 in $NaOH_{(aq)}$	25°C	fluorescent lamp	146 mW/cm^2	Wang et al.[15]
	NiO/$InTaO_4$ (1100°C)	1 wt% Ni		-	2.8 (μmol/g-cat/h)	0.0045% (CH_3OH)			25°C	(λ: 452, 543, 611 nm)		
				-	11.1 (μmol/g-cat/h)	0.063% (CH_3OH)	optical fiber photoreactor	CO_2, H_2O	25°C	100 W halogen lamp	327 mW/cm^2	
				-	21 (μmol/g-cat/h)				75°C	(λ = 400-1100 nm)		
				-	11.3 (μmol/g-cat/h)				32°C	solar concentrator		
2010	Ga_2SO_3	-	CO	0.72 (μmolCO/g-cat/h)	-		quartz reactor	CO_2, H_2O (1:1)	-	200 W Hg/Xe lamp	-	Tsuneoka et al.[50]
	MgO	-		0.71 (μmolCO/g-cat/h)	-							
	CaO	-		0.35 (μmolCO/g-cat/h)	-							
	ZrO_2	-		0.12 (μmolCO/g-cat/h)	-							
	Al_2O_3	-		0.07 (μmolCO/g-cat/h)	-							
	TiO_2	-		-	-							
	V_2O_5	-		-	-							
	Nb_2O_5	-		-	-							
2010*	TiO_2	-	CH_4, CH_3OH	3.3 (μmol/g-cat/h)	0.8 (μmol/g-cat/h)		inner-irradiated cell	CO_2 in $NaOH_{(aq)}$	-	8 W Hg lamp	1.41 mW/cm^2	Koci et al.[51]
	Ag/TiO_2	1 wt% Ag		5.2 (μmol/g-cat/h)	0.96 (μmol/g-cat/h)					(λ = 254 nm)		
		3 wt% Ag		4.2 (μmol/g-cat/h)	0.9 (μmol/g-cat/h)							
		5 wt% Ag		5.6 (μmol/g-cat/h)	1.2 (μmol/g-cat/h)							
		7 wt% Ag		8.5 (μmol/g-cat/h)	1.9 (μmol/g-cat/h)							
2010	TiO_2-SiO_2	12 wt% TiO_2	CO	-	-		continuous flow reactor,	CO_2, H_2O	-	Xe arc lamp	2.4 mW/cm^2	Li et al.[52]
	Cu/TiO_2-SiO_2	12 wt%TiO_2;0.5wt%Cu	CO, CH_4	13.2 (μmol/g-TiO_2/h)	-	0.56% (CH_4)	side-illuminated cell					
2010	$Zn2GeO_4$ (solid-state reaction)	-	CH_4	0.67 (μmol/g-cat/h)	-		top-illuminated cell	CO_2, injected H_2O	-	300 W Xe lamp	-	Liu et al.[53]
	$Zn2GeO_4$ (nanoribbons)	-		1.5 (μmol/g-cat/h)	-							
	Pt-loaded nanoribons	1 wt% Pt		2 (μmol/g-cat/h)	-							
	RuO_2-loaded nanoribbons	1 wt% RuO_2		2 (μmol/g-cat/h)	-							
	RuO_2+Pt-loaded nanoribbons	1 wt% RuO_2;1 wt% Pt		25 (μmol/g-cat/h)	-							
2010	$ZnGa_2O_4$ (solid-state reaction)	-	CH_4	-	-		top-illuminated cell	CO_2, injected H_2O	-	300 W Xe lamp	-	Yan et al.[54]
	meso-$ZnGa_2O_4$ (mesoporous)	-		5.3 (ppm/h)	-							
	RuO_2-loaded meso-$ZnGa_2O_4$	1 wt% RuO_2		50.4 (ppm/h)	-							
2010	CdSe quantum dots/Pt/TiO_2	1 at% Cd; 0.5 at% Pt	CO, H_2, CH_4, CH_3OH	48 (ppm/g-cat/h) [0.6 (μmol/g-cat/h)]	3.3 (ppm/g-cat/h)		stainless steel cube (quantified by FTIR)	CO_2, H_2O	-	300 W Xe lamp + filter (λ > 420 nm)	≤100 mW/cm^2	Wang et al.[16]

* stands for liquid phase photocatalytic CO_2 reduction. The rest is gas phase photocatalytic CO_2 reduction.

References

1. **M. Schiavello, *Heterogeneous Photocatalysis*, John Wiley & Sons, 1997.**
2. **M. Halmann, *Nature*, 1978, 275, 115-116.**
3. **C. H. Hamann and P. Schmode, *J. Power Sources*, 1976, 1, 141-157.**
4. **T. Inoue, A. Fujishima, S. Konishi and K. Honda, *Nature*, 1979, 277, 637-638.**
5. **K. R. Thampi, J. Kiwi and M. Gratzel, *Nature*, 1987, 327, 506-508.**
6. **M. Anpo and K. Chiba, *J. Mol. Catal.*, 1992, 74, 207-212.**
7. **F. Saladin, L. Forss and I. Kamber, *J. Chem. Soc., Chem. Commun.*, 1995, 533-534.**
8. **K. Hirano, K. Inoue and T. Yatsu, *J. Photochem. Photobiol., A*, 1992, 64, 255-258.**
9. **I. H. Tseng and J. C. S. Wu, *Catal. Today*, 2004, 97, 113-119.**
10. **H. Yamashita, A. Shiga, S. Kawasaki, Y. Ichihashi, S. Ehara and M. Anpo, *Energy Convers. Manage.*, 1995, 36, 617-620.**
11. **H. Yamashita, Y. Fujii, Y. Ichihashi, S. G. Zhang, K. Ikeue, D. R. Park, K. Koyano, T. Tatsumi and M. Anpo, *Catal. Today*, 1998, 45, 221-227.**
12. **J. S. Hwang, J. S. Chang, S. E. Park, K. Ikeue and M. Anpo, *Top. Catal.*, 2005, 35, 311-319.**
13. **O. K. Varghese, M. Paulose, T. J. LaTempa and C. A. Grimes, *Nano Lett.*, 2009, 9, 731-737.**
14. **P. W. Pan and Y. W. Chen, *Catal. Commun.*, 2007, 8, 1546-1549.**
15. **Z. Y. Wang, H. C. Chou, J. C. S. Wu, D. P. Tsai and G. Mul, *Appl. Catal., A*, 2010, 380, 172-177.**
16. **C. J. Wang, R. L. Thompson, J. Baltrus and C. Matranga, *J. Phys. Chem. Lett.*, 2010, 1, 48-53.**
17. **S. Campagna, F. Puntoriero, F. Nastasi, G. Bergamini and V. Balzani, in *Photochemistry and Photophysics of Coordination Compounds I*, Springer-Verlag Berlin, Berlin, 2007, vol. 280, pp. 117-214.**
18. **F. E. Lytle and D. M. Hercules, *J. Am. Chem. Soc.*, 1969, 91, 253-&.**
19. **J. Kiwi and M. Gratzel, *Angew. Chem. Int. Ed.*, 1978, 17, 860-861.**
20. **A. Harriman, M. C. Richoux, P. A. Christensen, S. Mosseri and P. Neta, *J. Chem. Soc., Faraday Trans. I*, 1987, 83, 3001-3014.**

21. A. Harriman, I. J. Pickering, J. M. Thomas and P. A. Christensen, *J. Chem. Soc., Faraday Trans. I*, 1988, 84, 2795-2806.

22. M. Hara, C. C. Waraksa, J. T. Lean, B. A. Lewis and T. E. Mallouk, *J. Phys. Chem. A*, 2000, 104, 5275-5280.

23. P. K. Ghosh, B. S. Brunschwig, M. Chou, C. Creutz and N. Sutin, *J. Am. Chem. Soc.*, 1984, 106, 4772-4783.

24. D. Y. C. Leung, X. L. Fu, C. F. Wang, M. Ni, M. K. H. Leung, X. X. Wang and X. Z. Fu, *ChemSusChem*, 2010, 3, 681-694.

25. A. L. Linsebigler, G. Q. Lu and J. T. Yates, *Chem. Rev.*, 1995, 95, 735-758.

26. J. F. Zhu and M. Zach, *Curr. Opin. Colloid Interface Sci.*, 2009, 14, 260-269.

27. O. Ishitani, C. Inoue, Y. Suzuki and T. Ibusuki, *J. Photochem. Photobiol., A*, 1993, 72, 269-271.

28. M. Anpo, H. Yamashita, Y. Ichihashi and S. Ehara, *J. Electroanal. Chem.*, 1995, 396, 21-26.

29. F. Saladin and I. Alxneit, *J. Chem. Soc., Faraday Trans.*, 1997, 93, 4159-4163.

30. S. Kaneco, Y. Shimizu, K. Ohta and T. Mizuno, *J. Photochem. Photobiol., A*, 1998, 115, 223-226.

31. M. Subrahmanyam, S. Kaneco and N. Alonso-Vante, *Appl. Catal., B*, 1999, 23, 169-174.

32. K. Ikeue, H. Mukai, H. Yamashita, S. Inagaki, M. Matsuoka and M. Anpo, *J. Synchrotron Radiat.,* 2001, 8, 640-642.

33. K. Ikeue, H. Yamashita, T. Takewaki, M. E. Davis and M. Anpo, *J. Synchrotron Radiat.*, 2001, 8, 602-604.

34. I. H. Tseng, W. C. Chang and J. C. S. Wu, *Appl. Catal., B*, 2002, 37, 37-48.

35. I. Keita, S. Nozaki, M. Ogawa and M. Anpo, *Catal. Today*, 2002, 74, 241-248.

36. G. Q. Guan, T. Kida and A. Yoshida, *Appl. Catal., B*, 2003, 41, 387-396.

37. G. R. Dey, A. D. Belapurkar and K. Kishore, *J. Photochem. Photobiol., A*, 2004, 163, 503-508.

38. I. H. Tseng, J. C. S. Wu and H. Y. Chou, *J. Catal.*, 2004, 221, 432-440.

39. P. Pathak, M. J. Meziani, L. Castillo and Y. P. Sun, *Green Chem.*, 2005, 7, 667-670.

40. Y. Ku, W. H. Lee and W. Y. Wang, *J. Mol. Catal. A: Chem.*, 2004, 212, 191-196.

41. J. C. S. Wu, H. M. Lin and C. L. Lai, *Appl. Catal., A*, 2005, 296, 194-200.

42. N. Sasirekha, S. J. S. Basha and K. Shanthi, *Appl. Catal., B*, 2006, 62, 169-180.

43. S. S. Tan, L. Zou and E. Hu, *Sci. Technol. Adv. Mater.,* 2007, 8, 89-92.

44. X. H. Xia, Z. H. Jia, Y. Yu, Y. Liang, Z. Wang and L. L. Ma, *Carbon*, 2007, 45, 717-721.

45. S. H. Liu, Z. H. Zhao and Z. Z. Wang, *Photochem. Photobiol. Sci.*, 2007, 6, 695-700.

46. G. H. Li, S. Ciston, Z. V. Saponjic, L. Chen, N. M. Dimitrijevic, T. Rajh and K. A. Gray, *J. Catal.*, 2008, 253, 105-110.

47. T. V. Nguyen and J. C. S. Wu, *Appl. Catal., A*, 2008, 335, 112-120.

48. H. C. Yang, H. Y. Lin, Y. S. Chien, J. C. S. Wu and H. H. Wu, *Catal. Lett.*, 2009, 131, 381-387.

49. Q. H. Zhang, W. D. Han, Y. J. Hong and J. G. Yu, *Catal. Today*, 2009, 148, 335-340.

50. H. Tsuneoka, K. Teramura, T. Shishido and T. Tanaka, *J. Phys. Chem. C*, 2010, 114, 8892-8898.

51. K. Koci, K. Mateju, L. Obalova, S. Krejcikova, Z. Lacny, D. Placha, L. Capek, A. Hospodkova and O. Solcova, *Appl. Catal., B*, 2010, 96, 239-244.

52. Y. Li, W. N. Wang, Z. L. Zhan, M. H. Woo, C. Y. Wu and P. Biswas, *Appl. Catal., B*, 2010, 100, 386-392.

53. Q. Liu, Y. Zhou, J. H. Kou, X. Y. Chen, Z. P. Tian, J. Gao, S. C. Yan and Z. G. Zou, *J. Am. Chem. Soc.*, 2010, 132, 14385-14387.

54. S. C. Yan, S. X. Ouyang, J. Gao, M. Yang, J. Y. Feng, X. X. Fan, L. J. Wan, Z. S. Li, J. H. Ye, Y. Zhou and Z. G. Zou, *Angew. Chem. Int. Ed.*, 2010, 49, 6400-6404.

Chapter 2

Artificial Photosynthesis over TiO_2-based Catalyst: Fact or Fiction?

Abstract: The mechanism of photocatalytic conversion of CO_2 and H_2O over Copper Oxide promoted Titania, Cu(I)/TiO_2, was investigated by means of in-situ DRIFT spectroscopy in combination with isotopically labeled $^{13}CO_2$. Besides small amounts of ^{13}CO, ^{12}CO was demonstrated to be the primary product of the reaction by the 2115 cm^{-1} Cu(I)-CO signature, indicating that carbon residues on the catalyst surface are involved in reactions with predominantly photo-catalytically activated surface adsorbed water. This was confirmed by prolonged exposure of the catalyst to light and water vapor, which significantly reduced the amount of CO formed in a subsequent experiment in the DRIFT cell. In addition, formation of carboxylates and (bi)carbonates was observed by exposure of the Cu(I)/TiO_2 surface to CO_2 in the dark. These carboxylates and (bi)carbonates decompose upon light irradiation, yielding predominantly CO_2. The finding that carbon residues are involved in photocatalytic water activation and CO_2 reduction might have important implications for the rates of artificial photosynthesis reported in many studies in the literature, in particular those using photo-active materials synthesized with carbon containing precursors, such as mesoporous materials and TiO_2-nanotubes.

Introduction

In photo-synthesis, solar energy is converted to chemical energy by reaction of CO_2 and H_2O to e.g. glucose and O_2. It has been reported that titania-based catalysts induce artificial photosynthesis, yielding single-carbon molecules in photocatalytic CO_2 reduction, such as CO, CH_4, CH_3OH, formaldehyde and formic acid. Titania catalysts were first used in aqueous suspension for photoelectrocatalytic CO_2 reduction.[1] Hirano et al. used copper-metal supported TiO_2 suspended in aqueous solution for photocatalytic CO_2 reduction.[2, 3] CH_3OH and HCHO were detected to be the main products. During illumination, trace amounts of formic acid were also detected in the liquid phase, while CO and CH_4 appeared in the gas phase. Tseng et al. confirmed these data, and reported that illumination of titania-supported copper catalysts (Cu/TiO_2) in the presence of CO_2 in the liquid phase resulted in the formation of methanol.[4, 5] For 2 wt-% Cu/TiO_2, methanol yield reached 12.5 μmol/g-cat./h after 20 h irradiation, which was around 25 times higher than obtained for TiO_2 (sol-gel method) and 3 times higher than Degussa P25 TiO_2 tested in the same system. Recently, Wu et al. also tested $Cu(I)/TiO_2$ materials in an optical-fiber reactor for gas phase photocatalytic CO_2 reduction. The maximum methanol yield for 1.2 wt% $Cu(I)/TiO_2$ was 0.46 μmol/g-catalyst/h under 365 nm UV irradiation.[6] Besides these studies on crystalline TiO_2 based catalysts, Ti-containing siliceous materials, such as TS-1, Ti-MCM-41, Ti-MCM-48[7-9], Ti-ZSM-5[10], Ti-zeolite Y[11-13] and Ti-SBA-15[14] were found to yield high methane production rates in gas phase photocatalytic CO_2 reduction. The production yield of highly dispersed titanium oxide catalysts (in μmol/g-Ti/h), was increased 10-300 times as compared to crystalline TiO_2. Pt was found to further enhance the performance of Ti-MCM-48, enhancing the CH_3OH over CH_4 selectivity 8 times. Despite these numerous studies on photoreduction of CO_2 over TiO_2 based catalysts, relatively little is known about the surface chemistry and the mechanism of the reaction. Anpo et al. proposed a mechanism for isolated excited $(Ti^{+III}\text{-}O^{-I})^*$ sites, based on EPR data[15], over which simultaneous reduction of CO_2 and decomposition of H_2O is proposed to lead to CO and C radicals, and H and OH radicals, respectively. Subsequently, these photoinduced C, H, and OH radicals recombine to final products, such as CH_4 and CH_3OH.

IR studies focused on photoinduced CO_2 activation are rare. Rasko et al.[16, 17] observed bent CO_2^- species on pre-reduced TiO_2 upon illumination at -83°C. CO was detected only on a pre-reduced Rh/TiO_2 catalyst. The most comprehensive IR study to date also focused on a Ti

silicalite molecular sieve (TS-1).[18] CO was observed as the initial redox product of gaseous CO_2 photoreduction. Through labeled CO_2 and CH_3OH experiments, the origin of CO was proposed to be the secondary photolysis of HCO_2H, which was the 2-electron reduction product of CO_2 over photo-excited Ti centers generated by a LMCT transition (Ti^{+IV}-O^{-II} $\rightarrow$ Ti^{+III}-O^{-I}).

In the present study the surface chemistry of crystalline Cu(I)/TiO_2 was further investigated employing a combination of DRIFT spectroscopy and isotopically labeled $^{13}CO_2$. The strong adsorption of CO on Cu(I) sites was used to identify the origin of this product, indicating that carbon residues are very important in determining the initial reactivity of photocatalysts active in CO_2 reduction. Moreover, a rich surface carbonate-chemistry was observed for Cu(I)/TiO_2, with an inter-conversion of CO_2 induced carbonate, formed in the dark, to CO induced carbonate formed upon illumination. The implications of this study for studies in the literature using photo-active materials synthesized with carbon containing precursors will be discussed.

Experimental Section

Material preparation. Cu(I)/TiO_2 was synthesized by a modified sol-gel method. The precursors titanium (IV) butoxide (TBOT, Ti-$(OC_4H_9)_4$) and copper nitrate ($Cu(NO_3)_2{\cdot}2.5H_2O$) were used as received. 17 mL TBOT, 0.15 g ($Cu(NO_3)_2{\cdot}2.5H_2O$), 2 g Polyethylene Glycol (PEG) and 102 mL 0.1 M nitric acid (HNO_3) were added to induce hydrolysis, and poly-condensation was achieved by thermal treatment at 80^{o}C for 28 h. The final sol was filtered, dried at 150^{o}C for 3 h, and then calcined at 500^{o}C for 5 h applying a heating rate of 1^{o}C/min. Based on elemental analysis, 1% (weight basis) copper was deposited. The as-synthesized Cu(I)/TiO_2 catalyst had a grass-green color. A reference Cu(I)/TiO_2 catalyst was prepared by the same procedure, in the absence of Polyethylene Glycol (PEG). Finally, TiO_2 was also prepared following the same procedure, only without adding copper nitrate.

In-situ Diffuse and Reflectance Infrared Fourier Transform spectroscopy. Photocatalytic CO_2 reduction experiments were carried out using a Nicolet Magna 860 spectrometer equipped with a Liquid N_2 cooled MCT detector, and a three window DRIFTS (Diffuse and Reflectance Infrared Fourier Transform Spectroscopy) cell. Two ZnSe windows allowed IR transmission, and a third (Quartz) window allowed the introduction of UV/Vis light into the

cell. Prior to the illumination experiments, 25 mg of the as-synthesized catalyst was heated up to 120°C in He (30 mL/min) for 0.5 h, in order to remove the majority of adsorbed water without changing the oxidation state of copper oxide. Before recording a background spectrum of the still grass-green catalyst, CO_2 (50 vol-% in He, 20 mL/min) was purged for 20 min. For experiments involving water vapor, CO_2 was bubbled through a saturator at room temperature (30°C), which added approximately 4 vol-% water vapor to the CO_2 feed. During illumination, reactants were held stationary in the cell at room temperature (30°C). In-situ IR signals were thus recorded every 10 min under UV/Vis light irradiation (100Watt Hg lamp, λ: 250 – 600 nm).

CO_2 (Linde Gas, 99.995%), $^{13}CO_2$ (ISOTEC, 99.9%^{13}C), CO (Linde Gas, 5% in He) and ^{13}CO (ISOTEC, 99%^{13}C) were used as received. CO (or ^{13}CO) adsorption experiments were performed by introducing CO (2500 ppm in He, 20 mL/min) over Cu(I)/TiO_2 for 20 min. To estimate the CO adsorption capacity, He (30 mL/min) was used to flush the catalyst and remove weakly adsorbed CO molecules. To further illustrate the role of carbonates in photocatalytic conversion of CO_2, an illumination experiment was conducted in the absence of CO_2, after pre-exposure of the surface of the catalyst to CO_2. Specifically a flush-dose cycle of exposure of the catalyst to $^{13}CO_2$ for 20 minutes, followed by flush in He, was repeated four times, to increase the surface concentration of ^{13}C-labeled carbonates.

Coking experiments. The catalyst under investigation was also pretreated to achieve different degrees of coking. Coked catalysts were prepared by introducing a batch of fresh Cu(I)/TiO_2 catalyst (70 mg) into an isobutane flow at 600°C (30 mL/min consisting of 1 % C_4H_{10} and 50 % CO_2). By varying the exposure time, variable amounts of coke were successfully deposited on Cu(I)/TiO_2.

Results

Illumination of Cu(I)/TiO_2 in different conditions. Figure 1 shows DRIFT spectra of the Cu(I)/TiO_2 catalyst after 80 min of illumination in different atmospheres, against background spectra of the catalyst obtained after respectively flushing with the different gas compositions for 20 min. The spectra are dominated by an absorption band at 2115 cm^{-1}, which can be assigned to the asymmetric υ_s mode of CO-Cu(I), consistent with literature.[19-21]

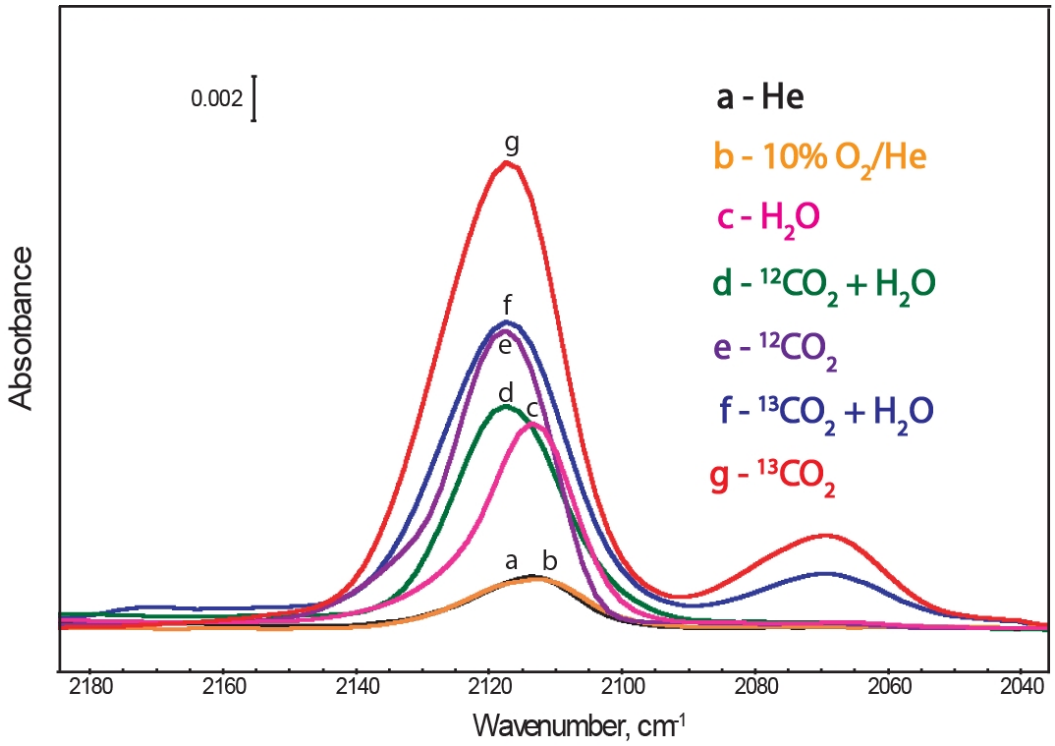

Figure 1. FT-IR spectra of Cu(I)/TiO_2 obtained after 80-min of irradiation in the presence of (a) He (b) 10 % O_2/He (c) water vapor (d) $^{12}CO_2$ and water vapor (e) $^{12}CO_2$ (f) $^{13}CO_2$ and water vapor, and (g) $^{13}CO_2$.

In inert (He) and oxidizing atmosphere (10% O_2/He), a small quantity of CO evolved after 80 min illumination. In the case of water vapor (spectrum 1c), a significantly higher intensity of the CO band at 2115 cm^{-1} can be observed. By introducing CO_2 and water vapor (1d), the CO band broadens and blue-shifts to 2117 cm^{-1}. The broadening of the CO band suggests that CO_2 co-adsorption slightly alters the nature of the Cu(I) site. Without H_2O co-feed (spectrum 1e), CO_2 leads to a CO band of even higher intensity, which might imply that in the presence of water subsequent hydrogenation of adsorbed CO takes place. $^{13}CO_2$ was used to identify the origin of the CO product. Spectrum 1f shows two CO bands, at 2069 and 2117 cm^{-1}. The former one is assigned to adsorbed ^{13}CO, in agreement with a calculation based on the harmonic equation[22] and spectra after dosing ^{13}CO over Cu(I)/TiO_2, which will be described later. Unexpectedly, there is still a majority of ^{12}CO formed during illumination, despite the absence of $^{12}CO_2$, demonstrating that carbon residues on the catalyst surface are involved in the reaction. Thermal Gravimetric Analysis (TGA) was performed for the as-synthesized

catalyst, which showed no distinguishable weight loss, indicating that these residues are present in small quantities and cannot be easily removed by calcination.

In the absence of water vapor, the intensity of the band of adsorbed CO was enhanced (compare spectra 1f and 1g), in agreement with the experiment conducted with $^{12}CO_2$. As expected, in reference experiments over pure TiO_2, CO absorption bands in the 2115 cm^{-1} region were absent, indicating that Cu(I)-sites serve as a probe to visualize CO formation in IR spectroscopy.

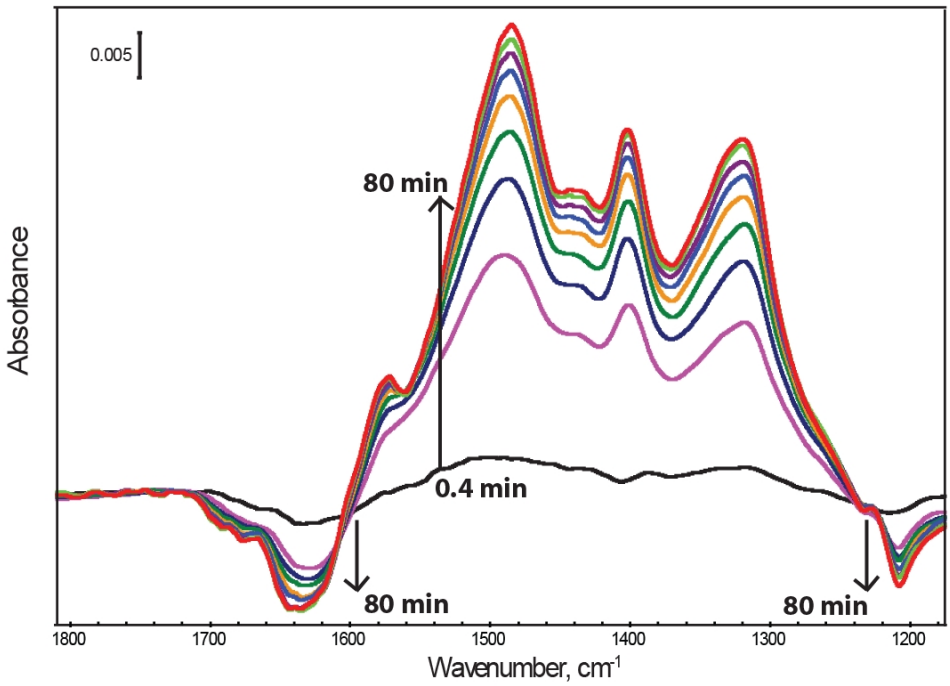

Figure 2. Trend in carbonate formation over Cu(I)/TiO_2 in the presence of $^{13}CO_2$ during 80 min of illumination. Time-profiled DRIFT spectra between 0.4 and 80 min. of illumination.

Figure 2 shows the spectral development in the region of carbonate absorptions (1200-1800 cm^{-1}) during an experiment where Cu(I)/TiO_2 is illuminated in an atmosphere of $^{13}CO_2$ (compare Figure 1g). In the presence of $^{13}CO_2$, irradiation enhances carbonate intensities. There are also decreasing bands observable (around 1650 cm^{-1}, and 1210 cm^{-1}), indicating that specific surface species are involved in the formation of CO.

To further evaluate the dynamics in the intensities of the carbonate vibrations, pre-saturation of the TiO_2 surface by treatment with $^{13}CO_2$ was conducted. The ^{13}Carbonate containing surface was subsequently illuminated in an He atmosphere. The spectral changes

are displayed in Figure 3. Clearly ^{12}CO (2115 cm^{-1}) is formed upon illumination, together with a minor amount of ^{13}CO, in agreement with the data shown in Figure 1. Rather than positive carbonate features, as observed in the presence of gas phase $^{13}CO_2$, negative features are observed in the spectral region of 1800 to 1200 cm^{-1}, including these at 1650 cm^{-1}, and 1210 cm^{-1}, indicating that carbonates are decomposing upon illumination. This mainly produces gas phase $^{13}CO_2$, as is evident from IR absorption features at 2280 cm^{-1}. In addition, the complex spectral signature in the carbonate region contains positive contributions at ~1560, 1420, and ~1350 cm^{-1}, which can be assigned to the formation of carbonate species formed by (re)adsorption of CO, as will be discussed in the following paragraph. Finally Figure 3 shows significant depletion in the hydroxyl region (3000 to 4000 cm^{-1}), suggesting that hydroxyl-groups and surface adsorbed water are participating in the surface reactions.

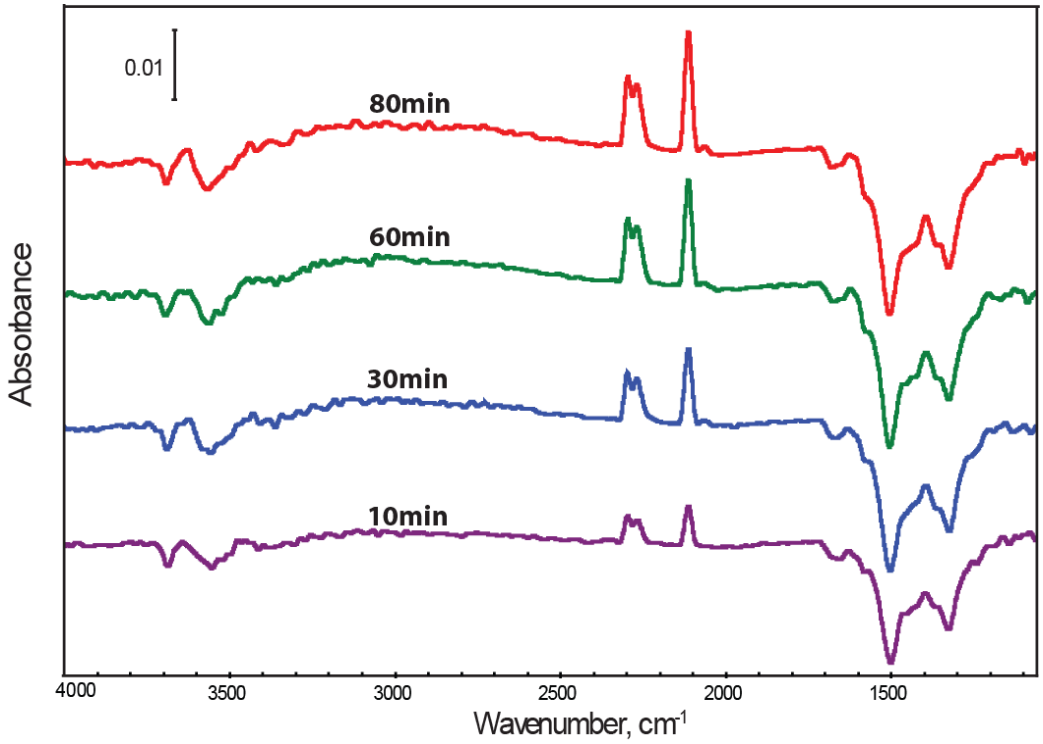

Figure 3. Time-profiled FT-IR spectra of Cu(I)/TiO_2, pre-loaded with $^{13}CO_2$, Spectra were recorded after illumination times of 10, 30, 60 and 80 min, respectively.

Reference spectra. To allow a better comprehension of the changes in the carbonate region (see Figure 2 and 3), Figure 4 shows the deconvolution of the region of the carbonate bands, formed by exposure of the Cu(I)/TiO_2 catalyst to CO_2 or $^{13}CO_2$, respectively. The corresponding band assignments are summarized in Table 1. In agreement with literature

data[23, 24], we assign the bands to bidentate carbonates (1363, 1554 cm^{-1} for CO_2 and 1319, 1508 cm^{-1} for $^{13}CO_2$), monodentate carbonates (1409 cm^{-1} for CO_2 and 1374 cm^{-1} for $^{13}CO_2$), bicarbonates (1481 cm^{-1} for CO_2 and 1461 cm^{-1} for $^{13}CO_2$) and carboxylates (1663 cm^{-1} for CO_2 and 1649 cm^{-1} for $^{13}CO_2$). In addition, bands at 1650 cm^{-1} and 1210 cm^{-1} have been assigned to a bent CO_2^- conformation, formed by CO_2 adsorption on Ti^{3+}-sites in the vicinity of Rh.[16, 17] Following this assignment, the 1650 cm^{-1} and 1210 cm^{-1} bands observed in the present study might be associated with CO_2 adsorption in the vicinity of the Cu(I)-centers. Among the surface species, bidentate carbonates dominate the spectra and are the thermally most stable species. It must be noted that the control experiments (CO_2 and $^{13}CO_2$) over pure TiO_2 synthesized by the same sol-gel method, showed similar surface species, which confirms that most carbonates, bicarbonates and carboxylates are adsorbed on titania, not on copper sites.

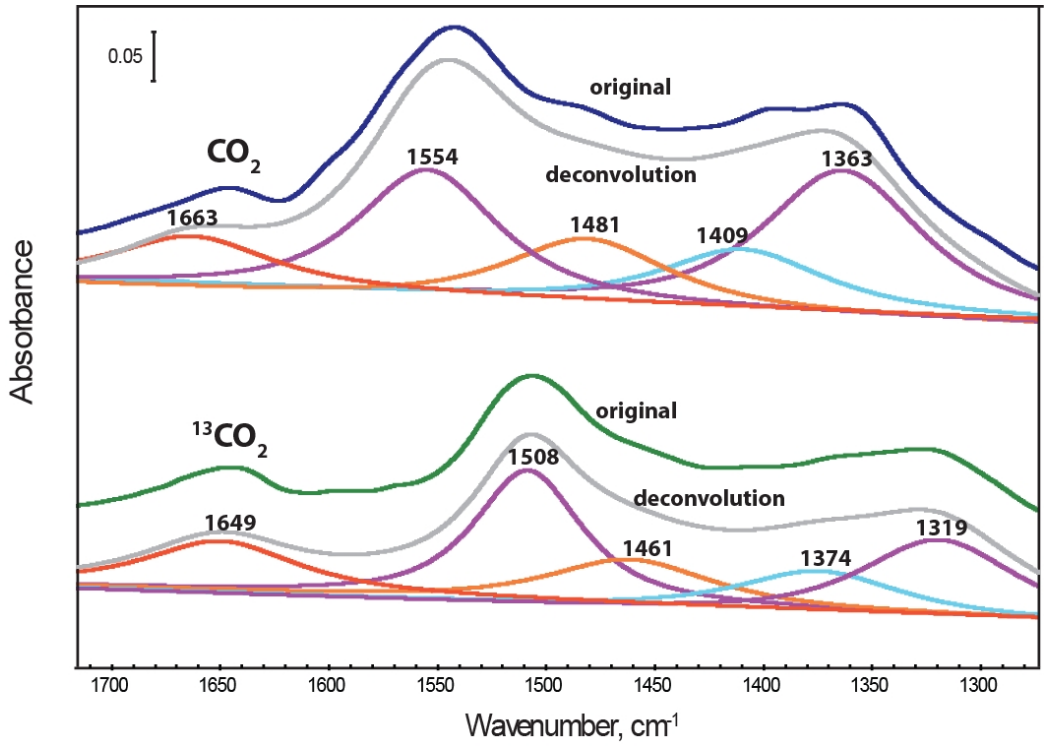

Figure 4. Deconvolution of IR spectra obtained by adsorption of CO_2 and $^{13}CO_2$ on the surface of Cu(I)/TiO_2.

Table 1. IR spectral assignment of surface species formation after inducing $^{12}CO_2$, $^{13}CO_2$, ^{12}CO, or ^{13}CO over Cu(I)/TiO_2.

adsorbed molecule	IR peak position (cm^{-1})	species	vibration mode
CO_2	1363	bidentate carbonate	. $\nu_{as}COO$
	1409	monodentate carbonate	. $\nu_{as}COO$
	1481	bicarbonate	. $\nu_{s}COO$
	1554	bidentate carbonate	. $\nu C=O$
	1663	bicarbonate / CO_2^- carboxylate	. $\nu_{s}COO$
$^{13}CO_2$	1319	bidentate carbonate	$\nu_{as}COO$
	1374	monodentate carbonate	. $\nu_{as}COO$
	1461	bicarbonate	. $\nu_{s}COO$
	1508	bidentate carbonate	. $\nu C=O$
	1649	bicarbonate / CO_2^- carboxylate	. $\nu_{s}COO$
CO	1349	bidentate carbonate	. $\nu_{as}COO$
	1419	monodentate carbonate	. $\nu_{as}COO$
	1492	bicarbonate	. $\nu_{s}COO$
	1569	bidentate carbonate	. $\nu C=O$
	1665	bicarbonate / CO_2^- carboxylate	. $\nu_{s}COO$
^{13}CO	1315	bidentate carbonate	. $\nu_{as}COO$
	1378	monodentate carbonate	. $\nu_{as}COO$
	1468	bicarbonate	. $\nu_{s}COO$
	1523	bidentate carbonate	. $\nu C=O$
	1645	bicarbonate / CO_2^- carboxylate	. $\nu_{s}COO$

Figure 5 contains reference spectra obtained by adsorption of CO and ^{13}CO on the catalyst surface, in the absence or presence of CO_2. Cu(I)/TiO_2 was first exposed to CO, followed by He flush. Strong adsorption of CO is observed, with a band composed of two contributions at 2107 and 2115 cm^{-1}. By introducing $^{13}CO_2$ the band at 2107 cm^{-1} rapidly disappears, and the band at 2115 cm^{-1} blue shifts to 2120 cm^{-1}, in agreement with observations reported in the literature. This blue shift was explained by a dynamic interaction between adsorbed CO and CO_2 molecules from the gas phase.[25, 26] After removing CO_2 by purging with He, the band of adsorbed CO gradually red shifts back to 2115 cm^{-1}. The stability of adsorbed CO under

illumination is shown in Figure 5b. Clearly desorption is stimulated by illumination, in view of the significant reduction in intensity of the band at 2070 cm^{-1}. A slight positive growth is observed at ~2115 cm^{-1}, again indicative of conversion of carbon residue by surface adsorbed water.

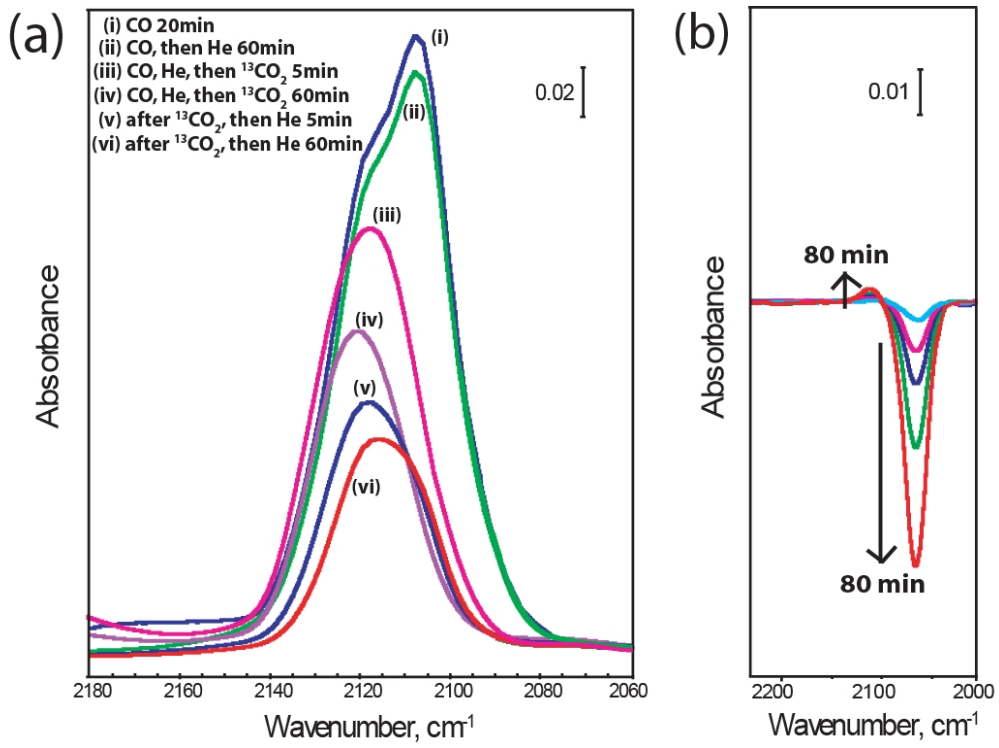

Figure 5. (a) $CO_{(ads)}$-$^{13}CO_{2(g)}$ interaction. FT-IR spectra of Cu(I)/TiO_2 after (i) 2500 ppm CO/He adsorption 20min (ii) flush with He 60min (iii) 2500ppm $^{13}CO_2$/He 5 min (iv) 2500ppm $^{13}CO_2$/He 60 min (v) flush again with He 5 min (vi) He 60min. (b) Time-profiled IR spectra of Cu(I)/TiO_2 pre-loaded with ^{13}CO during 80-min light irradiation.

Figure 6 shows the (deconvoluted) carbonate intensities formed upon exposure of the Cu(I)/TiO_2 catalyst to CO, and ^{13}CO, respectively. While the features are similar to those obtained by adsorption of CO_2 (compare Figure 4), intensity differences can be noted. In particular bands at 1569, 1419, and 1349 cm^{-1} are indicative for CO adsorbed on surface Ti(O)-sites as bidentate and monodentate carbonates, at 1492 cm^{-1} as bicarbonates and at 1665 cm^{-1} as carboxylates. A corresponding peak assignment can be made for ^{13}CO adsorbed on surface Ti(O)-sites at 1523, 1378, and 1315 cm^{-1} as bidentate and monodentate carbonates, at 1468 cm^{-1} as bicarbonates and at 1645 cm^{-1} as carboxylates.

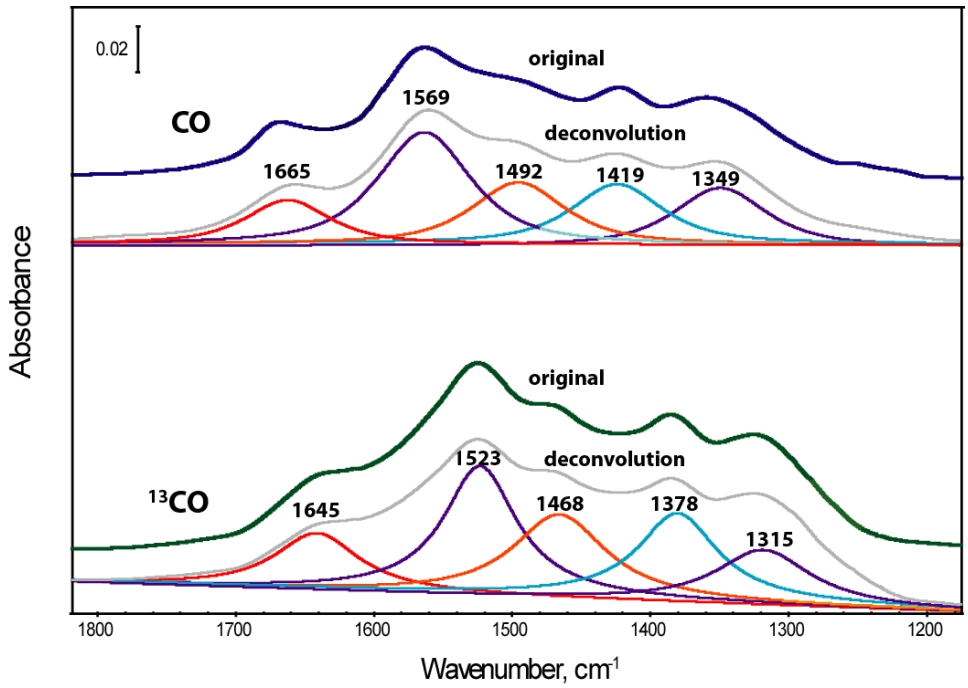

Figure 6. Deconvolution of IR spectra obtained by adsorption of CO and ^{13}CO on the surface of Cu(I)/TiO_2.

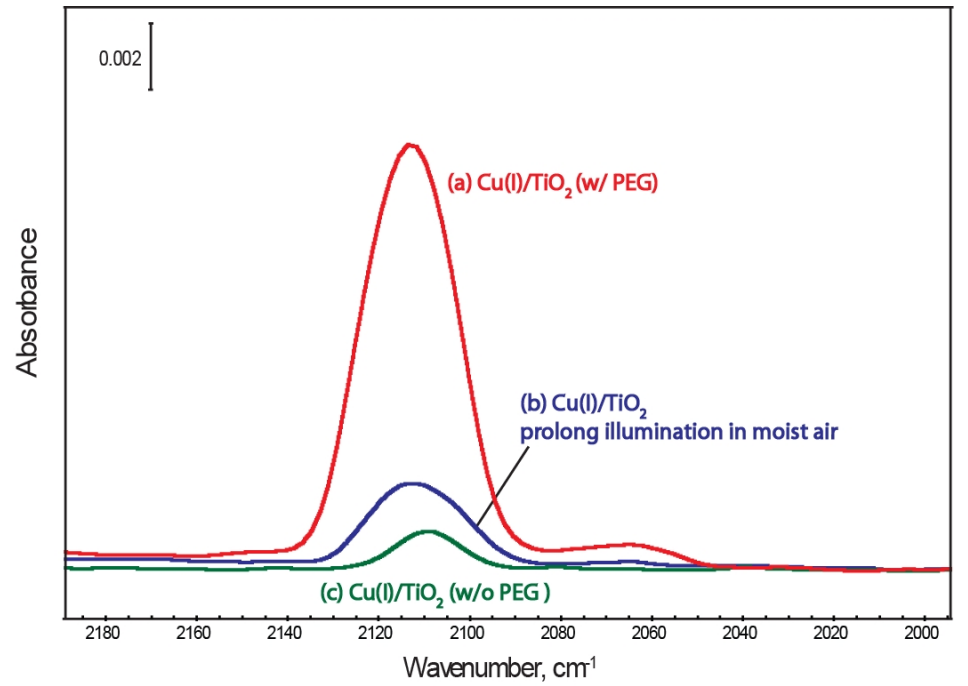

Figure 7. FT-IR spectra of Cu(I)/TiO_2 pre-loaded with $^{13}CO_2$ after 80 min-illumination. Comparison of (a) fresh Cu(I)/TiO_2 (synthesized with PEG), (b) Cu(I)/TiO_2 cleaned by illumination in humid air for 14h, and (c) reference Cu(I)/TiO_2 (synthesized without PEG).

Illumination of pretreated CuO/TiO_2. To eliminate the contribution of surface carbon species, the catalyst was pretreated for a prolonged period of time in moist air under UV illumination. The subsequent experiment with preloaded $^{13}CO_2$ is shown in Figure 7. As compared to the fresh catalyst, much less CO is produced upon illumination. Figure 7 also shows the amount of CO evolved for a catalyst that was prepared without PEG in the synthesis mixture. An even smaller CO formation rate is observed.

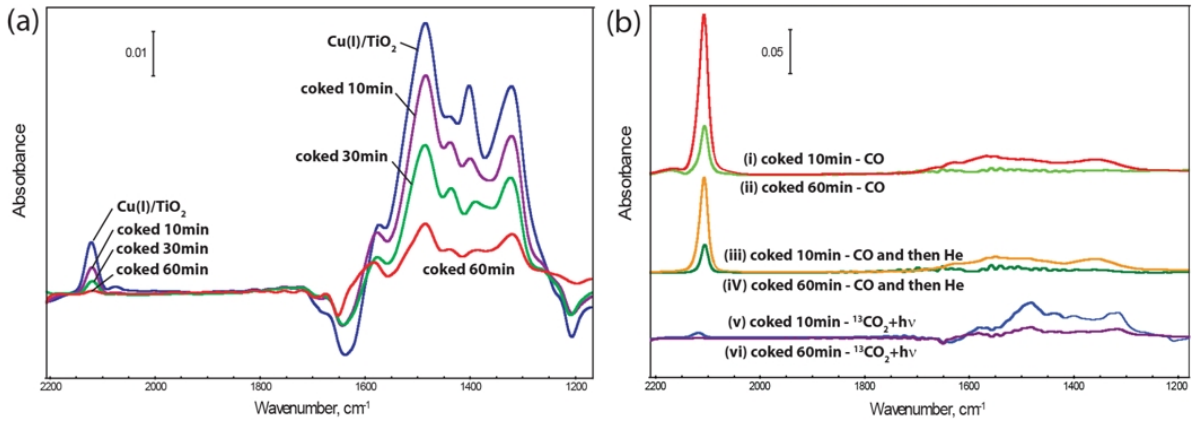

Figure 8. (a) FT-IR spectra after 80-min light irradiation in the presence of $^{13}CO_2$ for Cu(I)/TiO_2, the coked analogue for 10, 30, and 60 min; (b) CO adsorption capacity. Spectra of (i) coked 10 min catalyst in the presence of CO (ii) coked 60 min catalyst in the presence of CO (iii) coked 10 min catalyst loaded with CO and then flushed by He for 30 min (iv) coked 60 min catalyst loaded with CO and then flushed by He for 30 min (v) coked 10 min catalyst after 80-min light irradiation loaded with $^{13}CO_2$ (vi) coked 60 min catalyst after 80-min light irradiation loaded with $^{13}CO_2$.

To further evaluate the influence of carbon residues on CO_2 reduction rates over Cu(I)/TiO_2, coked catalysts were prepared with variable carbon content. By Thermal Gravimetric Analysis (TGA) it was determined that coke amounts of 0.009, 0.144 and 0.297 wt-% were obtained after reaction times in the applied iso-butene/CO_2 mixture of 10, 30, and 60 min., respectively. Figure 8(a) shows the DRIFT spectra of coked catalysts recorded after 80 min. illumination in the presence of $^{13}CO_2$. Only the ^{12}CO band at 2117 cm^{-1} was observed for all the coked catalysts. Furthermore, compared to as-synthesized Cu(I)/TiO_2, coked catalysts show a smaller CO production after 80 min. of illumination. The more coke is present on the surface of the Cu(I)/TiO_2 catalyst, the less CO is formed upon light irradiation.

In the spectral region of carbonates (1200-1600cm^{-1}), the same tendency is exhibited: less carbonates accumulate on the surface the higher the coke level of the applied catalyst.

To further characterize the coked Cu(I)/TiO_2 catalysts, DRIFT analyses of adsorbed CO were performed (Fig 8b), in the presence of gas phase CO (2500 ppm), and after subsequent He-flush. A significant amount of adsorbed CO can be observed in the presence of gas phase CO, which decreases as a function of increasing coke level. Furthermore, the stability of the adsorbed CO is smaller than observed for the as-synthesized Cu(I)/TiO_2 catalyst (see Figure 5), in view of the significant reduction in intensity after He-flush. It should be noted that the intensities of adsorbed CO are significantly higher than those obtained after 80 min illumination in the presence of CO_2, which demonstrates that there are still enough Cu(I) sites to allow CO adsorption. This shows that for coked catalysts the decreasing CO band (Fig 5a) is related to a smaller CO formation rate upon light irradiation. Finally, the intensity differences and changes in the carbonate region suggest that the Cu(I)/TiO_2 surface is indeed largely covered by coke, leading to lower intensities, and smaller stability of the CO induced carbonate species.

Discussion

Formation of CO by carbon assisted photocatalytic CO_2 reduction. The experimental data presented herein, demonstrate that CO is formed in significant quantities over Cu(I)/TiO_2 catalyst during illumination in the presence of CO_2, in particular if PEG is applied in the synthesis mixture. Using isotopically labeled $^{13}CO_2$, it is shown that carbon residues and surface adsorbed water significantly contribute to the formation of CO. The ratio of ^{12}CO over ^{13}CO is approximately 6. Two reactions can be proposed to explain the formation of ^{12}CO, i.e. the reverse Boudouard reaction, equation (1), and H_2O induced photocatalytic surface carbon gasification, equation (2):

$$^{13}CO_2 + \text{`}^{12}\mathbf{C}\text{'} \rightarrow {}^{13}CO + {}^{12}CO \qquad (1)$$

$$H_2O + \text{`}^{12}\mathbf{C}\text{'} \rightarrow {}^{12}CO + H_2 \qquad (2)$$

In view of the high ^{12}CO over ^{13}CO ratio, equation (2) must have a predominant contribution to the products formed. The source of H_2O is probably surface adsorbed water,

which is activated upon illumination. In addition it is well known that surface OH-groups are involved in oxidation reactions over TiO_2 surfaces, which might also contribute to CO formation.

As stated in the introduction, usually additional products are obtained upon illumination of a Cu(I)/TiO_2 catalyst in the presence of CO_2, including methanol or methane. In view of the small quantities produced, we have not observed any spectral features that can be related to these species. However, it is to be expected that by consecutive reaction with H_2, CO formed by equations (1) and (2) can be converted to e.g. CH_4.

Besides the isotopically labeled experiments, it was also demonstrated by prolonged exposure to UV-irradiation in the presence of water vapor, that equation (2) plays a major role in the formation of CO over Cu(I)/TiO_2. In a way it is surprising that adding additional coke did not lead to extensive formation of CO. Apparently the surface coverage achieved was that considerable, that the surface had become highly hydrophobic. This limits the reactive adsorption of CO_2, and more importantly significantly decreases the extent of surface hydration, as witnessed by the smaller intensity of the negative water bands in the 1620-1680 cm^{-1} region (Figure 8a). Clearly this is detrimental to the production of CO. Furthermore, the coke layer might simply prevent efficient light activation of the catalyst by absorption of light by the carbon layer, as was observed e.g. by Xia et al.[27] The surface chemistry of Cu(I)/TiO_2 in the photocatalytic CO_2 reduction is discussed in more detail in the following.

Surface carbonate chemistry. The Cu(I)/TiO_2 catalyst is very reactive towards CO_2 and CO at room temperature, leading to various carboxylate, bicarbonate and carbonate species. Generally IR intensities are higher upon exposure to CO_2. When CO_2 approaches Cu(I)/TiO_2, carbonate species likely form on titania sites which are not fully coordinated, i.e. in the vicinity of the Cu(I)-centers. This is in agreement with a study of Rasko et al., who investigated CO_2 adsorption and photocatalytic decomposition over pre-reduced Rh/TiO_2.[16, 17] It was demonstrated in their study that on pre-reduced Rh/TiO_2, oxygen vacancies in the vicinity of Rh offered sites for carboxylate formation, specifically with a C atom of CO_2 linked to Rh and one O atom of CO_2 bonded to the oxygen vacancy of titania. It is generally accepted that by illumination with light of high enough energy, electron-hole pairs are generated in titania. Rasko et al propose that electrons are transferred to CO_2, yielding CO, while holes are involved in neutralizing the Ti^{3+} sites to Ti^{4+}. It is thus proposed by Rasko et al that bent adsorbed CO_2 species are the precursor of CO, with the oxygen atom being

incorporated in the TiO_2, changing the oxidation state from Ti^{3+} to Ti^{4+}. Also in our study we observe a depletion of the 1650 and 1220 cm^{-1} bands upon illumination, suggesting that these might be involved in the formation of CO by CO_2 dissociation. However, rather than being incorporated in the Cu(I)/TiO_2 lattice, we believe the remaining oxygen is predominantly transferred to residual carbon, yielding an additional CO molecule, according to equation (1).

The experiment conducted on a $^{13}CO_2$ pretreated catalyst (Figure 3), demonstrates that besides carboxylates, CO_2 induced surface carbonates are also instable upon illumination, yielding $^{13}CO_2$. As previously discussed, the large selectivity for ^{12}CO in the experiment is related to water induced reactions of carbon residues, according to Equation (2). This is followed by ^{12}CO adsorption on Cu(I) sites (2115 cm^{-1}), and surface TiO_2 sites, yielding ^{12}CO induced carbonates, explaining the growth of the demonstrated features (at 1560, 1420, and 1350 cm^{-1}) in Figure 3.

It should be noted that the carbonate and carboxylate species formed are most likely a strong function of the extent of surface hydration of the applied TiO_2 catalysts. Morterra[28] has evaluated the interaction of CO with TiO_2 surfaces. He demonstrated that removal of water molecules and decomposition of surface hydroxyl groups (OH) leads to the formation of surface Lewis-acid sites, that reversibly chemisorb CO at ambient temperature. While Morterra removed water and hydroxyl groups by evacuation in a vacuum IR cell, it is obvious (Figure 3) that the degree of hydration is also largely affected by the illumination procedure.

Artificial photosynthesis, fact or fiction? Many (recent) studies discuss the performance of modified TiO_2 catalysts in the photocatalytic reduction of CO_2.[29] Generally methane and/or methanol are the products reported to be formed. In view of our study, the data reported in various of these studies should be interpreted with caution. Frei and coworkers already observed for mesoporous materials that carbon residues can be involved in the production of primary products in the photocatalytic reduction of CO_2.[30-32] In view of our data, also for crystalline TiO_2 materials, water induced gasification of these carbon residues might be affecting the product quantities and distribution (reaction (2)). This is particularly true if alkoxides (propoxide, butoxide) were used as the precursor[33], or if carbon supported TiO_2 was used.[27] Also in the synthesis procedure of N-doped TiO_2, organic solvents were used, the residue of which might have contributed to the observed activity.[34] Clearly, contribution of these reactions leads to an over-estimation of the rate of the real artificial photosynthesis reactions, such as $CO_2 + H_2O \rightarrow CH_3OH + O_2$. It is highly recommended to add to future

studies on photocatalytic CO_2 reactions a test of activity in the absence of CO_2, but in the presence of H_2O, to exclude the participation of catalyst associated carbon residues in the formation of products.

While there is no doubt that carbon residues contribute to catalytic performance, based on our study we can not entirely exclude artificial photosynthesis. ^{13}CO was formed in various experiments, and it is necessary to isolate the reversed Boudouard reaction from true artificial photosynthesis. This would require careful evaluation of the production of O_2. To close the oxygen balance is however extremely difficult, and usually irreproducible data are obtained due to fluctuations in background oxygen pressures. The most conclusive evidence that CO is formed in the absence of carbon residues is again provided by Frei and coworkers[18] in a high vacuum IR cell, in the case of isolated Ti-sites in mesoporous materials. Mechanistic studies on highly pure crystalline metal oxide systems are needed to definitively proof that artificial photosynthesis over these materials is fact, as well as to further reveal the chemical pathway of CO_2 reduction, including the complexity in the dynamics of surface carbonates.

Conclusions

Carbon residues are largely participating in the formation of CO over Cu-promoted crystalline TiO_2 catalysts, as demonstrated by the combined use of DRIFT spectroscopy and ^{13}C labeled CO_2. These residues are formed during the catalyst synthesis procedures, often involving the use of Ti-alkoxides and organic solvents, such as Poly-Ethylene-Glycol (PEG). Removal of these residues by thermal activation in air is incomplete, while prolonged exposure to water vapor and UV-irradiation is more efficient. Coking of $Cu(I)/TiO_2$ showed that extensive carbon coverage of $Cu(I)/TiO_2$ diminishes CO formation during illumination in the presence of CO_2. H_2O induced photocatalytic carbon gasification should be carefully considered for the evaluation of CO_2 photoreduction.

Acknowledgements

This work was supported by ACTS (NWO, The Netherlands), in the framework of an NSC-NWO project (Project Number NSC-97-2911-I-002-002). Dorette Spaans and Nienke Firet at Delft University of Technology are gratefully acknowledged of their experimental contribution to these investigations.

References

1. **T. Inoue, A. Fujishima, S. Konishi and K. Honda, *Nature*, 1979, 277, 637-638.**
2. **K. Hirano, K. Inoue and T. Yatsu, *J. Photochem. Photobiol,. A*, 1992, 64, 255-258.**
3. **K. Adachi, K. Ohta and T. Mizuno, *Sol. Energy*, 1994, 53, 187-190.**
4. **I. H. Tseng, W. C. Chang and J. C. S. Wu, *Appl. Catal., B*, 2002, 37, 37-48.**
5. **I. H. Tseng, J. C. S. Wu and H. Y. Chou, *J. Catal.*, 2004, 221, 432-440.**
6. **J. C. S. Wu, H. M. Lin and C. L. Lai, *Appl. Catal., A*, 2005, 296, 194-200.**
7. **S. G. Zhang, Y. Fujii, K. Yamashita, K. Koyano, T. Tatsumi and M. Anpo, *Chem. Lett.*, 1997, 659-660.**
8. **M. Anpo, H. Yamashita, K. Ikeue, Y. Fujii, S. G. Zhang, Y. Ichihashi, D. R. Park, Y. Suzuki, K. Koyano and T. Tatsumi, *Catal. Today*, 1998, 44, 327-332.**
9. **K. Ikeue, H. Yamashita, M. Anpo and T. Takewaki, *J. Phys. Chem. B*, 2001, 105, 8350-8355.**
10. **H. Yamashita, A. Shiga, S. Kawasaki, Y. Ichihashi, S. Ehara and M. Anpo, *Energy Convers. Manage.*, 1995, 36, 617-620.**
11. **M. Anpo, H. Yamashita, Y. Ichihashi, Y. Fujii and M. Honda, *J. Phys. Chem. B*, 1997, 101, 2632-2636.**
12. **H. Yamashita, Y. Fujii, Y. Ichihashi, S. G. Zhang, K. Ikeue, D. R. Park, K. Koyano, T. Tatsumi and M. Anpo, *Catal. Today*, 1998, 45, 221-227.**
13. **I. Keita, S. Nozaki, M. Ogawa and M. Anpo, *Catal. Today*, 2002, 74, 241-248.**
14. **J. S. Hwang, J. S. Chang, S. E. Park, K. Ikeue and M. Anpo, *Top. Catal.*, 2005, 35, 311-319.**
15. **M. Anpo, H. Yamashita, Y. Ichihashi and S. Ehara, *J. Electroanal. Chem.*, 1995, 396, 21-26.**
16. **J. Rasko and F. Solymosi, *J. Phys. Chem.*, 1994, 98, 7147-7152.**
17. **J. Rasko, *Catal. Lett.*, 1998, 56, 11-15.**
18. **N. Ulagappan and H. Frei, *J. Phys. Chem. A*, 2000, 104, 7834-7839.**
19. **K. Hadjiivanov, D. Klissurski, M. Kantcheva and A. Davydov, *J. Chem. Soc., Faraday Trans.*, 1991, 87, 907-911.**
20. **F. Coloma, F. Marquez, C. H. Rochester and J. A. Anderson, *Phys. Chem. Chem. Phys.*, 2000, 2, 5320-5327.**
21. **T. Venkov and K. Hadjiivanov, *Catal. Commun.*, 2003, 4, 209-213.**

22. Harmonic equation was useful for calculating the theoretical peak shift for isotopic molecules. The vibration frequency is inverse-proportional to the square root of reduced mass.

$$\nu = \frac{1}{2\pi}\sqrt{\frac{\kappa}{\mu}}, \mu = \frac{m_1 \times m_2}{m_1 + m_2}, \nu \propto \sqrt{\frac{1}{\mu}} \qquad \nu_{^{13}CO} = 2117 \times \sqrt{\frac{(12\times16)/(12+16)}{(13\times16)/(13+16)}} = 2069 cm^{-1}$$

23. A. A. Davydov, *Infrared spectroscopy of adsorbed species on the surface of transition metal oxides*, John Wiley & Sons, Chichester, 1990.

24. W. G. Su, J. Zhang, Z. C. Feng, T. Chen, P. L. Ying and C. Li, *J. Phys. Chem. C*, 2008, 112, 7710-7716.

25. A. A. Tsyganenko, L. A. Denisenko, S. M. Zverev and V. N. Filimonov, *J. Catal.*, 1985, 94, 10-15.

26. K. Hadjiivanov, B. M. Reddy and H. Knozinger, *Appl. Catal., A*, 1999, 188, 355-360.

27. X. H. Xia, Z. H. Jia, Y. Yu, Y. Liang, Z. Wang and L. L. Ma, *Carbon*, 2007, 45, 717-721.

28. C. Morterra, *J. Chem. Soc., Faraday Trans. I*, 1988, 84, 1617-1637.

29. K. Koci, L. Obalova and Z. Lacny, *Chem. Pap.*, 2008, 62, 1-9.

30. W. Y. Lin and H. Frei, *J. Am. Chem. Soc.*, 2005, 127, 1610-1611.

31. W. Y. Lin and H. Frei, *J. Phys. Chem. B*, 2005, 109, 4929-4935.

32. W. Y. Lin and H. Frei, *C. R. Chim.*, 2006, 9, 207-213.

33. K. Koci, L. Obalova, L. Matejova, D. Placha, Z. Lacny, J. Jirkovsky and O. Solcova, *Appl. Catal., B*, 2009, 89, 494-502.

34. O. K. Varghese, M. Paulose, T. J. LaTempa and C. A. Grimes, *Nano Lett.*, 2009, 9, 731-737.

Chapter 3

Effect of Carbonates on Promoting Photocatalytic CO_2 Reduction over Cu-TiO_2-based Catalyst

Abstract: To clarify the role of carbonates in photocatalytic CO_2 reduction over titania-based catalysts, CO_3^{2-}-impregnated Cu(I)/TiO_2 samples were evaluated in this reaction by applying the in-situ DRIFTS technique. Upon illumination, the depletion of various surface carbonate species introduced by impregnation, along with formation of CO, was demonstrated. Furthermore the added-on-carbonate samples were found to enhance adsorption of gaseous CO_2, mainly in the form of bicarbonate, thereby inducing higher CO formation rates during illumination in the presence of CO_2, as compared to untreated catalysts. Consecutive hydrogenation to e.g. surface adsorbed formaldehyde or methanol was not observed under the applied gas phase conditions. Various hypotheses for the photo-induced carbonate decomposition will be discussed.

Introduction

Photocatalytic CO_2 reduction is a promising route to reduce CO_2 emissions, and simultaneously generate useful hydrocarbons as renewable energy sources. The main difference from natural photosynthesis lies in conversion of CO_2 into small molecules and hydrocarbons, such as CO, CH_4 and CH_3OH, rather than big sugar molecules, such as glucose. To achieve energetically uphill reactions at room temperature requires catalysts with suitable physical and chemical properties to overcome the thermodynamic and kinetic barriers of CO_2-to-fuel conversion. Many researchers have focused on developing effective photocatalysts for CO_2 reduction. Titania-based catalysts have been found to be active materials.[1, 2] Anpo et al. demonstrated the photocatalytic activity for gas phase CO_2 reduction of isolated Ti-sites in various mesoporous oxide materials, yielding CH_4 and CH_3OH as major products.[3-5] Recently, Varghese et al. reported a high rate of photocatalytic conversion of CO_2 over nitrogen-doped titania nanotubes, with detectable increase in CH_4, alkane, and olefin concentrations, along with formation of CO and H_2.[6]

Semiconductors suspended in CO_2 saturated H_2O have also been tested for reduction of CO_2. The results demonstrate production of HCHO and CH_3OH during illumination.[7] In particular, Cu-promoted TiO_2 was found to be quite effective.[8-10] An optimum amount of copper of 2.0 wt-% was determined, corresponding to the highest dispersion of Cu on the TiO_2 surface. A preferred distribution of 25 mol-% of surface exposed Cu relative to that present in the bulk was found to yield the highest rates of $1000\mu mol_{products}/g_{catal}$. Experimental results indicated that the methanol yield was significantly increased by adding NaOH. Caustic solutions are preferred to dissolve CO_2. In addition, the OH^- in aqueous solution might also serve as a strong hole scavenger.

Dissolution of CO_2 in water initially results in formation of carbonates and bicarbonates, and the question arises if it is feasible to directly reduce these carbonates or bicarbonates upon illumination. Chandrasekaran et al. first demonstrated the photochemical reduction of carbonates into formaldehyde over TiO_2 powder.[11] The yield of formaldehyde was found independent of the concentration of $Na_2CO_{3(aq)}$ from 0.01 to 1 M. Raphael et al. reported activity of platinized titania suspended in a Na_2CO_3 solution under UV/visible light irradiation. Their results showed formation of CH_3OH, 'C', HCHO and $HCOO^-$ ions in the absence of CO_2, quantified by spectro-photometrical methods.[12]

While aqueous phase carbonate reduction has been reported, the role of surface adsorbed carbonates in gas phase conversion of CO_2 has been rarely addressed, and this is the topic of the present study. Recently we demonstrated the activity of a Cu(I)/TiO_2 catalyst in gas phase CO_2 activation by following the formation of adsorbed CO using DRIFT spectroscopy.[13] The presence of Cu(I) was demonstrated beneficial for photocatalytic performance previously, assigned to an electron trapping effect of the Cu(I) sites at the surface and improved light absorption properties.[14] Here we conclusively demonstrate effective decomposition of carbonates introduced on the surface of this catalyst by impregnation, yielding CO. Furthermore we disclose an enhancement as a result of carbonate impregnation in CO_2 reduction activity of Cu(I)/TiO_2 catalysts. We will discuss the data on the basis of available literature and a tentative proposal for the surface chemistry.

Experimental Section

Material preparation. Cu(I)/TiO_2 was synthesized by a modified sol-gel method as described elsewhere.[15] The precursors titanium (IV) butoxide (TBOT, Ti-$(OC_4H_9)_4$) and copper nitrate ($Cu(NO_3)_2{\cdot}2.5H_2O$) were used as received. 17 mL TBOT, 0.15 g ($Cu(NO_3)_2{\cdot}2.5H_2O$), 2 g Polyethylene Glycol (PEG) and 102 mL 0.1 M nitric acid (HNO_3) were added to induce hydrolysis, and poly-condensation was achieved by thermal treatment at 80^{o}C for 28 h. The final sol was filtered, dried at 423 K for 3 h, and then calcined at 500^{o}C for 5 h applying a heating rate of 1^{o}C/min. Based on elemental analysis, 1% (weight basis) copper was deposited. The as-synthesized Cu(I)/TiO_2 catalyst had a grass-green color. The characterization of the samples was reported elsewhere. XRD, XPS and XAS analysis reveal that the active Cu-state in inducing the photoreaction of CO_2 is highly dispersed Cu(I).[15]

Impregnation procedure. Sodium carbonate (Na_2CO_3) was used to modify Cu(I)/TiO_2 by impregnation. In particular, 2 g of Cu(I)/TiO_2 was added to 80 mL of a Na_2CO_3 solution of variable concentration ranging from 0.01 M to 0.1 M. It should be noted that the pH of the 0.01-0.1 M $Na_2CO_{3(aq)}$ solutions increases from 9 to about 11. After stirring for 1 or 2 hours at room temperature, respectively, the solid was filtered off and re-suspended in 100 mL of deionized water, treated for 10 minutes and again filtered. The filter cake was subsequently resuspended for a second time in 500 mL deionized water, and filtered to minimize the accumulation of sodium on the catalyst surface. The solid was finally dried at 120^{o}C

overnight in static air. According to elemental analysis by ICP, the residual sodium level was below the detection limit (ppb). We assume that the carbonate has replaced OH^- groups on the surface of the catalyst, to maintain a neutral charge balance upon exchange.

Attenuated Total Reflection Fourier Transform Infrared spectroscopy (ATR-FTIR). The ATR-FTIR device applied consists of a Harrick Horizon multiple internal reflections accessory, equipped with a flow cell containing a ZnSe crystal (45^o internal reflection). Spectra were recorded using a Nicolet 8700 FTIR spectrometer equipped with a DTGS detector. IR spectra were recorded for Cu(I)/TiO_2 coated on a ZnSe crystal in the presence of either a 0.5 M Na_2CO_3 or $NaHCO_3$ solution, respectively.

In-situ Diffuse Reflectance Infrared Fourier Transform spectroscopy (DRIFTS). Photocatalytic CO_2 reduction experiments were carried out using a Nicolet Magna 860 spectrometer equipped with a Liquid N_2 cooled MCT detector, and a three window DRIFTS (Diffuse and Reflectance Infrared Fourier Transform Spectroscopy) cell. Two ZnSe windows allowed IR transmission, and a third (Quartz) window allowed the introduction of UV/Vis light into the cell. CO_2 (Linde Gas, 99.995%), and $^{13}CO_2$ (ISOTEC, 99.9% $^{13}CO_2$ were used as received. The Cu(I)/TiO_2 catalysts, with or without pretreatment by carbonate impregnation, were firstly heated up to 120^oC in the cell, and cooled down to 303K in a dry He stream of 30 mL/min in order to remove surface adsorbed water.

Characterization of samples. Spectra of the CO_3-impregnated samples were recorded (against a background of pure Cu(I)/TiO_2), and subsequently various experiments were performed. In particular, the adsorption of CO_2 on the carbonate pretreated surfaces was evaluated. To this end, the pretreated samples were exposed to a CO_2 stream (50 vol % in He, 20 mL/min) for 20 minutes, followed by changing the feed to pure He for 5 minutes. Repeating this procedure four times was found to maximize the concentration of surface adsorbed species. Spectra of these CO_2 pretreated catalysts were recorded against a background of the native CO_3-impregnated samples.

Illumination. During illumination the cell was kept at room temperature (30^oC). In-situ IR spectra were recorded every 10 min under UV/Vis light irradiation (100 W Hg lamp, λ: 250 – 600 nm), in the presence of a Helium atmosphere, against a background of the catalyst 'as is'.

For comparison, other experiments were performed in the presence of $^{13}CO_2$, recorded against background spectra of the corresponding samples after saturation of the surface by exposure for 20 minutes to $^{13}CO_2$. For comparison, time-profiled DRIFT spectra of Cu(I)/TiO_2 during 80 min of illumination in the presence of ^{12}CO and ^{13}CO, respectively, were recorded after saturation of the surface by exposure (equilibration) for 20 minutes to ^{12}CO or ^{13}CO (2500 ppm in He, 20 mL/min), respectively.

Results

Characterization of Na_2CO_3-impregnated samples. Figure 1 (a) shows the DRIFT spectra of Cu(I)/TiO_2 impregnated with different concentrations of a Na_2CO_3 solution (0.01, 0.05 and 0.1M), and additionally two impregnation times (1 or 2h) for the applied 0.1 M concentration. The DRIFT spectra demonstrate carbonate and bicarbonate deposition was successfully achieved. In between 1200 and 1800 cm^{-1}, bands are observed at 1598, 1553, 1543, 1434, 1388, and 1360 cm^{-1} for the 0.01M and 0.05M Na_2CO_3-impregnated samples. When the concentration of sodium carbonate is further increased to 0.1 M, the intensity of the bands appearing at 1506, 1330, 1282, and 1250 cm^{-1} increases. By extending the impregnation time from 1 h to 2 h for the 0.1 M Na_2CO_3 solution, bands at 1516 and 1287 cm^{-1} appear. The two dominant bands at 1543 and 1360 cm^{-1} are assigned to bidentate carbonates.[13] This clearly shows that deposition predominantly in the form of bidentate carbonates is achieved by exposing TiO_2 to carbonate solutions. This is confirmed by the ATR spectra shown in Figure 1 (b). Except for the massive water band around 1650 cm^{-1}, a broad absorption band at 1388 cm^{-1} can be assigned to the C=O stretching mode of carbonates. This stretching mode shifts from 1388 to 1360 cm^{-1} when the saturated solution is replaced by 0.1M $NaHCO_{3(aq)}$. An additional band at 1300 cm^{-1} appears in the presence of $NaHCO_{3(aq)}$. This band is corresponding to the bending mode of C-OH.[16, 17]

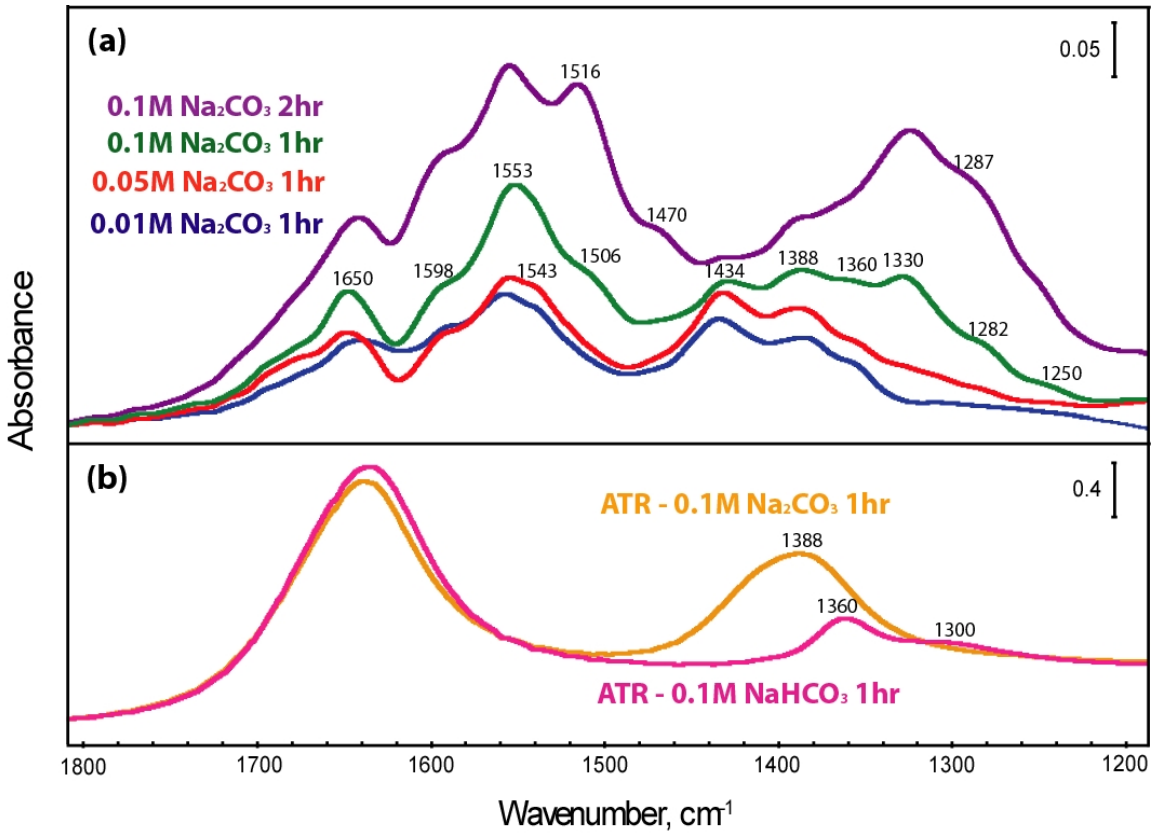

Figure 1. (a) DRIFT spectra of Na_2CO_3-impregnated samples prepared at different concentrations, recorded in He. The spectrum of the Cu(I)/TiO_2catalyst without carbonate impregnation was used as background; (b) ATR spectra of Cu(I)/TiO_2 in the presence of Na_2CO_3 or $NaHCO_3$ solution. The spectrum of the catalyst coated on the crystal and exposed to ambient air was used as background.

To illustrate the capacity for CO_2 chemisorption of the impregnated samples, Figure 2 shows the DRIFT spectra of a 0.1M Na_2CO_3-impregnated sample saturated with CO_2 (or $^{13}CO_2$) for 20 minutes, in comparison to the sample without carbonate impregnation. By introducing the samples to a CO_2 stream for 20 min, appreciable spectral enhancement is observed at 1675, 1650, 1598, 1565, 1427, 1353, and 1290 cm^{-1} for CO_2; 1640, 1570, 1530, 1385, 1320, and 1250 cm^{-1} for $^{13}CO_2$. The spectral increase is more dominant for the impregnated sample, suggesting a stronger affinity for CO_2 adsorption.

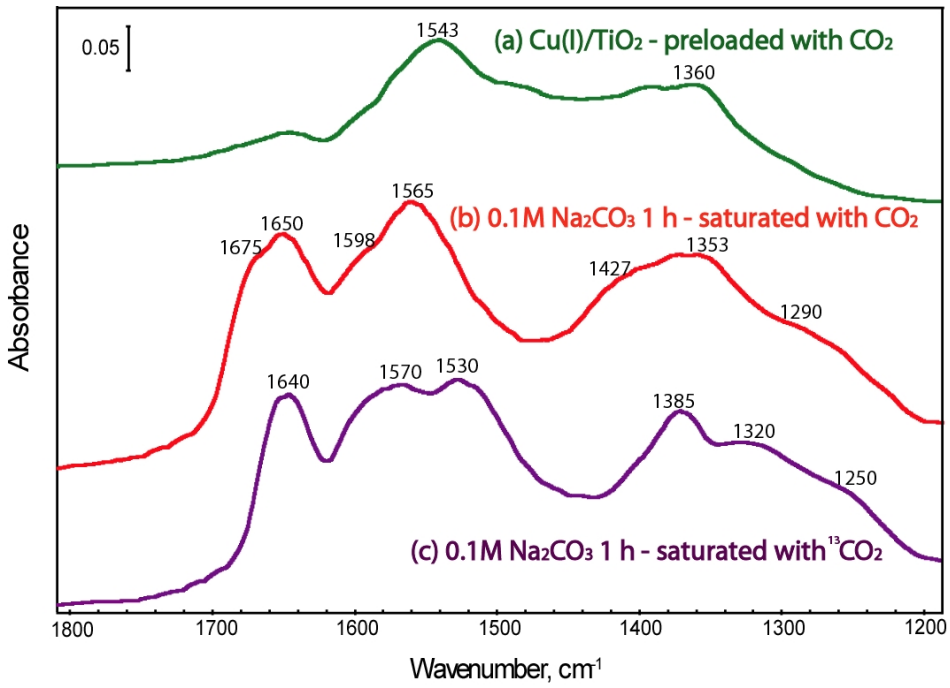

Figure 2. DRIFT spectra of (a) Cu(I)/TiO_2 preloaded with CO_2; (b) Cu(I)/TiO_2 impregnated with 0.1M Na_2CO_3 for 1 h saturated with CO_2 and (c) Cu(I)/TiO_2 impregnated with 0.1M Na_2CO_3 for 1 h saturated with $^{13}CO_2$. The spectra of the respective catalysts recorded in He without exposure to CO_2, were used as background.

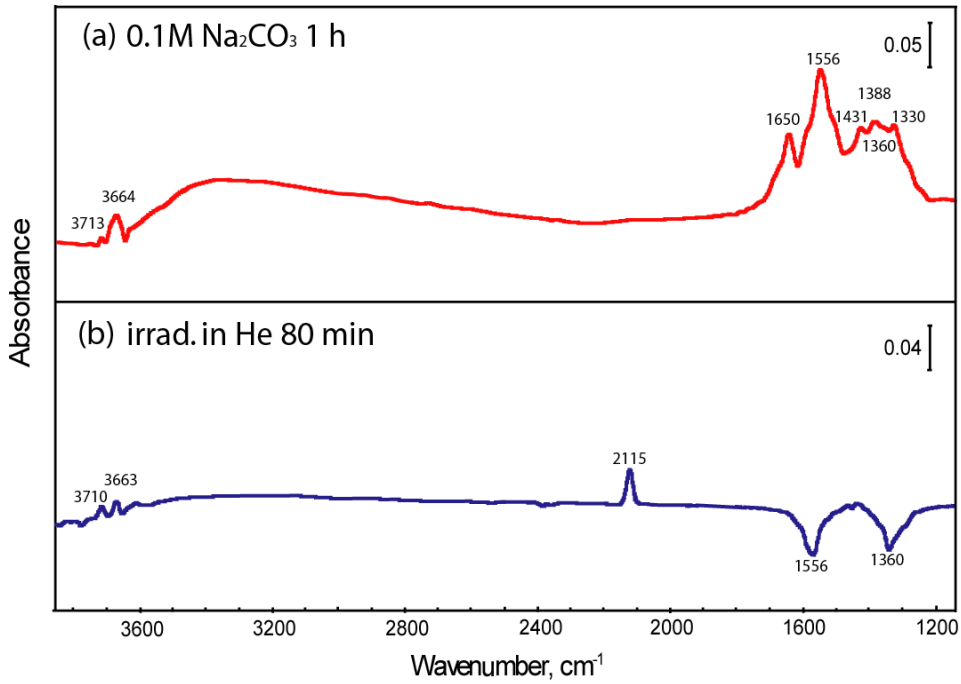

Figure 3. DRIFT spectra of (a) 0.1M Na_2CO_3-impregnated Cu(I)/TiO_2; (b) the corresponding spectra after 80 min of illumination in He. For the spectrum displayed in (b), spectrum (a) was used as background.

Illumination of Na_2CO_3-impregnated samples. Figure 3 (a) shows the spectrum of the sample impregnated with 0.1 M Na_2CO_3 over the entire spectral range (compare Figure 1 (a)). Besides the bands previously assigned to carbonates, additional bands can be observed at 3713 and 3664 cm^{-1}. These bands are assigned to OH vibrations of TiO_2. Figure 3 (b) demonstrates that CO formation is induced upon illumination of the catalyst in the absence of CO_2, in agreement with the depletion of specific carbonate bands at 1556 and 1360 $cm^{-1.}$ It should be noted that the intensity of the 2117 cm^{-1} band of Cu(I)-CO is approximately a factor of 15 higher than observed in the case of the untreated catalyst.[13]

Figure 4 (a) shows the DRIFT spectra of Cu(I)/TiO_2 and Na_2CO_3-impregnated Cu(I)/TiO_2 at variable conditions, after 80 min of illumination in the presence of $^{13}CO_2$, recorded against the background of the respective samples saturated with $^{13}CO_2$ for 20 minutes. For untreated Cu(I)/TiO_2, the spectra shows absorption bands increasing at 2117, 1484, 1400, and 1315 cm^{-1}, and depleting at 1640 and 1210 cm^{-1}. The slight blue-shift from 2115 to 2117 cm^{-1} for the Cu(I)-CO band is due to the dynamic interaction between adsorbed CO and CO_2 molecules from the gas phase.[18] Except for CO production as evident from the 2117 cm^{-1} band, growth at 1484, 1400, and 1315 cm^{-1} is due to formation of novel carbonates. The band intensity decrease at 1640 and 1210 cm^{-1} represents unstable surface carboxylate and bicarbonate species, converting due to light illumination.[13] The band at 2117 cm^{-1} shows higher intensity as a function of increasing concentration of the applied Na_2CO_3-solution in the preparation of the impregnated samples. The trend is shown in Figure 4 (b), showing non-linear behavior, suggesting that at some point an enhancement of the surface carbonate concentration no longer leads to enhanced CO formation rates. This might be related to a depleting surface OH-concentration upon carbonate impregnation. Also a slight increase of a band positioned at 2069 cm^{-1} is apparent, assigned to Cu(I)-^{13}CO, with much smaller extent of increase as function of increasing carbonate concentration (Figure 4 (b)). The spectral development of the samples in between 1200 and 1800 cm^{-1}, as well as the negative bands at 1640 and 1210 cm^{-1}, are also evident for the carbonate impregnated samples in Figure 4 (a).

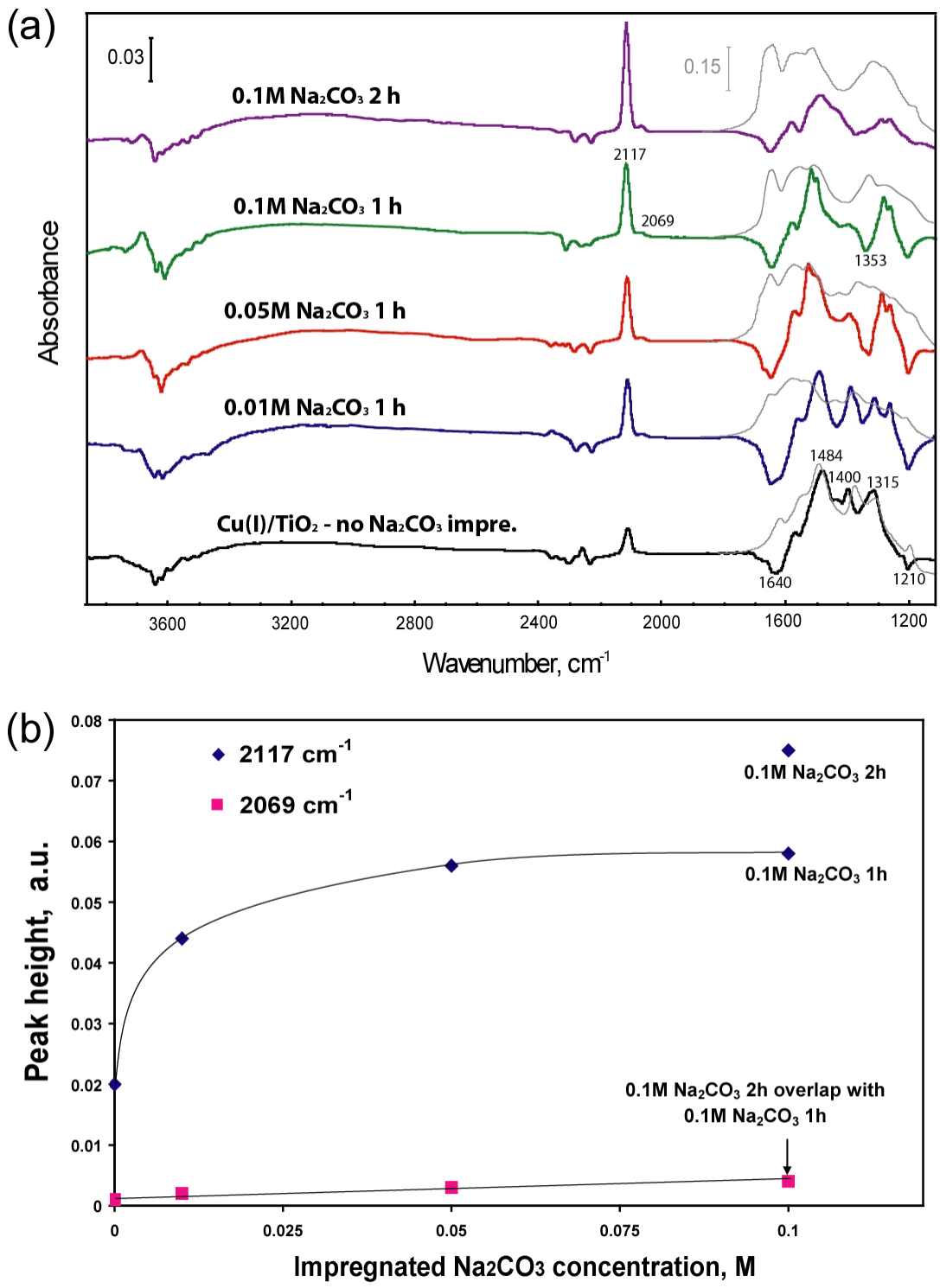

Figure 4. (a) DRIFT spectra of different Na_2CO_3-impregnated Cu(I)/TiO_2 samples after 80 min-illumination in the presence of $^{13}CO_2$; the spectra (grey curves) in the region of 1200-1800 cm^{-1} represent the applied background spectra of the corresponding samples, recorded after saturation of the surface with $^{13}CO_2$. (b) The evolution of the peak height of the 2117 and 2069 cm^{-1} bands for different Na_2CO_3-impregnated Cu(I)/TiO_2 samples.

Furthermore, it should be noted that band depletion around 1353 cm^{-1} is more pronounced for the 0.05 M and 0.1 M Na_2CO_3-impregnated catalysts. Compared to the background (gray) spectra for the corresponding impregnated samples, two additional absorption band depletions become more pronounced, i.e. at around 1640, and 1210 cm^{-1}. The depletion at 1640 cm^{-1} is presumably also the result of desorption of water, as the bending mode of adsorbed water is located at this wavenumber. The top spectra in Figure 4 (a) were recorded for the 0.1 M impregnated sample after treatment for 2 h. Not only is the 2117 cm^{-1} band the highest, but also the band signature in the 1200-1800 cm^{-1} region different from the other analyzed samples.

Illumination of Cu(I)/TiO_2 saturated with CO. Cu(I)/TiO_2 saturated with CO (or isotopically labeled ^{13}CO) was tested under illumination, in order to evaluate the changes in surface carbonate composition in the presence of CO (or ^{13}CO) triggered by light irradiation. Figure 5 shows the spectral development for the corresponding conditions. After 20 min exposure of Cu(I)/TiO_2 to carbon monoxide, several bands become apparent at 1667, 1569, 1557, 1495, 1426, 1418, 1360, 1319, 1247, and 1221 cm^{-1} as a result of CO adsorption (Figure 5 (a)). Peaks at 1641, 1519, 1468, 1376, and 1322 cm^{-1} formed for ^{13}CO adsorption (Figure 5 (b)). These bands indicate an increasing amount of surface carbonates, bicarbonates and carboxylates under irradiation.[13]

In the case of CO present in the gas phase, predominant peak growth occurs at 1557, 1418 and 1360 cm^{-1} during illumination. For Cu(I)/TiO_2 saturated with ^{13}CO, Figure 5 (b), bands at 1557, 1380 and 1360 cm^{-1} dominate the spectral growth during illumination, assigned to ^{12}CO induced species. Although no ^{12}CO was introduced, the spectral developing signature of ^{12}C labeled species results from carbon-residue left during the synthesis procedure.[13]

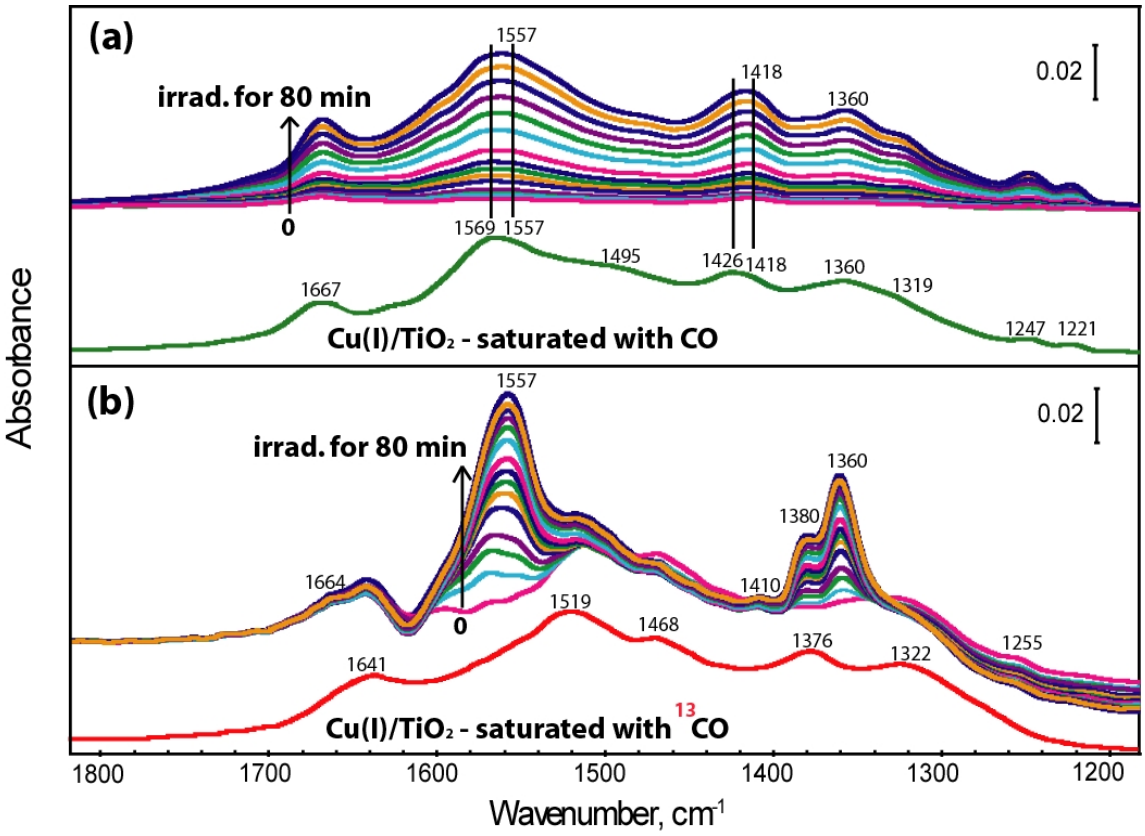

Figure 5. Time-profiled DRIFT spectra of Cu(I)/TiO_2 during 80 min of illumination, after saturation of the surface with (a) CO and (b) ^{13}CO (equilibration for 20 minutes). Irradiation was performed in the presence of gas phase CO.

Discussion

Surface composition of Na_2CO_3-impregnated TiO_2 samples. The relative concentration of CO_3^{2-} and HCO_3^- in the applied impregnation solutions is dependent on the pH. CO_3^{2-} is the dominant species, increasing to nearly 98 % CO_3^{2-} when the pH is higher than 12.[19] The results shown in Figure 1 clearly demonstrate that CO_3^{2-} adsorbes on the Cu(I)/TiO_2 surface in the form of bidentate carbonate, in view of the IR signature at 1553 and 1388 cm^{-1}. In view of the pH of the applied solutions for impregnation (9 to 11), a certain amount of HCO_3^- can be anticipated to additionally deposit on Cu(I)/TiO_2 during impregnation. This is confirmed by the developing broad absorption band around 1282-1287 cm^{-1}.[20] Probably OH^- groups are displaced by carbonate to account for the charge balance of the system. The ATR-IR result of Cu(I)/TiO_2 saturated with $NaHCO_3$ shown in Figure 1 (b) confirms that absorptions of C-OH

bending modes contribute to spectral features of the catalysts at around 1300 cm^{-1}, as well as the feature at 1360 cm^{-1}. Finally, besides bidentate carbonate and bicarbonates, the pronounced 1434 cm^{-1} band is evidence for monodentate carbonate, showing a mild relative decrease at increasing carbonate solution concentrations or impregnation times.

Interactions of TiO_2 surfaces with carbonate solutions have been reported previously.[11] The adsorption of carbonate on the surface was reported to be complete at approximately 0.01 M. Contrary to these literature results, the spectra in Figure 1 demonstrate an increase in surface carbonate composition after exposure to higher (0.1 M) concentrations, which might be related to the type of TiO_2, and pH applied. In conclusion, the impregnation procedure as applied here leads to a carbonate surface of mixed signature, with bidentate carbonate being dominant, followed by bicarbonate and monodentate carbonate species.

Carbonate/bicarbonate decomposition leads to CO formation. The illumination test in He of the 0.1 M Na_2CO_3-impregnated sample shown in Figure 3 (b), clearly demonstrates CO formation, accompanied by decomposition of carbonates/bicarbonates. This is the first conclusive evidence that surface adsorbed carbonates can be photo-reduced in non-aqueous conditions. Rather than CO, formaldehyde, formic acid, and methanol were reported as products of carbonate decomposition over illuminated TiO_2 in solution.[11, 12, 21] When H_2O is abundantly present, this might be involved in various ways in the reaction path, including as a reductant of carbonate. We will discuss the carbonate reduction pathway in more detail in the following paragraph and limit ourselves here by stating that the absence of reductants makes further hydrogenation of CO to hydrocarbons unlikely. This is supported by the absence of C-H stretching vibrations in the region of 2700-3000 cm^{-1}.

When present, $^{13}CO_2$ enhances the amount of predominantly ^{12}CO formed (compare Figure 3 and 4 (a)). This might be related to fast exchange of $^{13}CO_2$ with ^{12}C-containing carbonate sites, as well as exchange reaction of the produced CO.[22, 23] Irradiation was indeed found to initiate the formation of novel ^{13}C-carbonates, evident by spectral growth at 1484, 1400, and 1315 cm^{-1}, in particular for the pure Cu(I)/TiO_2 sample. While the growth in bands is less pronounced for the Na_2CO_3-impregnated samples, this is likely the result of a higher degree of surface site saturation with carbonates already deposited during the impregnation procedure. It should be mentioned that the spectral development is complicated and affected by overlapping decreasing and increasing absorption bands, which makes a detailed analysis of the carbonate dynamics ambiguous. An additional factor contributing to formation of ^{12}CO in

the presence of $^{13}CO_2$ has been previously addressed [13], and is most likely related to the involvement of carbon residue in the catalyst, the result of the precursors used for the synthesis of the Cu(I)/TiO_2 catalyst. Since these residues are present in extremely small concentrations, their nature is hard to assess. Based on the data presented in Figure 5, ^{13}CO is formed, but predominantly adsorbes in the form of surface carbonates, contributing to the dynamics of the carbonates demonstrated in Figure 4.

Figure 4 (b) demonstrates a significant improvement in ^{12}CO production rate by incorporation of increasing quantities of carbonates on the catalyst surface. The ^{13}CO peak at 2069 cm^{-1} only slowly, but continuously increases as a function of increasing Na_2CO_3 concentration used during impregnation. Besides the direct involvement of the carbonates in producing CO, also the reactivity of OH^- groups towards CO_2 might be affected by carbonate deposition. These hydroxyl groups could be considered as candidates for CO_2 and (in situ formed) CO adsorption. This is in agreement with the negative intensities of these bands in Figure 4 (a), being the result of CO or CO_2 insertion in the Ti-OH entities.

Mechanism of carbonate reduction? As stated in the introduction, carbonate reduction has been studied previously, and some aspects of the decomposition mechanism on TiO_2 surfaces have been addressed.[12, 21, 24] There is no agreement on this mechanism, however. In particular, Chandrasekaran et al. suggest that the carbonate ion is a hole acceptor, and oxidized, as demonstrated by laser flash pyrolysis experiments [11]. The carbonate neutral radical is then proposed to decompose into CO and O_2. The electron is scavenged either by oxygen, or involved in proton reduction to hydrogen, eventually leading to catalytic reduction of CO to form the product formaldehyde. Contrary to this mechanism, Raphael and Malati [12, 24], and later Ku et al.[21] argue that carbonate is the electron acceptor, and propose a route in which carbonate is first reduced to formate, and subsequently to formaldehyde and methanol. Water is oxidized by holes resulting in the formation of O_2. An argument used by Raphael [12] against carbonate oxidation proposed by Chandrasekaran [11], is the incompatibility of this mechanism with the formation of formaldehyde.

Based on the exclusive formation of CO, and the absence of (surface adsorbed) formates and formaldehyde, we tend to follow the mechanism proposed by Chandrasekaran et al. under our experimental conditions, also considering that the laser flash pyrolysis experiments provide for solid evidence of carbonate interactions with holes.[11] It should finally be mentioned, however, that the nature of the site on which the carbonate is adsorbed affects the

pathway, as experiments have demonstrated that holes and electrons might preferentially accumulate on specific crystal facets.

Conclusions

Surface adsorbed carbonates on Cu(I)/TiO_2, introduced by impregnation, can be decomposed to CO upon illumination. Furthermore, decomposition of CO_2 to CO over illuminated Cu(I)/TiO_2 is enhanced by carbonate impregnation, because of the higher affinity for CO_2 adsorption, as demonstrated by DRIFTS. Since formates have not been observed in our study, we favor a carbonate decomposition mechanism in which carbonate is oxidized by holes, eventually leading to the formation of CO. Subsequent hydrogenation of CO was not observed, possibly because of the absence of significant concentration of H_2 formed by proton reduction likely in aqueous environment.

Acknowledgements

This work was supported by ACTS (NWO, the Netherlands), in the framework of an NSC-NWO project (Project Number NSC-97-2911-I-002-002). Dorette Spaans and Nienke Firet at Delft University of Technology are gratefully acknowledged of their experimental contribution to the study.

References

1. **J. C. Hemminger, R. Carr and G. A. Somorjai, *Chem. Phys. Lett.*, 1978, 57, 100-104.**
2. **V. P. Indrakanti, J. D. Kubicki and H. H. Schobert, *Energy Environ. Sci.*, 2009, 2, 745-758.**
3. **H. Yamashita, N. Kamada, H. He, K. Tanaka, S. Ehara and M. Anpo, *Chem. Lett.*, 1994, 855-858.**
4. **S. G. Zhang, Y. Fujii, K. Yamashita, K. Koyano, T. Tatsumi and M. Anpo, *Chem. Lett.*, 1997, 659-660.**
5. **J. S. Hwang, J. S. Chang, S. E. Park, K. Ikeue and M. Anpo, *Top. Catal.*, 2005, 35, 311-319.**

6. **O. K. Varghese, M. Paulose, T. J. LaTempa and C. A. Grimes, *Nano Lett.*, 2009, 9, 731-737.**
7. **T. Inoue, A. Fujishima, S. Konishi and K. Honda, *Nature*, 1979, 277, 637-638.**
8. **I. H. Tseng, W. C. Chang and J. C. S. Wu, *Appl. Catal., B*, 2002, 37, 37-48.**
9. **I. H. Tseng and J. C. S. Wu, *Catal. Today*, 2004, 97, 113-119.**
10. **I. H. Tseng, J. C. S. Wu and H. Y. Chou, *J. Catal.*, 2004, 221, 432-440.**
11. **K. Chandrasekaran and J. K. Thomas, *Chem. Phys. Lett.*, 1983, 99, 7-10.**
12. **M. W. Raphael and M. A. Malati, *J. Photochem. Photobiol., A*, 1989, 46, 367-377.**
13. **C. C. Yang, Y. H. Yu, B. van der Linden, J. C. S. Wu and G. Mul, *J. Am. Chem. Soc.*, 2010, 132, 8398-8406.**
14. **S. C. Roy, O. K. Varghese, M. Paulose and C. A. Grimes, *ACS Nano*, 2010, 4, 1259-1278.**
15. **Y. Q. Wu, G. X. Lu and S. B. Li, *Catal. Lett.*, 2009, 133, 97-105.**
16. **D. L. Bernitt, K. O. Hartman and Hisatsun.Ic, *J. Chem. Phys.*, 1965, 42, 3553-&.**
17. **G. Lefevre, *Adv. Colloid Interface Sci.*, 2004, 107, 109-123.**
18. **K. Hadjiivanov, B. M. Reddy and H. Knozinger, *Appl. Catal., A*, 1999, 188, 355-360.**
19. **H. Lambers, F. S. Chapin III and T. L. Pons, *Plant physiological ecology*, second ed., Springer New York, Berlin, 1998.**
20. **F. A. Miller and C. H. Wilkins, *Anal. Chem.*, 1952, 24, 1253-1294.**
21. **Y. Ku, W. H. Lee and W. Y. Wang, *J. Mol. Catal. A: Chem.*, 2004, 212, 191-196.**
22. **G. Liuti, S. Dondes and P. Harteck, *J. Chem. Phys.*, 1966, 44, 4052-&.**
23. **O. Dunn and S. Dondes, *J. Phys. Chem.*, 1973, 77, 878-883.**
24. **M. A. Malati, L. Attubato and K. Beaney, *Sol. Energy Mater. Sol. Cells*, 1996, 40, 1-4.**

Chapter 4

A Parallel Screening Device for Photocatalytic Activity Evaluation in Gas Phase CO_2 Reduction

Abstract: We present a novel device for reproducible screening of heterogeneous photocatalysis. The device consists of multiple batch reactors, applicable for gas- and liquid phase reactions, and is equipped with fully automated gas sampling. Up to 12 catalysts can be evaluated simultaneously, and quick analysis for hydrocarbon products (80 seconds for C_3 alkanes and alkenes) is facilitated by compact GC. For the first time, several catalysts reported effective in the literature for CO_2 reduction, varying from crystalline semiconductors, to porous materials with isolated metal centers, and Ti-nanotubes, were tested under identical conditions. For various catalysts, carbon residues were found an important factor in producing quantities of CH_4. Of the catalysts investigated with stable performance, Ti-SBA-15 shows the highest activity. Still, the turnover frequency of Ti-SBA-15 needs to be improved at least by a factor of 1000, to allow practical application in photocatalytic CO_2 reduction.

Introduction

Artificial photosynthesis is currently receiving a high level of attention, as this is a promising technology for energy-to-fuel conversion and reduction of the emission of greenhouse gas CO_2. In Chapter 1, Table 1 shows a summary of recent literature reports on photocatalytic CO_2 reduction in either liquid or gas phase applications. Different semiconductors, porous materials with isolated metal centers, and Ti-nanotubes have been tested for this target reaction. A valid comparison of the catalysts' performance in CO_2 reduction is difficult, as a result of the following issues:

1) As Table 1 shows, the activity tests were carried out under various specific reaction conditions, such as conducting the reaction in the gas-, or liquid phase, composition of the CO_2 and water (vapor) feed, the reaction temperature, and the applied light source. Furthermore, the diversity of the applied photoreactors, and unavailability of any "standard" reference sample, makes it virtually impossible to compare the performance of various catalytic formulations.
2) Catalytic activity variations among different materials are best compared by evaluating the Turnover Frequency. Unfortunately, the determination of the nature and quantity of active sites is usually not reported, and requires extensive characterization. As listed in Table 1, the product yield was mostly determined based on the amount of titania (per gram of TiO_2) or titanium (per gram of Ti). For silica-supported titania samples, like Ti-ZSM-5, Ti-MCM-41, Ti-MCM-48, Ti-SBA-15, Ti-PS, the titania loading is low, ranging from 0.5 wt% to at most 10 wt%, and quantification of the amount by ICP or XRF analyses with small error margins is difficult. Furthermore, since the product yields are very small, the role of impurities in the catalyst formulations should not be underestimated.
3) Another relevant parameter to evaluate photocatalytic performance is the affectivity of the catalyst to convert light into chemical energy. Only few papers report a quantum yield. This requires measurement of the quantity of photons absorbed by the catalysts. This can be achieved by the subtraction of the photon flux (mol of photon/sec-m^2) into a specific reactor in the presence of catalyst from the one in the absence of catalyst. Inaccuracy arises from how precisely the light is probed. Similar issues arise when comparing materials in photocatalytic hydrogen production from water, as discussed by Maschmeyer et al.[1]

We present a custom-built apparatus to establish activity evaluation of heterogeneous photocatalytic activity of similar materials reported in Table 1 (Chapter 1) in gas phase CO_2 reduction under identical conditions. The reproducibility of the photoreactor system will be evaluated. Time-profiled quantitative data will be reported [2]. The impact of the results on the perspective of artificial photosynthesis in practice will also be discussed.

Experimental Section

Catalyst preparation. Degussa P25 TiO_2, ZnO and SiC are commercially available, and were used as received from Sigma-Aldrich. Modification of TiO_2 yielding CuO/TiO_2 and FeO/TiO_2 was achieved by sol-gel and hydrothermal synthesis, described in our previous study.[3] The only modification was not to include the addition of polyethylene glycol (PEG) to the synthesis procedure, in order to reduce the amount of potential carbon residues left in the catalysts. Titanium (IV) butoxide (TBOT, $Ti\text{-}(OC_4H_9)_4$) was the applied titania source. The used metal-salt precursors were 0.15 g of $Cu(NO_3)_2{\cdot}2.5H_2O$ and 0.3 g of $Fe(NO_3)_3{\cdot}9H_2O$ (both from Sigma-Aldrich, ≥ 98 %), added to 17 mL of TBOT, respectively, in 102 mL of 0.1 M $HNO_{3(aq)}$ solution After poly-condensation at 80°C for 28 h, filtration, washing, and drying at 150°C for 3 h in air, the powders were calcined at 500°C for 5 h (1°C /min). ZnO/TiO_2, NiO/TiO_2, and Pt/TiO_2 were synthesized by the incipient wetness impregnation method with aqueous solutions of $Zn(CH_3COO)_2{\cdot}2H_2O$, $Ni(NO_3)_2{\cdot}6H_2O$ (both from Sigma-Aldrich, ≥ 98 %), and $H_2PtCl_6{\cdot}6H_2O$ (from Sigma-Aldrich, ≥ 37.5 % Pt basis), respectively. Based a target for the metal content of 1.2 wt %, an appropriate amount of metal-salt solution was drop-wise added to 2 g of Degussa P25 TiO_2. After drying at 80°C over overnight and calcination at 500°C for 6 hours (1°C /min), ZnO/TiO_2, NiO/TiO_2, and Pt/TiO_2 were obtained. Au/TiO_2 was synthesized by a deposition precipitation method.[4] $HAuCl_4{\cdot}3H_2O$ was used as the gold precursor and Degussa P25 TiO_2 as support. After suspending P25 TiO_2 in the gold solution (pH 6, pre-adjusted by addition of an aliquot of a 0.1 M NaOH solution) and stirring at 80°C for 1h, washing with de-ionized water, and drying at 120°C, Au/TiO_2 was obtained. Based on the elemental analysis (ICP), the metal loading of the above samples was 1.0 wt% Cu, 1.5 wt% Fe, 1.2 wt% Zn, 1.1 wt% Ni, 1.0 wt% Pt, and 0.8 wt% Au, respectively.

For dispersed titania on porous materials, Ti-SBA-15 was synthesized by dissolving the surfactant, pluronic P123 ($EO_{20}PO_{70}EO_{20}$), in $HCl_{(aq)}$ and water. After mixing overnight, TEOS (tetraethylorthosilicate) and TBOT (titanium (IV) butoxide) were added under vigorous

stirring, which was maintained for 7.5 h at 45°C. The solution was aged overnight at 80°C in an oil bath. After filtration, washing, drying and calcination at 550°C for 6h (1°C /min), Ti-SBA-15 was obtained.[5] Titianium-silicalite-1 (TS-1) was prepared by mixing 20% TPAOH (tetrapropylammonium oxide) with water. TBOT and TEOS were added to the solution, stirring at room temperature for 1.5 h, followed by aging at 70°C for 3 days. After hydrothermal treatment at 150°C for 7 days under autogeneous pressure, filtration, washing, drying and calcination at 550°C for 6h (1^{o}C/min), TS-1 zeolites was collected. For dispersed TS-1 over SBA-15, the previously described TS-1 procedure was followed, up to 3 days of aging. This TS-1 seed solution was prepared followed a similar procedure reported by Meng et al.[6] It is used to impregnate TS-1 particles on pre-calcined SBA-15 materials (550°C for 6h). The solution used for impregnation was highly basic, with a pH of around 13. After drying at room temperature and calcination at 550°C for 6h, TS-SBA-15 was obtained. Cobalt oxide loaded on SBA-15 was synthesized by impregnation of a 3M cobalt nitrate solution., in a similar procedure as reported by Wolters et al.[7] SBA-15 (surface area = 600 m^2/g, pore volume = 0.7 mL/g, desorption pore diameter = 8 nm) was prepared similarly to the above methods. Prior to the impregnation, the SBA-15 support was dried at 80^{o}C in dynamic vacuum to remove water from the pores. Subsequently, SBA-15 was impregnated to incipient wetness with the $Co(NO_3)_2$ solution. After impregnation, the mixture was dried at 60^{o}C for 12 h in stagnant air and calcined at 500^{o}C for 5 h in air (1^{o}C /min). Co_3O_4-SBA-15 was obtained.

Cr-Ti-TUD-1 with variable Cr:Ti ratio (x:y) was synthesized by aging, drying and calcination of a homogeneous mixture, as follows. Triethanolamine (TEA) and H_2O were mixed, followed by the addition of orthosilicate (TEOS), chromium (III) nitrate nonahydrate, and titanium (IV) n-butoxide. Tetraethylammonium hydroxide (TEAOH) was added dropwisely and the obtained clear mixture after 2 hours was vigorously stirred. The resulting mixture was subsequently aged at room temperature for 24 hours and then dried at 98^{o}C for another 24 hours. The obtained solid was ground and hydrothermally treated in a 50 mL Teflon-lined stainless steel autoclave at 178^{o}C for 24 hours. After calcination at 600^{o}C for 10 hours, Cr-Ti-TUD-1 was collected. The molar ratio of TEOS: Cr: Ti: TEAOH: TEA: H_2O is 1: x: y: 0.5: 1: 11, x and y being variable. Synthesis details can be found elsewhere.[8]

Trititanate nanotube (Ti-nanotube) was prepared using a hydrothermal synthesis method.[9] The titanium dioxide source used for the preparation of Ti-nanotube is commercial Riedel De Haen powder, 100% anatase nanoparticles with a surface area of 12 m^2/g. In a typical

nanotube preparation, TiO_2 was dispersed into a 10 M NaOH solution under vigorous stirring. Afterwards, the mixture was stirred for 1h, transferred into an autoclave, followed by hydrothermal treatment at 150°C for 48 h. After hydrothermal treatment, the solid (Na-TNT) was recovered by centrifugation. After washing with deionized water, the wet cake was dispersed in 0.1 M HCl solution and stirred for 30 min. The solid was recovered again by centrifugation, and further washed with 0.1 M $HCl_{(aq)}$ until the pH of the solution reached ca. 6.5-7. After filtration, washing with water and ethanol, drying at 100°C for several days, and calcination at 350°C for 6h, Ti-nanotube was thus obtained.

Development of screening device and quantitative analysis. As shown in Figure 1, the experimental apparatus consists of three parts: the assembly of multiple batch photoreactors, a compact gas chromatograph, and a valve system controlled by a user interface in LabView. The 12 cylindrical reactors (inner volume 50 mL) are connected by a loop for gas dosage and sampling. To avoid cross-talking among reactors and disturbance from air, a diaphragm pump is used to evacuate the reactors and sampling loop. An oil based pump has been avoided to prevent possible contamination from lubricating oils during evacuation, possibly affecting the measurement of the organic products from CO_2 reduction, such as methane.

Fast quantitative analysis is achieved by a compact gas chromatograph, equipped with TCD and FID detectors. Molsieve 5A (5 m) and a capillary Porabond Q column (10 m), are connected to a TCD detector and used for the separation of H_2, O_2, N_2, CO, and CH_4. A Porabond Q column (10 m) was also coupled to an FID detector, used for the separation of C_1 to C_4 alkanes and alkenes. Due to the short column length, and absence of a ramping procedure, quantitative data representing each reactor can be obtained within 80 sec. The followed procedure of gas dosage and sampling is illustrated in Figure 2.

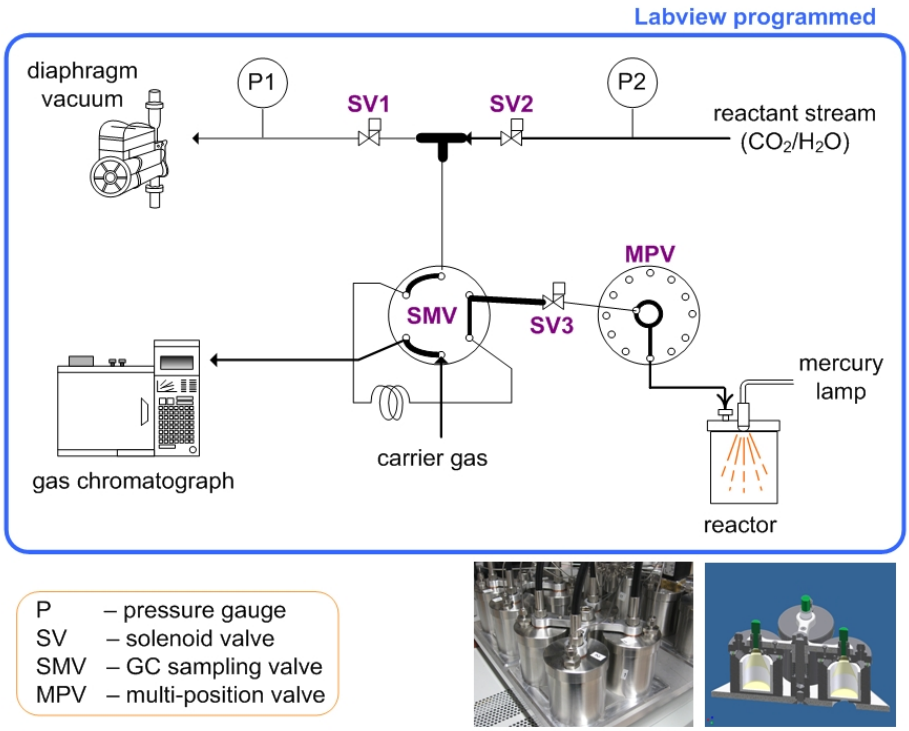

Figure 1. Principle of the developed apparatus for secondary screening of photocatalytic activity under identical conditions.

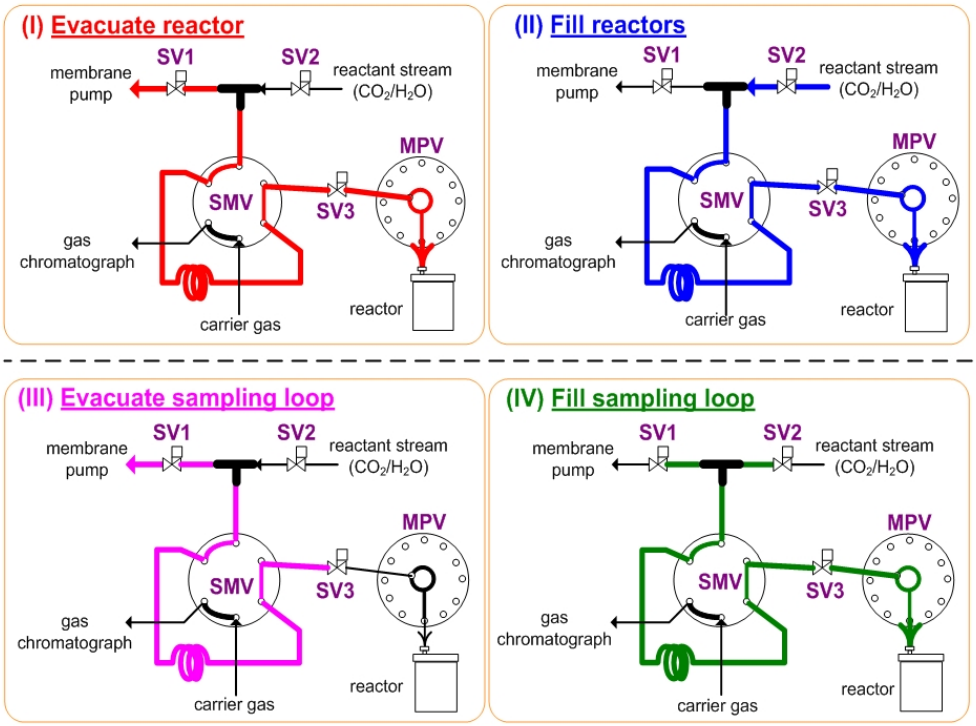

Figure 2. Sketch of the principle of how reactants were dosed (I, II), and products sampled by gas chromatography (III, IV).

A diaphragm pump was used to degas the reactor down to 3 mbar within 30 sec. During the filling procedure, the reactor is open to the gas stream, containing CO_2 and water vapor. Three cycles of evacuation and filling minimized the air content inside the reactors. Before sampling, the loop shared by the reactor effluent is evacuated, to discard the leftover products from the previous analysis (gas-dosing or sampling). All tubing is made of 1/16 inch stainless steel, to reduce the dead volume in joining reactors and valves.

The applied light source is a 120 Watt high pressure mercury lamp, from Dr. Gröbel UV-Elektronik GmbH. The spectrum of this mercury lamp ranges from 280 to 650 nm. The life time of the lamp is around 1400 hours with a maximum intensity decay of 30 %, and 2500 hours for a maximum decay of 50 % in light intensity. A bundle of 12 quartz light guides is used to introduce the light source into 12 of the reactors. When placing the light guide on the cover of the reactor, the illumination area is 60 mm in diameter, fully covering the bottom area inside the reactor (35 mm in diameter). The material of the window on the cover is fused silica, allowing 90 % of transmission between 180 and 1000 nm. The irradiance profile in each reactor is shown as in Figure 3. The spectra demonstrate a homogeneous light distribution among the 12 reactors.

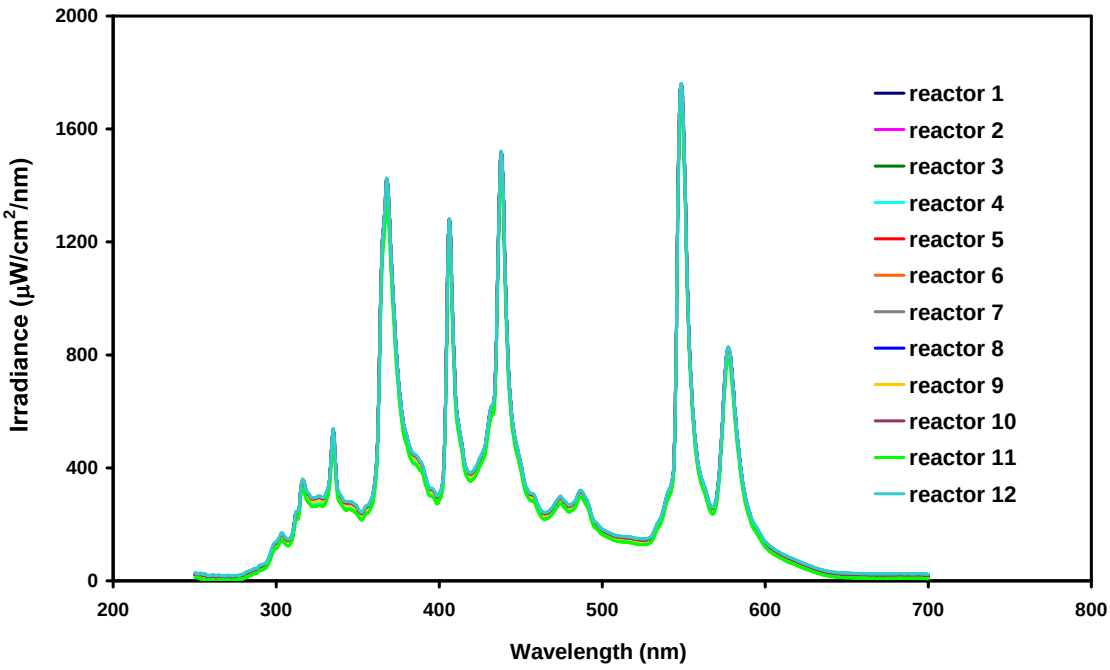

Figure 3. Irradiance profiles detected in each reactor (light source: 120 W mercury lamp).

CO_2 reduction experiment. The presented apparatus is designed for evaluation of heterogeneous photocatalysis. In this chapter, we discuss the evaluation of photocatalytic materials in gas phase CO_2 reduction, which was performed by introducing a CO_2/He stream saturated with water vapor. He was used to maintain the overall pressure at 1.03 bar. 200 mg of the catalysts was placed in each photoreactor. In Chapter 2, the contribution of carbon residue to the CO production rate was discussed for a Cu(I)/TiO_2 sample, which can be greatly reduced by prolonged illumination in moist air.[3] Hence, in order to minimize the influence of any possible carbon residue, the samples were illuminated firstly for 7 h in humid Helium. After the pre-illumination in humid Helium, three evacuation-gas dosage cycles was completed by evacuated the reactor down to 3 mbar followed by dosing the CO_2/He stream saturated with water vapor. All the reactors were operated in batch mode, and illuminated for 7 h. Production of hydrocarbons was quantified by the FID detector of the GC. The reaction was conducted with a CO_2/H_2O ratio of 0.5, containing 38 μmole of CO_2 and 76 μmole of water vapour. The temperature was maintained at 40^oC (± 2^oC) during the 7 h of illumination. Each catalyst was tested for three runs, in order to check the reproducibility. After each run, the leftover gas reactants and products were removed by evacuation to 3 mbar. Subsequently, evacuation-gas dosage cycles were conducted three times. The error in methane quantification was less than 0.5 ppm for all the tested samples.

Results and Discussion

Screening of catalysts active in CO_2 reduction. Figure 4 shows the amount of CH_4 produced by various catalysts after 7 h of illumination. The tested catalysts can be divided into five groups, dense phase semiconductors (TiO_2, ZnO, SiC), metal or metal oxide promoted titania materials (CuO/TiO_2, ZnO/TiO_2, FeO/TiO_2, NiO/TiO_2, Pt/TiO_2, Au/TiO_2), dispersed titania on porous materials (Ti-SBA-15, TS-SBA-15), Cr-Ti co-deposited TUD-1 materials (Cr-Ti-TUD-1), and a Trititanate nanotube (TNT) catalyst.

For the dense phase semiconductors, CH_4 production follows the order TiO_2 > ZnO > SiC. TiO_2, ZnO and SiC possess different conduction/valence band positions, but have a similar band gap (3.2 eV for ZnO, and 3.0 eV for TiO_2 and SiC). [10] TiO_2 still shows a higher CH_4 production rate than ZnO and SiC. Compared to TiO_2 and ZnO, SiC holds a larger potential for electron transfer to CO_2, as shown in Figure 5.[10-13] However, CH_4 yield was the lowest. The low surface area and the hydrophobic, non-catalytic, surface properties of SiC apparently

limit the adsorption of CO_2 and H_2O, and do not result in an appreciable kinetic rate for the reaction.[3] ZnO generally is less effective for photocatalytic transformation as compared to TiO_2[13, 14], and obviously this is confirmed by the data reported in Figure 4.

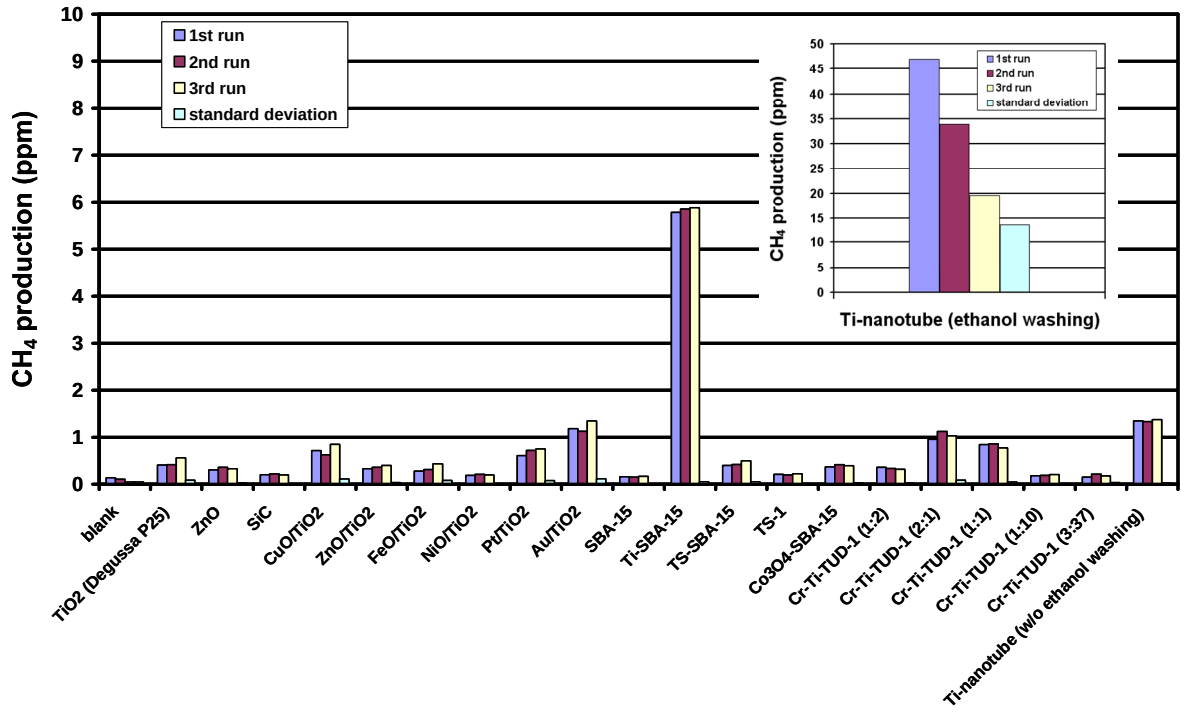

Figure 4. CH_4 quantity produced as determined for various catalysts after 7 h of illumination in a CO_2/H_2O mixture (38 μmol CO_2, 76 μmole H_2O, and balanced with Helium). The insert shows the extremely high CH_4 quantity obtained for Ti-nanotube, washed with ethanol.

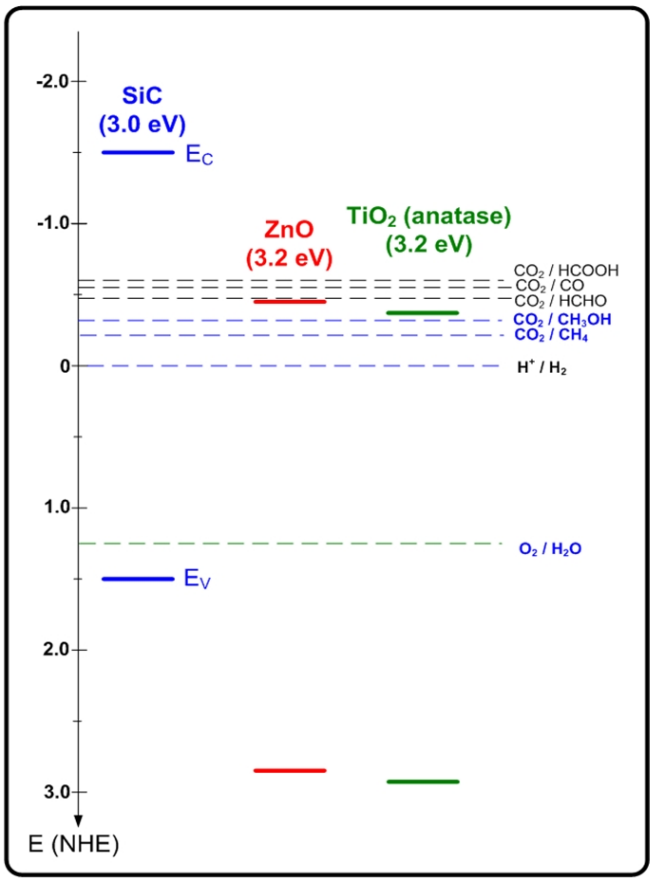

Figure 5. Schematic diagram of valence and conduction band levels of SiC, ZnO, and anatase TiO_2.[10, 11, 13] The redox potential of CO_2 towards various C1 molecules is also shown..[12]

For the metal or metal oxide promoted titania samples, the sequence of CH_4 production is: $Au/TiO_2 > Pt/TiO_2 \approx Cu(O)/TiO_2 > ZnO/TiO_2 \approx FeO/TiO_2 \approx NiO/TiO_2$. Au/TiO_2 shows the highest production rate, 1.2 ppm of CH_4 after 7 h of illumination. Among the tested samples, metal promoted titania is more active in CH_4 production than metal oxide promoted titania, which was to be expected. Metal particles, especially nano-gold particles, serve as electron trap, which reduces recombination of photo-induced electrons and holes. Furthermore, Au might be effective in electron transfer to adsorbed CO_2, inducing the reduction. This hypothesis requires further in depth studies.

For dispersed titania on porous materials, Ti-SBA-15 shows the highest production of CH_4 (5.8 ppm after 7 h of illumination). This observation is in agreement with what has been reported in the literature. Isolated titania over porous materials displays an increase of two orders of magnitude in terms of CH_4 yield per Ti site, as compared to crystalline TiO_2.[15] We

also tested titanium-silicalite (TS-1) and dispersed TS-1 over SBA-15 for activity in the reduction of CO_2. TS-1 is less effective than TiO_2, yielding only 0.2 ppm after 7 h of illumination. TS-1-SBA-15 shows somewhat higher CH_4 production (0.4 ppm for 7h illumination) as compared to the pure TS-1 sample. Catalysts containing nano-structured cobalt oxide clusters in mesoporous silica are active in water oxidation, yielding O_2, which is the required half reaction in CO_2 activation [16] CH_4 production over Co_3O_4-SBA-15 after 7h of illumination was only 0.4 ppm, demonstrating that Co_3O_4-SBA-15 requires an efficient reduction catalyst to establish a catalytic cycle.

For the Cr-Ti co-deposited TUD-1 materials, Cr-Ti-TUD-1 (2:1) shows a CH_4 production of 1.0 ppm after 7 h of illumination. The CH_4 production sequence of the various Cr/Ti compositions is: Cr-Ti (2:1) > (1:1) > (1:2) > (1:10) ≈ (3:37). Two conclusions can be drawn based on this trend. First, a relatively low loading of Ti is beneficial for the performance, since increasing the Ti content, decreased performance [(1:1) > (1:2) > (1:10) ≈ (3:37)]. Second, enhancing the Cr-content was found beneficial [Cr-Ti (2:1) > (1:1)]. The effect of Ti content is consistent with the hypothesis that isolated, tetrahedral Ti-sites are most active in photocatalytic CO_2 reduction, as suggested by Anpo and Frei.[15, 17] We speculate that the higher Cr content leads to some visible light response of the catalytic system, but this requires further investigation.

It is noteworthy that CH_4 production over the fresh Ti-nanotube catalyst was spectacular in the first test of reaction. However, CH_4 production decreased significantly for the 2nd and 3rd time test. Even after pre-illumination 7h in moist Helium, the results of CH_4 production were still inconsistent in repeating tests. Considering that in the sample synthesis an ethanol-washing procedure was included, we speculate that decomposition of remaining ethanol may influence the extent of methane producted during illumination. A new batch of Ti-nanotubes was synthesized without the ethanol-washing procedure, and the results shown in Figure 4. A consistent, but dramatic decrease in CH_4 production (1.3 ppm) can be observed, demonstrating the contribution from ethanol to the production of CH_4. This suggests that results of photocatalytic CO_2 reduction obtained for catalysts treated with organic solvents should be analyzed with care. This observation also agrees with the results of our previous study on Cu(I)/TiO_2, which demonstrated an effect of carbonaceous residue on conversion of CO_2 into CO over titania-based catalysts.[3]

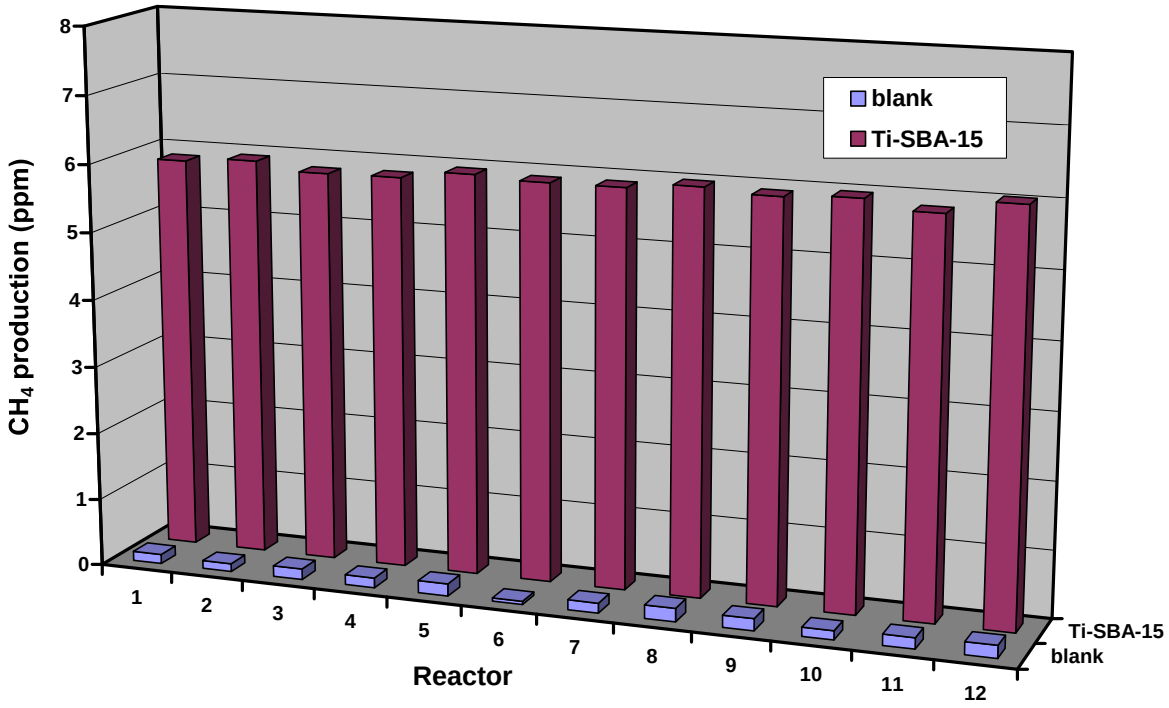

Figure 6. Quantities of CH_4 produced using Ti-SBA-15 in 12 different photoreactors after 7 h of illumination in a CO_2/H_2O mixture (38 μmol CO_2, 76 μmole H_2O, and balanced with Helium).

Among the screened catalytic formulations, Ti-SBA-15 showed the highest consistent production of CH_4, 5.8 ppm, after 7h of illumination. To confirm the reproducibility of our screening facility, Ti-SBA-15 was inserted in various reactors, and the performance evaluated. Figure 6 shows that CH_4 production for each of the 12 photoreactors were nearly the same, around 5.8 ppm. This result demonstrates the consistency of the activity evaluation among the 12 reactors. The reproducibility of the activity on Ti-SBA-15 in these reactors is consistent with the identical irradiance profile in each of the reactors, as shown in Figure 3. The same test was carried out in the absence of any catalyst under the same experimental conditions. Less than 0.1 ppm of CH_4 was detected in each of the reactors. This is consistent with a background level to be expected in air.

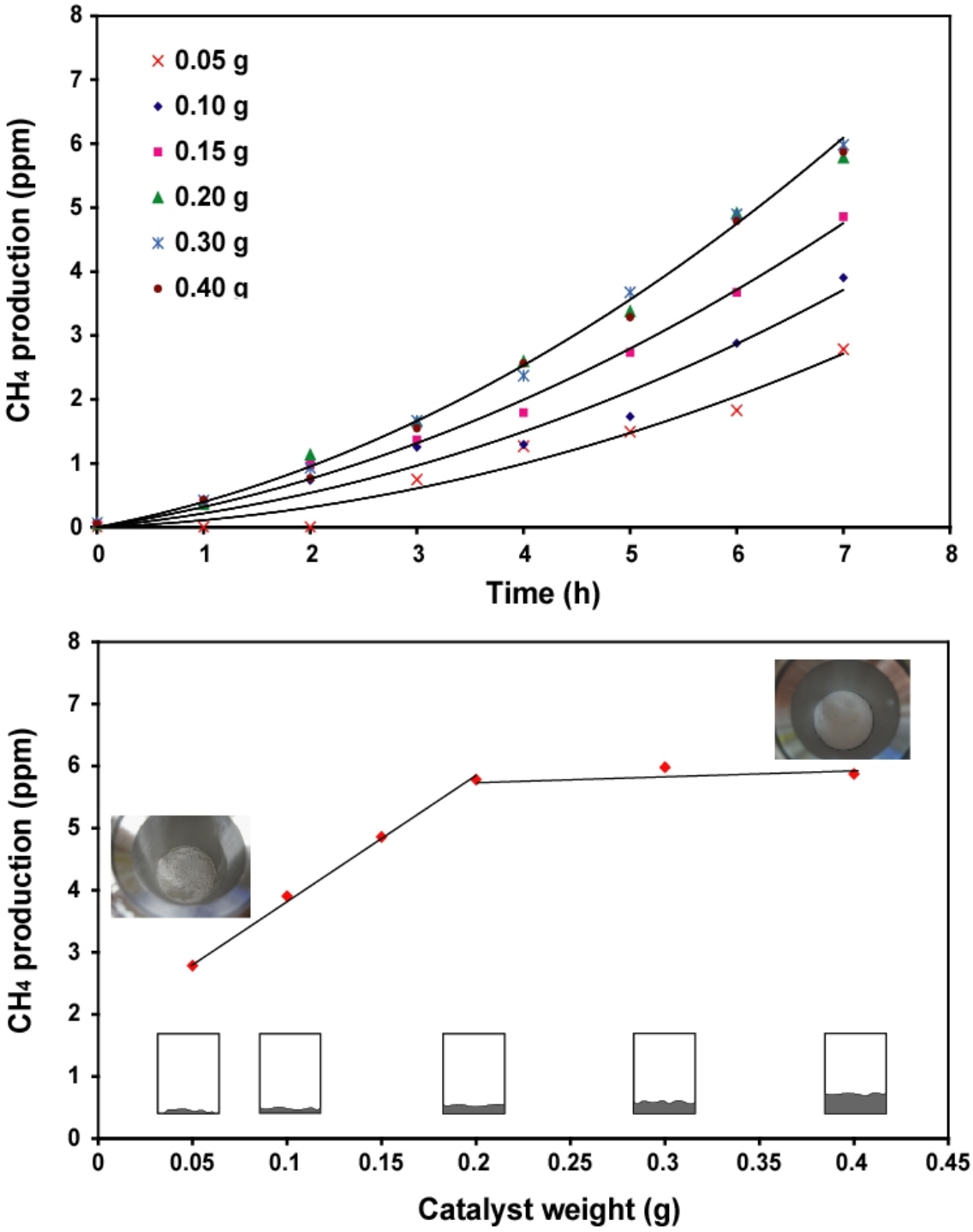

Figure 7. Effect of sample weight on CH_4 production profile for Ti-SBA-15. Top – time profiled CH_4 production of various amounts of sample; bottom – the quantity of CH_4 produced after 7 hours as a function of sample weight.

Effect of Catalyst weight on CH_4 production. Figure 7 shows the time-profiled production of CH_4 over different amounts of Ti-SBA-15. When the amount of Ti-SBA-15 was increased from 0.05 g to 0.2 g, CH_4 production increased linearly accordingly. If the amount of catalyst is larger than 0.2 g, CH_4 production remains constant, i.e. 5.8 ppm after 7 h of illumination. Clearly, a certain amount of light is no longer available for the reaction, when too much catalyst is used, explaining the leveling-off in CH_4 production. Optimization of the catalyst weight can thus be easily achieved in this multiple batch photoreactor system.

Another observation displayed in Figure 7 is the apparent 2-step profile in CH_4 production. An increase in production rate of CH_4 was observed after 2 or 3 h of illumination. This might be related to the mechanism of CO_2 reduction. First, CO_2 might yield CO in the early stages of illumination, which is followed by hydrogenation to CH_4.[18] How well H_2 or H_2O enable activation of CO or CO_2 over Ti-SBA-15 materials will be discussed in Chapter 5.

Correlating CH_4 production yields to literature data. An amount of 5.8 ppm CH_4 produced in the present study can be calculated to be the equivalent of 0.012 μmol after 7h of illumination. The production rate is thus 0.002 μmol/h. Considering that 0.2 g of Ti-SBA-15 catalyst was used, the CH_4 yield equals 0.008 μmol/g-cat/h. Based on the elemental analysis (ICP) of the Ti-loading in Ti-SBA-15 (0.05 wt%), the CH_4 yield is 16.6 μmol/g-Ti/h. Compared to the yield of Ti-SBA-15 reported in the literature[15], i.e. 106 μmol/g-Ti/h, our catalyst performs 6 times worse. This factor might be the result of various differences in reaction conditions between ours, and the study of Anpo and coworkers, such as Ti-loading (0.05 wt% Ti, *vs* 0.29 wt%, based on a Si/Ti ratio of Ti-SBA-15 of 270), the applied reaction conditions (CO_2/H_2O ratio of 1:2, *vs* a CO_2/H_2O ratio of 1:5) and type of irradiance (160 mW/cm^2 *vs* 1.3 mW/cm^2). Another fact is that we did not detect any CH_3OH in our system, which was observed by Anpo and coworkers. At the same time, we observed considerable formation of C_2 products - C_2H_4 and C_2H_6 - over this catalyst. We will further discuss the mechanistic evaluation of CH_4 and other C2 products in Chapter 5.

Another point of importance is the comparison of the performance of the supported Ti-sites with that of dense phase TiO_2, Degussa P25. We observed an amount of 0.46 ppm of CH_4 for P25 after 7 h of reaction, as shown in Figure 3. This is 0.0009 μmol of CH_4. The CH_4 product rate can be estimated as 0.00013 μmol/h or 0.00064 μmol/g-cat/h or 0.00107 μmol/g-Ti/h. This is 12.6 times lower than observed for the Ti-SBA-15 catalyst on a g^{-1} catalyst basis, and

15500 times lower on a g^{-1} Ti basis, obviously the result of the fact that Ti in the bulk of TiO_2 is not contributing to catalytic activity.

From a catalytic point of view, it is crucial to determine the turnover frequency of the materials. Even for Ti-SBA-15, the turn over frequency is only 8.6×10^{-4} h^{-1}. Such small turnover frequency is far from needed for an efficient catalytic process, and efficiency improvement of at least 3 orders of magnitude is needed to bring artificial photosynthesis close to reality.

Apparent quantum yield of Ti-SBA-15. Another comparison of photocatalytic performance is often based on the apparent quantum yield. First it is needed to evaluate the absorption spectrum of the catalyst. When Ti atoms occupy a tetrahedral position in a SiO_2 network, this yields significant absorption at around 200-250 nm. Titanium-silicate (TS-1) showed UV absorptions with maxima around 215-220 nm.[19] For Ti-MCM-41, with 2 wt% Ti loading, the absorption band is centered at around 230 nm.[20] A similar band in the region of 200-240 nm was reported for Ti-SBA-15, with 0.29 wt% Ti content. The strong band at 205 nm and the small tail around 230 nm are assigned to $Ti(OH)(OSi)_3$ and $Ti(OSi)_4$ sites, respectively.[15] As shown in Figure 8, our Ti-SBA-15 catalyst gives rise to a clear absorption band around 208 nm and a tailing small band at around 230 nm, in agreement with the literature[15]. The spectra of SBA-15 and dense phase TiO_2 are shown for comparison.

The irradiance, as detected on the surface where the samples are placed in the reactor, is also shown in Figure 8. If counting the photon flux entering the reactor in the 280-650 nm range, in total there are 1.97×10^{4} μmol photons entering the reactor every hour. The apparent quantum yield (AQY) for CH_4 is then 6.7×10^{-5} %. This low quantum yield is expected, however, since the isolated tetrahedral sites in Ti-SBA-15 do not absorb in the visible region. If we only consider the photons from 280 to 300 nm, the AQY is 1.1×10^{-2} %. While this number is still very low, the applied wavelength range for the calculation is still a considerable mismatch to the main absorption bands of the catalyst, suggesting that our light source is not the most suitable. Still the data are comparable to the studies of Anpo and coworkers[15], who also applied wavelengths larger than 250 nm to excite these types of catalyst. Recent attempts[21] of the group of Frei and coworkers to shift the absorption spectrum towards the visible by using isolated sites linked through oxygen bridges in mesoporous

structures appear to be an interesting way forward to improve quantum yield and use solar radiance more effectively.

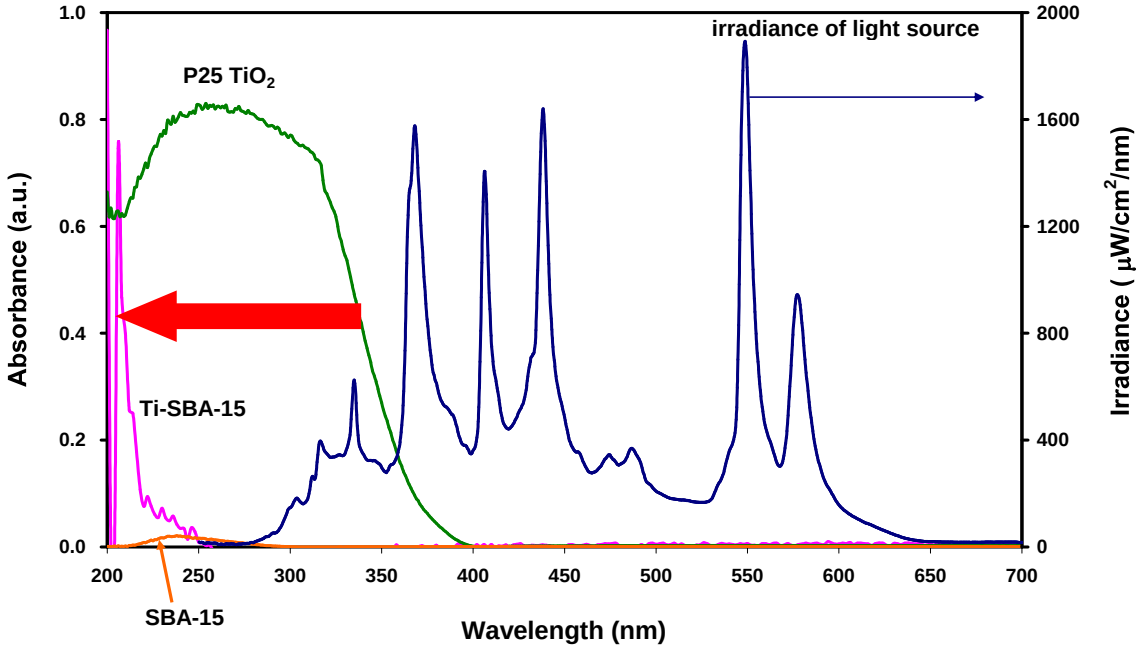

Figure 8. Diffuse reflectance UV/VIS absorption spectra of P25 TiO_2 (× 0.3), Ti-SBA-15, and SBA-15; the irradiance of the applied light source in photocatalytic CO_2 reduction experiments is shown for comparison.

Conclusions

A multiple batch screening facility for photocatalysis has been developed, and demonstrated effective for catalyst evaluation in the photocatalytic reduction of CO_2. The gas product, CH_4, was detected by gas chromatography with an automated sampling program. A consistent light distribution and temperature profile among the 12 photoreactors was confirmed by identical data for one specific catalyst. Among the tested catalysts, isolated titania on porous silica, Ti-SBA-15, shows the highest production rate for CH_4.

Acknowledgements

This work was supported by ACTS (NWO, the Netherlands), in the framework of an NSC-NWO project (Project Number NSC-97-2911-I-002-002). The author thank to Jarian Vernimmen and Stefan Ribbens at University of Antwerp, Mariska Wolters and Tamara

Eggenhuisen at Utrecht University, Yi-Hui Yu at National Taiwan University for catalysts syntheses. Nico Alberts and Bart Boshuizen at Delft University of Technology are gratefully acknowledged of their technical supports.

References

1. **T. Maschmeyer and M. Che, *Angew. Chem. Int. Ed.*, 2010, 49, 1536-1539.**
2. **J. A. Moulijn, J. Perez-Ramirez, R. J. Berger, G. Hamminga, G. Mul and F. Kapteijn, *Catal. Today*, 2003, 81, 457-471.**
3. **C. C. Yang, Y. H. Yu, B. van der Linden, J. C. S. Wu and G. Mul, *J. Am. Chem. Soc.*, 2010, 132, 8398-8406.**
4. **J. T. Carneiro, C. C. Yang, J. A. Moma, J. A. Moulijn and G. Mul, *Catal. Lett.*, 2009, 129, 12-19.**
5. **Y. Segura, P. Cool, P. Kustrowski, L. Chmielarz, R. Dziembaj and E. F. Vansant, *J. Phys. Chem. B*, 2005, 109, 12071-12079.**
6. **X. J. Meng, D. F. Li, X. Y. Yang, Y. Yu, S. Wu, Y. Han, Q. Yang, D. Z. Jiang and F. S. Xiao, *J. Phys. Chem. B*, 2003, 107, 8972-8980.**
7. **M. Wolters, L. J. W. van Grotel, T. M. Eggenhuisen, J. R. A. Sietsma, K. P. de Jong and P. E. de Jongh, *Catal. Today*, 2011, 163, 27-32.**
8. **S. Telalovic, A. Ramanathan, G. Mul and U. Hanefeld, *J. Mater. Chem.*, 2010, 20, 642-658.**
9. **S. Ribbens, V. Meynen, G. Van Tendeloo, X. Ke, M. Mertens, B. U. W. Maes, P. Cool and E. F. Vansant, *Microporous Mesoporous Mater.*, 2008, 114, 401-409.**
10. **T. Inoue, A. Fujishima, S. Konishi and K. Honda, *Nature*, 1979, 277, 637-638.**
11. **A. Mills and S. LeHunte, *J. Photochem. Photobiol., A*, 1997, 108, 1-35.**
12. **M. Schiavello, *Heterogeneous Photocatalysis*, John Wiley & Sons, 1997.**
13. **M. Miyauchi, A. Nakajima, T. Watanabe and K. Hashimoto, *Chem. Mat.*, 2002, 14, 2812-2816.**
14. **L. B. Khalil, W. E. Mourad and M. W. Rophael, *Appl. Catal., B*, 1998, 17, 267-273.**
15. **J. S. Hwang, J. S. Chang, S. E. Park, K. Ikeue and M. Anpo, *Top. Catal.*, 2005, 35, 311-319.**
16. **F. Jiao and H. Frei, *Angew. Chem. Int. Ed.*, 2009, 48, 1841-1844.**
17. **W. Y. Lin, H. X. Han and H. Frei, *J. Phys. Chem. B*, 2004, 108, 18269-18273.**

18. S. S. Tan, L. Zou and E. Hu, *Sci. Technol. Adv. Mater.,* 2007, 8, 89-92.

19. M. A. Uguina, D. P. Serrano, G. Ovejero, R. Vangrieken and M. Camacho, *Appl. Catal., A*, 1995, 124, 391-408.

20. L. Marchese, T. Maschmeyer, E. Gianotti, S. Coluccia and J. M. Thomas, *J. Phys. Chem. B*, 1997, 101, 8836-8838.

21. H. Frei, *Chimia*, 2009, 63, 721-730.

Chapter 5

Mechanistic Study of Hydrocarbon Formation in Photocatalytic CO_2 Reduction over Ti-SBA-15

Abstract: Ti-SBA-15 was exposed to illumination in the presence of different gas mixtures containing CO or CO_2, and H_2O or H_2, in order to clarify the route to hydrocarbon formation in photocatalytic CO_2 reduction over this photocatalyst. A mixture of CO and H_2O led to the highest quantities of CH_4, C_2H_4, and C_2H_6 after 7 hours of reaction, whereas a mixture of CO_2 and H_2 lead to the lowest production rate of these products. H_2O has been identified as more efficient in activation of CO and CO_2 than H_2. CH_3OH was not detected as significant product, and when fed to the catalyst, did not yield extensive product formation. Formaldehyde was found very reactive over the catalytic system, yielding a product distribution (C_1-C_2) of similar nature as obtained by CO activation. Finally, backward reactions, i.e. oxidation of hydrocarbon products into CO or CO_2, were found significant over this catalyst system. Based on the experimental activity profiles, results indicated above, and available literature, a mechanism for photocatalytic CO_2 reduction is proposed involving formation of CO in the initial stages, followed by consecutive formation of formaldehyde, which converts to CH_4, C_2H_4, and C_2H_6, presumably by reaction with photo-activated H_2O (OH radicals).

Introduction

Photocatalytic conversion of H_2O and CO_2 to fuel-like molecules is an ideal reaction to store solar energy in the form of chemical energy, and to close the carbon cycle. However, there are several challenges to make this technology a reality. Predominantly a poor conversion over various catalytic materials hinders practical application. TiO_2 was the first catalyst to be reported active in liquid phase photocatalytic CO_2 reduction by Inoue et al. in 1979 [1]. Later in 1987, ruthenium loaded TiO_2 was found active in gas phase photocatalytic CO_2 reduction, as reported by Thampi et al. [2]. Isolated Ti-sites in micro- and mesoporous materials were found very effective in CO_2 reduction by Yamashita et al. in 1995, including Ti-ZSM-5 [3]. Hwang et al. showed Ti-SBA-15 increased the CH_4 yield by two orders of magnitude as compared to TiO_2, and the CH_3OH yield by one order of magnitude in terms of μmol produced per gram Ti per hour[4]. In recent years other materials effective in CO_2 reduction have been reported, such as Ti-nanotubes [5], metal loaded TiO_2 [6-10], and different novel types of semiconductors – like Ga_2SO_3 [11], $InTaO_4$ [12, 13], Zn_2GeO_4 [14], $Zn_2Ga_2O_4$ [15], and CdSe [16].

Among the above identified investigated catalysts, isolated titania in porous silica materials still holds the best reported performance upon UV exposure. Tetrahedrally coordinated Ti-sites are considered to be the active centers for catalyzing CO_2 into hydrocarbons [3, 4]. However, various aspects of the catalysis are still unresolved. Anpo and coworkers have proposed a mechanism involving dissociation of CO_2 into CO and C, and H_2O into H and OH radicals, followed by recombination of the radicals to final products, CH_4 and CH_3OH, with traces of C_2-products, and the co-product O_2 [17]. In a recent advanced IR study on Ti supported on MCM-41, however, only CO could be demonstrated as the product of reaction, and only if H_2O was co-fed to the IR cell [18]. The excitation of the Ti-O ligand-to-metal charge transfer was proposed to lead to transient Ti^{+III} and a hole on the framework oxygen. Electron transfer from Ti^{+III} to CO_2 splits the molecule into CO and O^-. O^- is spontaneously protonated by a Si-OH group or H^+ co-generated upon H_2O oxidation, to yield a surface adsorbed OH radical. The OH radicals either combine to yield H_2O_2 or dismutate to give O_2 and H_2O [18] .

Further understanding of the mechanism of UV light-induced reduction of CO_2 by H_2O in Ti silicate sieves can lead to design rules for improved systems. Of particular interest is the identification of the individual reaction steps leading to the final products. Moreover, possible destructive reactions of final products need to be identified, since they will limit the quantum

efficiency. In this chapter, the performance of Ti-SBA-15 is further evaluated. To better understand how isolated Ti sites interact with potential intermediates, various gas mixtures including CO or CO_2, and H_2O or H_2 were used in illumination tests. By using standard C_1-C_3 gas mixtures, or pretreatment in formic acid, methanol or formaldehyde, the backward reactions of hydrocarbons into CO or CO_2 were also investigated. The results will be discussed on the basis of potential mechanistic steps.

Experimental Section

Catalysts preparation. Ti-SBA-15 was synthesized by dissolving the surfactant, 4 g pluronic P123 ($EO_{20}PO_{70}EO_{20}$), in 20 mL $HCl_{(aq)}$ and 130 mL water. After mixing overnight, 9.14 mL TEOS (tetraethylorthosilicate) and 300 μL TBOT (titanium (IV) butoxide) were added under vigorous stirring, which was maintained for 7.5 h at 45°C. The solution was aged overnight at 80°C in an oil bath. After filtration, washing, drying and calcination at 550°C for 6h (1°C/min) in air, Ti-SBA-15 was obtained. Pure SBA-15 was also prepared following a similar synthesis procedure, but without the addition of TBOT.

Catalytic evaluation. Gas phase photocatalytic tests were performed in a custom-built combinatorial photoreactor system. The apparatus consists of three parts: the assembly of multiple batch photoreactors, a compact gas chromatograph, and a valve system controlled by a user interface in LabView. The 12 cylindrical reactors (inner volume 50 mL) are connected by a loop for gas dosage and sampling. To avoid cross-talk among reactors and disturbance from air, a diaphragm pump is used to evacuate the reactors and sampling loop down to 3 mbar. Fast quantitative analysis is achieved by a compact gas chromatograph, equipped with TCD and FID detectors. A combination of a Molsieve 5A column (5 m) and a capillary Porabond Q column (10 min) is connected to a TCD detector and used for the separation of H_2, O_2, N_2, CO, and CH_4. A Porabond Q column (10 m) is coupled to the FID detector, used for the separation and detection of C_1 to C_4 alkanes and alkenes. Due to the short column length, and absence of a ramping procedure, quantitative data representing each reactor can be obtained within 80 seconds. The applied light source is a 120 Watt high pressure mercury lamp. The spectrum of this mercury lamp ranges from 280 to 650 nm. A bundle of 12 quartz light guides is used to introduce the light source into the 12 reactors, in a homogeneous

irradiance profile. The overall light irradiance (from 280 to 650 nm) reaching the bottom of the reactor is 1.5×10^5 μW/cm^2, as described in Chapter 4.

The production of hydrocarbons was monitored while Ti-SBA-15 was illuminated in the presence of various gas compositions of CO or CO_2, and H_2 or water vapor. By mixing a CO_2/He or CO/He stream with a H_2/He stream or Helium stream saturated with water vapor, these different initial gas compositions were obtained. Helium was used to maintain the overall pressure at 1.03 bar. 50 mg of Ti-SBA-15 was used for testing in the target reactions. The catalyst samples were spread flatly at the bottom surface (35 mm in diameter) of the reactor. All the samples were pretreated by illumination for 7 h in static humid Helium containing c.a. 4 mol-% of water vapor (saturated at room temperature) to remove possible hydrocarbon contaminants. The effectiveness and details of contaminant removal will be addressed in the description of the results. After pre-illumination, three evacuation-gas dosage cycles were completed using evacuation of the reactor down to 3 mbar. Subsequently, the CO_2/He stream saturated with water vapor was introduced. All the reactors were operated in the batch mode, and illuminated for 7 h. Production of hydrocarbons was quantified by the FID detector of the GC. The reaction was conducted with a ratio 0.5 of CO_2 (or CO) to H_2O (or H_2), containing 38 μmole of CO_2 (or CO) and 76 μmole of H_2O (or H_2). The temperature was maintained at 40^{o}C (± 2^{o}C) during the 7 hours of illumination. After each run of catalyst testing, the leftover gas reactants and products were removed by evacuation to 3 mbar. Three evacuation-gas dosage cycles were applied. The standard deviation in methane production was less than 0.5 ppm for all tests.

Additional experiments for evaluation of potential backreactions of intermediates and products were conducted as follows: CH_4, C_2H_2, C_2H_4, C_2H_6, C_3H_4, C_3H_6, and C_3H_8 were used as initial reactants by the introduction of a standard gas mixture (Scotty analyzed gases, 15 ppm of each component in balance of nitrogen, 4 liters, 120 psig, 21^{o}C) into a helium stream saturated with or without water vapor (4 mol-% water vapor). For liquid reagents the following procedure was applied: an amount of 50 mg of Ti-SBA-15 was dried at 120^{o}C overnight. The sample was then suspended in 10 mL of 99.9% CH_3OH (Sigma-Aldrich), 98 % HCOOH (Merck), or 36.5 % $HCHO_{(aq)}$ (Riedel – de Haën) (used as received) for 30 min. After filtration, the thus 'impregnated' samples were collected and directly used in illumination tests without drying.

Catalyst characterization.

Textural properties. N_2 adsorption-desorption isotherms were obtained at liquid Nitrogen temperature using a Quantachrome Quadrasorb-SI automated gas adsorption system. Prior to an experiment, the sample was degassed at 200°C for 16 h. The Brunauer–Emmet–Teller (BET) method was applied in a relative pressure range from 0.05 to 0.30 to calculate the specific surface area. The pore size distributions were deduced from the desorption branches of the isotherms using the Barrett–Joyner–Halenda (BJH) method. The total pore volumes were calculated from the amount of N_2 vapor adsorbed at a relative pressure of 0.95. ICP (Inductively Coupled Plasma) and EPMA (Electron Probe Micro Analysis) were applied for the elemental analysis. ICP was performed by using a PerkinElmer Optima 3000 dV apparatus The EPMA analyses were performed on a JEOL JXA 733 apparatus to determine the Ti-loading of the Ti-SBA-15 sample.

In-situ Diffuse Reflectance Infrared Fourier Transform Spectroscopy (DRIFTS). In-situ DRIFTS experiments were carried out using a Nicolet Magna 860 spectrometer equipped with a liquid N_2 cooled MCT detector, and a three window DRIFTS (Diffuse and Reflectance Infrared Fourier Transform Spectroscopy) cell. Two ZnSe windows allowed IR transmission, and a third (Quartz) window allowed the introduction of UV/Vis light into the cell. CO_2 (Linde Gas, 99.995%) was used as received. Prior to illumination, SBA-15 or Ti-SBA-15 were heated up to 120°C in the cell, and maintained at this temperature for 60 minutes, followed by cooling down to 30°C in a dry He stream of 30 mL/min in order to remove physisorbed water. During illumination the cell was kept at room temperature (30°C). In-situ IR spectra were recorded under UV/Vis light irradiation (100 Watt mercury lamp, λ: 250 – 600 nm), in the presence of a Helium atmosphere, against a background of the pre-treated catalyst. For comparison, other spectra were recorded accordingly against background spectra of the corresponding pre-treated samples, after saturation of the surface by exposure for 20 minutes to water vapor or CO_2 saturated with 4 mol-% of water vapor.

Results

Pre-illumination of Ti-SBA-15 in moist Helium. In Chapter 2, the contribution of carbon residue to CO production was demonstrated for Cu(I)/TiO_2, which can be greatly reduced by

prolonged illumination in moist air [19]. Hence, in order to minimize the influence of any possible carbon residue, the Ti-SBA-15 samples were all illuminated during 7 h in humid Helium conditions prior to evaluation in photocatalytic reactions. Figure 1 (a) shows the formation of 3.5 ppm of CH_4, 1.4 ppm of C_2H_4 and 2.3 ppm of C_2H_6 as a result of illumination in humid Helium (1st illumination). Apparently reactions of carbon residue yield the observed products, which even after calcination at 550°C for 6 h (1°C/min) is still present in Ti-SBA-15. As shown in Figure 1 (b) and 1 (c), the production of CH_4, C_2H_4 and C_2H_6 largely decreased in subsequent illumination experiments in humid Helium, and reached values of the same order as measured in an empty reactor as shown in Figure 1 (d). All data reported in the remainder of this study were obtained after application of pre-illumination in humid Helium environment.

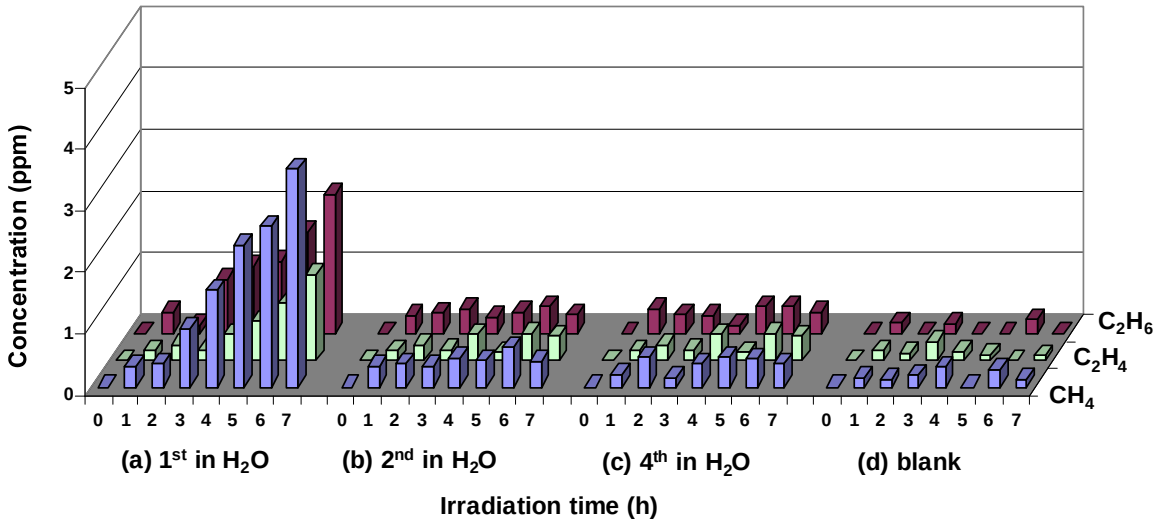

concentration (ppm)	(a) 1st in H_2O	(b) 2nd in H_2O	(c) 4th in H_2O	(d) blank
CH_4	3.54	0.47	0.37	0.12
C_2H_4	1.40	0.40	0.40	0.07
C_2H_6	2.26	0.31	0.35	-

Figure 1. CH_4, C_2H_4, and C_2H_6 production over Ti-SBA-15 during 7 h of illumination in water vapour/Helium environment: (a) 1st illumination, (b) 2nd illumination, (c) 4th illumination, and (d) blank test. In-between illumination periods, the reactor was evacuated to 3 mbar, before reloading with humid He. The table shows the respective concentrations after 7 h of illumination.

Illumination of Ti-SBA-15 in various gas mixtures. To investigate possible pathways to hydrocarbon formation over Ti-SBA-15, CH_4 and C_2-product formation in various mixtures of CO_2 or CO, and H_2O or H_2 was evaluated during illumination. As Figure 2 demonstrates, CH_4, C_2H_4, and C_2H_6 are the primary products of CO_2 or CO activation. The highest yield was found for a mixture of CO and H_2O, i.e. 4.3 ppm CH_4, 2.5 ppm C_2H_4, and 3.7 ppm C_2H_6. Lower yields were obtained for a CO and H_2 mixture, a CO_2 and H_2O mixture, while the lowest yield was obtained for a CO_2 and H_2 mixture, i.e. 2.1 ppm CH_4, 1.4 ppm C_2H_4, and 0.8 ppm C_2H_6. The absence of CH_4 formation in the initial 3 h may be the result of the detection limit of the FID detector, being approximately 0.5 ppm. We therefore assume a relatively constant rate in CH_4 production in all conditions.

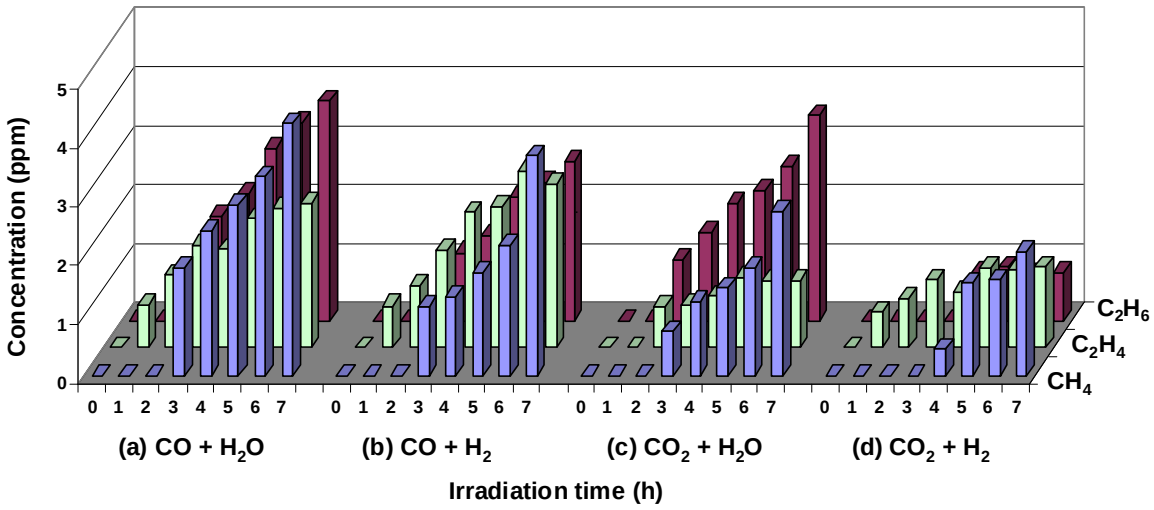

production (ppm)	(a) $CO + H_2O$	(b) $CO + H_2$	(c) $CO_2 + H_2O$	(d) $CO_2 + H_2$
CH_4	4.28	3.74	2.78	2.11
C_2H_4	2.46	2.79	1.15	1.39
C_2H_6	3.74	2.71	3.50	0.81

Figure 2. CH_4, C_2H_4, and C_2H_6 production over Ti-SBA-15 during 7 h of illumination in various gas mixtures: (a) CO/H_2O = 0.5, (b) CO/H_2 = 0.5, (c) CO_2/H_2O = 0.5, and (d) CO_2/H_2 = 0.5. The table shows the respective concentrations after 7 h of illumination.

Taking the most productive condition (in the mixture of CO and H_2O) as an example, the amount of 4.3 ppm CH_4, 2.5 ppm C_2H_4 and 3.7 ppm C_2H_6 produced in the present study can be calculated to be the equivalent of 0.009 μmol CH_4, 0.005 μmol C_2H_4, and 0.007 μmol C_2H_6 after 7 h of illumination. The production rates of CH_4, C_2H_4 and C_2H_6 are thus 0.001, 0.0007 and 0.001 μmol/h, respectively. Considering that 0.05 g of Ti-SBA-15 catalysts was used, the yield of CH_4, C_2H_4 and C_2H_6 equals to 0.025, 0.014 and 0.021 μmol/g-cat/h. Based on the elemental analysis (ICP) of the Ti-loading in Ti-SBA-15 (0.05 wt%), the yields of CH_4, C_2H_4 and C_2H_6 are 49.75, 28.93 and 42.81 μmol/g-Ti/h. Assuming that all the Ti sites were accessible for the reaction, the turnover frequency of CH_4, C_2H_4 and C_2H_6 can also be calculated as 2.4×10^{-3}, 1.4×10^{-3} and 2.0×10^{-3} h^{-1}. In this regard, after 7 hours of reaction time roughly only 1 out of 1000 Ti-sites has been active in producing CH_4, C_2H_4 and C_2H_6 by conversion of CO and H_2O.

Backward reaction, C1-C3 hydrocarbons into CO_2. Ti-SBA-15, pre-illuminated in humid Helium, was illuminated in a gas mixture of CH_4, C_2H_2, C_2H_4, C_2H_6, C_3H_4, C_3H_6, and C_3H_8 to analyze the rate of oxidation of these hydrocarbons. Figure 3 (a) demonstrates the absence of concentration changes in various components in the dark. During 7 h of illumination, Figure 3 (b), the concentration of all C_1-C_3 alkanes, alkenes, and alkynes decreased. CH_4 decreased from 9.2 ppm to 2.3 ppm. The other C_2 and C_3 compounds also decreased in concentration with conversion levels higher than 50 %. Physisorbed water on the catalyst and traces of oxygen left in the reactor after evacuation probably initiated the conversion of the C_1-C_3 compounds into CO or CO_2. Summarizing, the backward reaction – hydrocarbon oxidation to CO or CO_2 – is feasible during illumination.

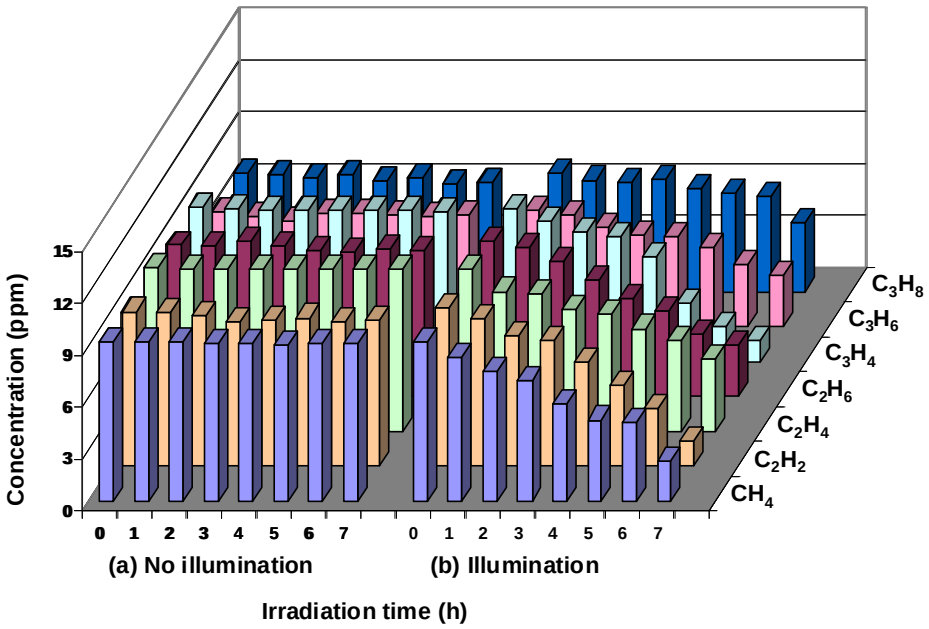

condition		concentration (ppm)						
		CH_4	C_2H_2	C_2H_4	C_2H_6	C_3H_4	C_3H_6	C_3H_8
(a) no illumination	0th h	9.22	8.92	9.44	8.73	8.89	6.63	6.85
	7th h	9.08	8.44	9.38	8.40	8.63	6.45	6.35
(b) illumination	0th h	9.16	9.17	9.39	8.99	8.84	6.73	6.86
	7th h	2.29	1.42	4.14	2.92	1.24	2.97	4.00

Figure 3. Concentrations of C1-C3 alkanes, alkenes, and alkynes in the presence of Ti-SBA-15: (a) no illumination and (b) illumination for 7 h. The initial concentrations are 9 ppm CH_4, C_2H_2, C_2H_4, C_2H_6, C_3H_4, and 7 ppm C_3H_6, C_3H_8, respectively. Total pressure: 1.03 bar Helium. The table shows the respective concentrations after 7 h of illumination.

Oxygenates? Contrary to the sole production of alkanes and alkenes (mainly CH_4) observed in the present study, CH_3OH was found as primary product in the literature over Ti-ZSM-5 [3], Ti-MCM-41, Ti-MCM-48 [20], Ti-FSM-16 [21], Ti-Beta zeolites [22], Ti-containing nanoporous silica films [23], and Ti-SBA-15 [4]. To further clarify whether and how CH_3OH or other oxygenates are involved in CO_2 reduction, CH_3OH, HCHO, and HCOOH-impregnated Ti-SBA-15 samples were prepared and exposed to illumination. As shown in Figure 4 (a), 1.3 ppm CH_4, 0.9 ppm C_2H_4, and 0.9 ppm C_2H_6 was detected for the CH_3OH-impregnated Ti-SBA-15 sample after 7 h of illumination in Helium. 1.9 ppm CH_4, 0.8 ppm C_2H_4, and 0.9 ppm C_2H_6 was found to be formed after illuminating a HCOOH-impregnated Ti-SBA-15 sample

for 7 h. Compared to illumination of Ti-SBA-15 in CO_2 and water vapor (Figure 4 (d)), the improvement in CH_4, C_2H_4, and C_2H_6 production was not significant for the CH_3OH and HCOOH-impregnated samples. Contrary, for the HCHO-impregnated Ti-SBA-15 sample, a huge amount of CH_4 and C_2H_6 was produced (insert in Figure 4). As much as 436 ppm of CH_4 and 19.4 ppm of C_2H_6 were produced after 7 h of illumination. Surprisingly, C_2H_4 was detected in only very little amounts. This observation implies that formaldehyde is extremely reactive over Ti-SBA-15, although direct photolysis reactions are also contributing to conversion, as will be discussed later.

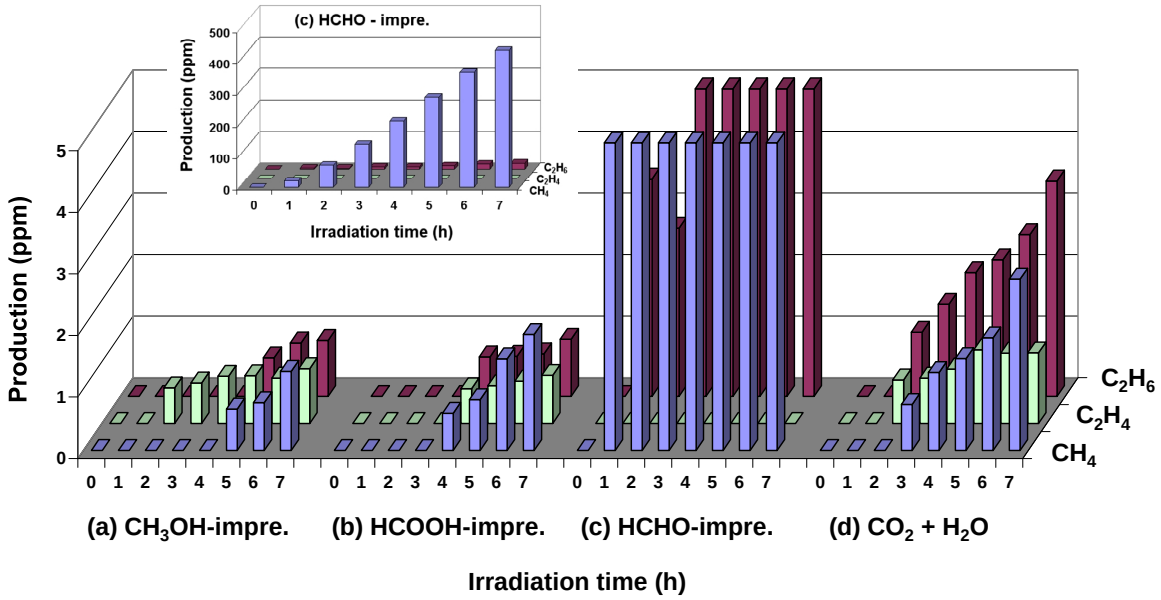

production (ppm)	(a) CH_3OH-impre.	(b) HCOOH-impre.	(c) HCHO-impre.	(d) CO_2 + H_2O
CH_4	1.28	1.88	436.05	2. 78
C_2H_4	0.89	0.78	-	1.15
C_2H_6	0.91	0.93	19.38	3.50

Figure 4. CH_4, C_2H_4, and C_2H_6 production over Ti-SBA-15 impregnated with (a) CH_3OH, (b) HCOOH, and (c) HCHO during 7 h of illumination in Helium environment, compared to Ti-SBA-15 illuminated in (d) CO_2/H_2O. The table shows the respective concentrations after 7 h of illumination.

Catalyst stability. It has been demonstrated in the literature that the meso-structure of SBA-15 will largely collapse as a result of steam treatment at temperatures higher than 600^oC [24, 25]. Hydrolysis and dehydrolysis can cause the recombination of Si-O-Si bonds on the amorphous silica walls of SBA-15, especially where numerous silanol groups are located. Although the working temperature and conditions of photocatalytic CO_2 reduction with water vapor are not as severe as steam at elevated conditions, it is essential to evaluate whether the pore structure remains intact during illumination. Figure 5 shows N_2 adsorption-desorption isotherms, and the pore size distribution (based on the desorption curve) of Ti-SBA-15. The characteristic feature of a Type IV isotherm with hysteresis loop is evident, which is associated with capillary condensation in mesopores [26]. Based on the isotherm in Figure 5 (a) and the pore size distributions in Figure 5 (b), the pore structure was established to be stable during illumination in the presence of CO_2 and H_2O. Table 1 indicates a slight decrease in BET surface (from 852 to 816 cm^2/g) and pore volume (from 0.96 to 0.93 cm^3/g), comparing fresh Ti-SBA-15 and Ti-SBA-15 illuminated in the presence of CO_2/H_2O. The isotherm of SBA-15 shows the same hysteresis profile as Ti-SBA-15, in agreement with the low Ti loading of the used Ti-SBA-15 catalyst (0.05 wt% from ICP and 0.1 wt% from EPMA).

Figure 6 shows the DRIFT spectra of Ti-SBA-15 and SBA-15 in specific working conditions, recorded against the spectra of the respective dehydrated samples. As shown in Figure 6 (a), in addition to the signature of the broad band in the region of 2800 and 3800 cm^{-1} assigned to chemisorbed water and H-bonded OH groups, spectral enhancement is visible at 910 and 950 cm^{-1}, and depletion at 3744 cm^{-1}, when exposing Ti-SBA-15 to water vapor for 20 min. A similar spectral signature, Figure 6 (b), was observed for SBA-15, except for the absorption at 910 cm^{-1}. The 910 cm^{-1} absorption has been assigned to the vibration of Si-O-Ti bonds [27], while the 950 cm^{-1} band is assigned to dangling $\nu(Si\text{-}O_d)$ vibrations associated with Si-OH and $Si\text{-}O^-$ groups [28-30] The 3744 cm^{-1} band is the corresponding OH stretching vibration of isolated surface silanol groups [31]. After 7 h of illumination in the presence of water vapor, the 910 and 950 cm^{-1} bands increased, while a further depletion at 3744 cm^{-1} was observed for Ti-SBA-15. The spectra of SBA-15 remained practically unchanged during illumination.

In the case of exposing Ti-SBA-15 or SBA-15 to CO_2 and water vapor, similar spectral profiles were observed. The only difference is the presence of two doublet absorption bands at 3600-3630 and 3715-3740 cm^{-1}, which are assigned to gas phase CO_2 [32]. The depletion of silanol groups at 3744 cm^{-1} needs to be considered when CO_2 and water vapor are introduced.

The enhancement of the CO_2 doublet around 3715-3740 cm^{-1} overlaps with the depletion of silanol groups at 3744 cm^{-1}, resulting in various negative features around 3715-3740 cm^{-1}. Upon illumination, irrespective of the present gas mixture (water vapour in the absence or presence of CO_2) for Ti-SBA-15 the 910 and 950 cm^{-1} absorption bands increased, while the band at 3744 cm^{-1} decreased. In contrast, these bands remained similar for SBA-15 in all conditions.

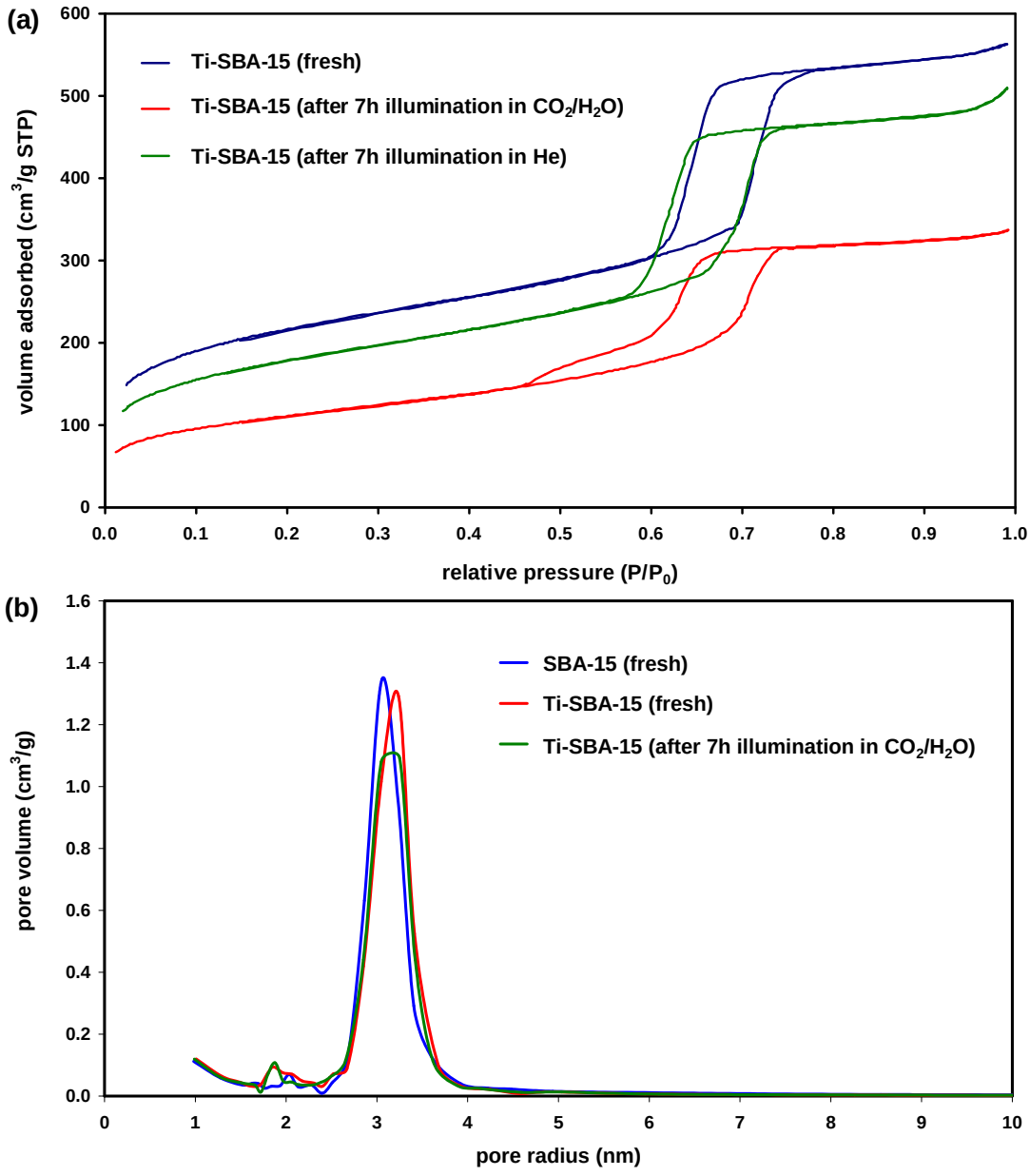

Figure 5. (a) Isotherm of N_2 adsorption and (b) desorption pore size distribution of the SBA-15 and Ti-SBA-15 samples: fresh, and after 7 h of illumination in CO_2/H_2O.

Table 1. Textural properties of SBA-15 and Ti-SBA-15.

	BET surface area (m^2/g)	total pore volume (cm^3/g)	average pore radius* (nm)
SBA-15	**751**	**0.93**	**3.1**
Ti-SBA-15	**852**	**0.96**	**3.2**
Ti-SBA-15 illum. in CO_2/H_2O	**816**	**0.93**	**3.2**

* the average pore radius was determined by the desorption isotherm of the investigated samples.

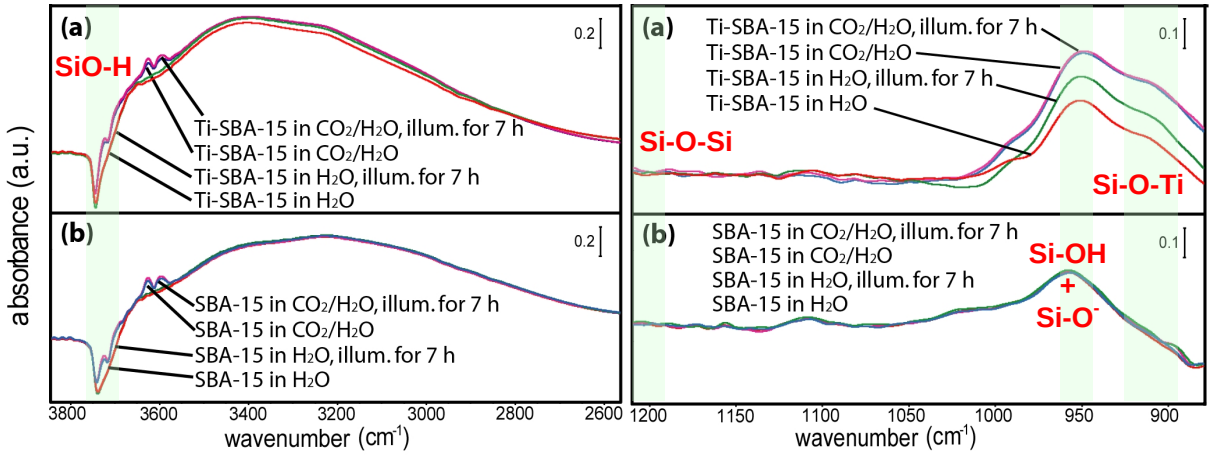

Figure 6. DRIFT spectra of (a) Ti-SBA-15 and (b) SBA-15, under various conditions: (1) after dosing H_2O/He for 20 min, (2) after illumination in H_2O/He for 7 h, (3) after dosing CO_2/H_2O for 20 min, and (4) after illumination in CO_2/H_2O for 7 h. All the spectra were recorded against the spectra of the respective dehydrated samples after heat treatment at 120°C.

Discussion

CO_2 reduction over Ti-SBA-15: mechanistic considerations. First, it is important to mention that carbon residues might contribute to product formation in CO_2 reduction in the presence of H_2O. This is clearly demonstrated by the data reported in Figure 1. Carbon containing reagents are often used in Ti-catalyst synthesis, such as for Ti-nanotube materials [5], as well as the SBA-15 catalysts reported herein. It is difficult to establish the nature of the carbon residues left after material synthesis [19]. It is clear, however, that illumination pretreatment of the catalyst in the presence of water, is a more efficient way to remove carbon

residue than calcination in air at elevated temperatures. Figure 2 clearly demonstrates that CO_2 reduction is feasible in the presence of H_2O, to yield CH_4 and C_2 products. It is proposed that CO is an important intermediate in the conversion of CO_2 to CH_4. This is in agreement with various observations. First, Figure 2 demonstrates that CO is quite reactive to form a similar product distribution as observed by activation of CO_2. The reason CO was not observed in the present experiments is that the rate of formation of CO by CO_2 activation is apparently slower than the rate of conversion of CO to CH_4 and C_2- hydrocarbons. Second, various literature reports have appeared that discuss the conversion of CO_2 to CH_4 such as e.g. Saladin et al. over Degussa P25 TiO_2 catalyst [33]. CO was proposed as intermediate in the production of CH_4, based on their experimental data. Also in-situ IR studies of Cu(I)/TiO_2 [19] suggest CO formation is quite feasible by photo-activation of CO_2 [21].

Comparing Figure 2 (c) to 2 (d) shows that H_2O is more efficient than H_2 to reduce CO_2 into CH_4 over Ti-SBA-15. Considering the bond energy of the H-H bond (436 kJ/mol, at 25^oC) is slightly lower than of the O-H bond in water (464 kJ/mol, at 25^oC) [34], this appears remarkable. However, the interaction of H_2 or H_2O with the "active sites" of the catalyst, and the necessity of an electron donor (water oxidation with formation of O_2) also need to be considered. Figure 6 (a) shows the increase of dangling bond ν(Si-O_d) and decrease of isolated surface silanol groups, when exposing Ti-SBA-15 to water vapor. Moreover, in comparison with SBA-15 (Figure 6 (b)), Ti-SBA-15 (Figure 6 (a)) shows a clear increase in intensity of the dangling bond ν(Si-O_d) vibration upon exposure to CO_2/H_2O (with and without illumination). These spectral observations indicate strong interaction between H_2O and Ti-SBA-15 [29]. Furthermore, Nakamura et al. reported FT-IR spectroscopic evidence of the formation of hydroperoxo (Ti-OOH) as an intermediates in photocatalytic reaction on nanocrystalline TiO_2 films in contact with aqueous solution [35]. In this respect, hydroxyl radicals or hydroperoxo (intermediates toward O_2) are demonstrated important transient species, which are not very likely to be formed in dehydrated conditions in the presence of hydrogen.

Role of Oxygenates? In the literature, besides methane and hydrocarbons, CH_3OH was found to be one of the primary products in gas phase CO_2 reduction over isolated titania in porous materials [3, 4, 20-23]. However, in this study, CH_3OH was not detected in illumination tests using various gas compositions, as shown in Figure 2. Moreover, the IR spectra of Ti-SBA-15 while illuminated in the presence of CO_2 and H_2O showed no signature of adsorbed CH_3OH or

other absorption bands indicative of adsorbed oxygenates (e.g. formates or aldehydes) (Figure 6). In particular, absorptions related to methyl stretching vibrations in the region between 2600 and 3000 cm^{-1} are absent, in agreement with the absence of CH_3OH production over Ti-SBA-15. Figure 4 shows that conversion of CH_3OH into C_1-C_2 hydrocarbons occurs only to a limited extent, which makes methanol also an unlikely intermediate in the conversion of CO_2 to methane. The observed (slow) conversion of CH_3OH might be related to primary decomposition into CO or CO_2, and consecutive reaction of CO or CO_2 into hydrocarbons. Pretreatment of Ti-SBA-15 by HCOOH-impregnation resulted in even lower production of C_1-C_2 hydrocarbons than after CH_3OH-impregnation, which excludes HCOOH as significant intermediate in CO_2 reduction. However, a dramatic increase of CH_4 production was observed after HCHO addition to Ti-SBA-15, suggesting HCHO might be an important intermediate. Besides photocatalytically, this compound is also easy to decompose photochemically, as will be discussed later. The fact that this species was not observed in the IR spectra, is the consequence of the low photocatalytic and/or photochemical stability of this intermediate and the thus low transient concentration of this species.

Mechanism. Based on the above discussed observations, we propose a tentative mechanism of CO_2 reduction by H_2O over Ti-SBA-15, as shown in Figure 7. We follow the proposed route by Frei et al. to explain formation of CO. In this route, a Ti-OH site serves as the active site for the adsorption of CO_2 and H_2O. The photo-induced [Ti(III)-O(I)]* site delivers electrons to CO_2, splitting this into CO [36]. Oxidation of H_2O is proposed to occur among others through a hydroperoxo – Ti-OOH – intermediate. These reactions are most likely the primary steps in the formation of hydrocarbons as well. Due to the limited amount and short lifetime, Ti-OOH was not successfully detected by IR spectroscopy in the present study. Besides decomposition of the peroxide to oxygen [36], we propose a subsequent reaction of the peroxide with CO and H_2O to form HCHO, in which the hydroperoxo species is converted to Ti-OH by releasing one molecule of O_2. Based on the very high rate of CH_4 formation by the HCHO-pretreated Ti-SBA-15 system observed in Figure 4, the conversion of HCHO to CH_4 occurs effectively and fast by reaction with photo-activated H_2O, another molecule of O_2 being produced consequently. Unfortunately, the generation of O_2 was not demonstrated experimentally, probably because this is consumed by consecutive reactions, leading to e.g. CO, which was found to be formed in high quantities.

C_2H_4 and C_2H_6 are potential products of the reaction of two molecules of HCHO, in the presence or absence of H_2O, respectively. As shown in Figure 4, illumination of HCHO-impregnated Ti-SBA-15 yields CH_4 and C_2H_6, while C_2H_4 is barely formed. This suggest a significant quantity of water was still present in Ti-SBA-15 during this experiment, which is very likely given the followed procedure of pretreating Ti-SBA-15 with HCHO. It should be mentioned that the extremely high conversion of formaldehyde to hydracarbons is remarkable. In the literature, the photodecomposition of formaldehyde has been studied by mixing different quantities of formaldehyde in synthetic air [37]. CO and H_2 were found to be the major products upon illumination in the wavelength range of 290 – 330 nm. Pope and his coworkers have recently discussed the photochemistry in more detail. Besides the photon induced splitting of formaldehyde into CO and H_2, also other reactions have been proposed, in particular between OH-radicals and formaldehyde, leading to HCO and H_2O, or direct decomposition to HCO and H (below 330 nm). Subsequent oxidation of HCO by oxygen leads to HO_2 and CO. Photochemistry thus very likely significantly contributes to the observed product distribution in the formaldehyde experiment, including the formation and decomposition of peroxide intermediates [38]. However, the formation of CH_4 and C_2 products is not disclosed in these photochemistry studies, and potentially involves photocatalytic steps, as tentatively proposed in Figure 7.

Furthermore, it should be mentioned that our mechanism is a rather ‘global’ description. Obviously various additional intermediate steps have to be involved, but we cannot evaluate these based on the data presented in the present study. We like to mention the ESR data reported by Anpo and coworkers [17], which appear to indicate the presence of various radical fragments on the surface of the catalyst formulation during illumination, again in agreement with various pathways proposed for the photochemical decomposition of formaldehyde.

$$\text{-Ti-OH} + CO_2 \rightarrow \text{-Ti-OOH} + CO$$
$$[\ \text{-Ti-OH} + H_2O \rightarrow \text{-Ti-OOH} + H_2\ ]$$

$$\text{-Ti-OOH} + CO + H_2O \rightarrow \text{-Ti-OH} + H_2CO + O_2$$

$$\text{-Ti-OH} + H_2CO + H_2O \rightarrow \text{-Ti-OH} + H_2CH_2 + O_2$$

$$CO_2 + 2\ H_2O \rightarrow CH_4 + 2\ O_2$$

$$\text{-Ti-OH} + H_2CO + H_2CO \rightarrow \text{-Ti-OH} + H_2C{=}CH_2 + O_2$$

$$\text{-Ti-OH} + H_2CO + H_2CO + H_2O \rightarrow \text{-Ti-OH} + H_3C\text{-}CH_3 + {}^3/_2\ O_2$$

Figure 7. Proposed mechanism of photocatalytic CO_2 reduction with H_2O over Ti-SBA-15.

Catalyst alterations for improving performance. A significant extent of oxidation of hydrocarbons into CO or CO_2 was observed in Figure 3 (a) and (b). This is an important observation, which suggests that if oxygen produced in the reaction by water oxidation is not efficiently removed from the catalytic sites, this will inevitably lead to lower quantum efficiencies. Achieving this by for example pore structure optimization would be an important means to further improve performance of this intriguing photocatalytically active system. Another way forward would be to increase the number of "active sites" for CO_2 reduction. Trukhan et al. showed that a certain amount of Ti species might be embedded in the thick amorphous silica walls, with poor catalytic activity in oxidation reactions [39]. Extraction of these sites by e.g. mild steam treatment, might create a higher effective quantity of active sites. This might also improve the accessibility. An adverse effect might be the structural degradation of the catalysts and condensation of isolated sites to form TiO_2 nanocrystals after contact with water, which should be prevented [40].

Surface modification to enhancing CO_2 adsorption may be another solution to boost the effectivity of the catalytic sites. SBA-15 functionalization with Lewis bases (primary,

secondary and tertiary amines) was reported to increase the number of active sites for CO_2 activation, utilized in cyclic carbonate synthesis [41]. Future studies are needed to verify if the above mentioned structural changes will lead to improved performance.

Conclusions

In this chapter, a mechanism of CO_2 reduction over Ti-SBA-15 is presented, based on the reactivity of the catalyst in various initial gas mixtures of CO or CO_2, and H_2O, or H_2. The results indicate that the highest rate of hydrocarbon production is achieved with a mixture of CO and H_2O. H_2 activation is not as efficient as H_2O activation, probably due to a poor interaction with isolated Ti sites. We believe in a mechanism for CO_2 reduction in which CO and formaldehyde are important intermediates, and in which transient Ti-OOH species are likely involved.

Acknowledgements

This work was supported by ACTS (NWO, the Netherlands), in the framework of an NSC-NWO project (Project Number NSC-97-2911-I-002-002). The author kindly thanks Jarian Vernimmen, Vera Meynen and Pegie Cool at University of Antwerp for the fruitful collaboration and discussions on the Ti-SBA-15 catalysts. Ruben Lubkemann at University of Twente is gratefully acknowledged for technical support.

References

1. T. Inoue, A. Fujishima, S. Konishi and K. Honda, *Nature*, 1979, 277, 637-638.

2. K. R. Thampi, J. Kiwi and M. Gratzel, *Nature*, 1987, 327, 506-508.

3. H. Yamashita, A. Shiga, S. Kawasaki, Y. Ichihashi, S. Ehara and M. Anpo, *Energy Convers. Manage.*, 1995, 36, 617-620.

4. J. S. Hwang, J. S. Chang, S. E. Park, K. Ikeue and M. Anpo, *Top. Catal.*, 2005, 35, 311-319.

5. O. K. Varghese, M. Paulose, T. J. LaTempa and C. A. Grimes, *Nano Lett.*, 2009, 9, 731-737.

6. N. Sasirekha, S. J. S. Basha and K. Shanthi, *Appl. Catal., B*, 2006, 62, 169-180.

7. **I. H. Tseng, J. C. S. Wu and H. Y. Chou, *J. Catal.*, 2004, 221, 432-440.**
8. **H. C. Yang, H. Y. Lin, Y. S. Chien, J. C. S. Wu and H. H. Wu, *Catal. Lett.*, 2009, 131, 381-387.**
9. **K. Koci, K. Mateju, L. Obalova, S. Krejcikova, Z. Lacny, D. Placha, L. Capek, A. Hospodkova and O. Solcova, *Appl. Catal., B*, 2010, 96, 239-244.**
10. **Q. H. Zhang, W. D. Han, Y. J. Hong and J. G. Yu, *Catal. Today*, 2009, 148, 335-340.**
11. **H. Tsuneoka, K. Teramura, T. Shishido and T. Tanaka, *J. Phys. Chem. C*, 2010, 114, 8892-8898.**
12. **P. W. Pan and Y. W. Chen, *Catal. Commun.*, 2007, 8, 1546-1549.**
13. **Z. Y. Wang, H. C. Chou, J. C. S. Wu, D. P. Tsai and G. Mul, *Appl. Catal., A*, 2010, 380, 172-177.**
14. **Q. Liu, Y. Zhou, J. H. Kou, X. Y. Chen, Z. P. Tian, J. Gao, S. C. Yan and Z. G. Zou, *J. Am. Chem. Soc.*, 2010, 132, 14385-14387.**
15. **S. C. Yan, S. X. Ouyang, J. Gao, M. Yang, J. Y. Feng, X. X. Fan, L. J. Wan, Z. S. Li, J. H. Ye, Y. Zhou and Z. G. Zou, *Angew. Chem. Int. Ed.*, 2010, 49, 6400-6404.**
16. **C. J. Wang, R. L. Thompson, J. Baltrus and C. Matranga, *J. Phys. Chem. Lett.*, 2010, 1, 48-53.**
17. **M. Anpo, H. Yamashita, Y. Ichihashi and S. Ehara, *J. Electroanal. Chem.*, 1995, 396, 21-26.**
18. **N. Ulagappan and H. Frei, *J. Phys. Chem. A*, 2000, 104, 7834-7839.**
19. **C. C. Yang, Y. H. Yu, B. van der Linden, J. C. S. Wu and G. Mul, *J. Am. Chem. Soc.*, 2010, 132, 8398-8406.**
20. **H. Yamashita, Y. Fujii, Y. Ichihashi, S. G. Zhang, K. Ikeue, D. R. Park, K. Koyano, T. Tatsumi and M. Anpo, *Catal. Today*, 1998, 45, 221-227.**
21. **K. Ikeue, H. Mukai, H. Yamashita, S. Inagaki, M. Matsuoka and M. Anpo, *J. Synchrotron Radiat.*, 2001, 8, 640-642.**
22. **K. Ikeue, H. Yamashita, T. Takewaki, M. E. Davis and M. Anpo, *J. Synchrotron Radiat.*, 2001, 8, 602-604.**
23. **I. Keita, S. Nozaki, M. Ogawa and M. Anpo, *Catal. Today*, 2002, 74, 241-248.**
24. **K. Cassiers, T. Linssen, M. Mathieu, M. Benjelloun, K. Schrijnemakers, P. Van Der Voort, P. Cool and E. F. Vansant, *Chem. Mater.*, 2002, 14, 2317-2324.**

25. F. Q. Zhang, Y. Yan, H. F. Yang, Y. Meng, C. Z. Yu, B. Tu and D. Y. Zhao, *J. Phys. Chem. B*, 2005, 109, 8723-8732.

26. K. S. W. Sing, D. H. Everett, R. A. W. Haul, L. Moscou, R. A. Pierotti, J. Rouquerol and T. Siemieniewska, *Pure Appl. Chem.*, 1985, 57, 603-619.

27. C. Beck, T. Mallat, T. Burgi and A. Baiker, *J. Catal.*, 2001, 204, 428-439.

28. J. Pires, M. Pinto, J. Estella and J. C. Echeverria, *J. Colloid Interface Sci.*, 2008, 317, 206-213.

29. A. Fidalgo and L. M. Ilharco, *Chem. Eur. J.*, 2004, 10, 392-398.

30. G. Ricchiardi, A. Damin, S. Bordiga, C. Lamberti, G. Spano, F. Rivetti and A. Zecchina, *J. Am. Chem. Soc.*, 2001, 123, 11409-11419.

31. J. P. Gallas, J. C. Lavalley, A. Burneau and O. Barres, *Langmuir*, 1991, 7, 1235-1240.

32. K. E. Dierenfeldt, *J. Chem. Educ.*, 1995, 72, 281-283.

33. F. Saladin, L. Forss and I. Kamber, *J. Chem. Soc. Chem. Commun.*, 1995, 533-534.

34. R. T. Sanderson, *Chemical bonds and bond energy* 2nd ed., Academic Press, New York, 1976.

35. R. Nakamura, A. Imanishi, K. Murakoshi and Y. Nakato, *J. Am. Chem. Soc.*, 2003, 125, 7443-7450.

36. W. Y. Lin, H. X. Han and H. Frei, *J. Phys. Chem. B*, 2004, 108, 18269-18273.

37. G. K. Moortgat and P. Warneck, *J. Chem. Phys.*, 1979, 70, 3639-3651.

38. F. D. Pope, C. A. Smith, P. R. Davis, D. E. Shallcross, M. N. R. Ashfold and A. J. Orr-Ewing, *Faraday Discuss.*, 2005, 130, 59-72.

39. N. N. Trukhan, V. N. Romannikov, A. N. Shmakov, M. P. Vanina, E. A. Paukshtis, V. I. Bukhtiyarov, V. V. Kriventsov, I. Y. Danilov and O. A. Kholdeeva, *Microporous Mesoporous Mater.*, 2003, 59, 73-84.

40. M. J. Elser, T. Berger, D. Brandhuber, J. Bernardi, O. Diwald and E. Knozinger, *J. Phys. Chem. B*, 2006, 110, 7605-7608.

41. R. Srivastava, D. Srinivas and P. Ratnasamy, *Microporous Mesoporous Mater.*, 2006, 90, 314-326.

Chapter 6

Effect of Particle Size and Silica Scaffold on H_2O Oxidation Activity of Dispersed Cobalt Oxide

Abstract: Water oxidation over highly dispersed cobalt oxide particles in porous silica was studied, applying photo-activation of the $Ru(bpy)_3^{2+}$ photosensitizer complex and a sacrificial electron acceptor ($S_2O_8^{2-}$). 4 nm crystalline particles of Co_3O_4 dispersed in SBA-15, obtained by calcination of impregnated $Co(NO_3)_2$ in an NO/N_2 atmosphere, showed higher O_2 evolution rates than 7 nm Co_3O_4 particles, obtained by air calcination of the same catalyst precursor. A similar trend was observed for Co_3O_4 embedded in MCM-41, while MCM-41 catalysts showed lower O_2 production rates than SBA-15 catalysts of comparable Co_3O_4 sizes. The effect of the Co_3O_4-particle size is related to the amount of the Ru complex interacting with the surface sites of Co_3O_4, which subsequently induce water oxidation. The effect of the scaffold was demonstrated to be the consequence of the higher surface area of MCM-41 *vs* SBA-15 (~1000 m^2/g *vs* 600 m^2/g) and the consequently higher content of the $[Ru(bpy)_3]^{2+}$ photosensitizer complex adsorbed on the silica walls, which renders this inactive for water oxidation. However, the extent in differences in adsorption determined experimentally cannot entirely account for the activity difference between the two scaffolds. Therefore the lower accessibility of the Co_3O_4 surface sites in the MCM-41 scaffold for the Ru-complex is considered an additional factor for the lower activity of MCM-41 as compared to SBA-15. Furthermore, decreasing oxygen evaluation rates were observed, assigned to the degradation of the photosensitizer and leaching of Co^{2+} in solution as the result of acidic pH conditions.

Introduction

Photocatalytic water oxidation is an essential half reaction in the conversion of photon energy into useful fuels by reduction of CO_2. To evaluate the performance of inorganic oxides[1, 2], H_2O oxidation experiments are typically performed in the presence of the photosensitizer - $[Ru(bpy)_3]Cl_2 \cdot 6H_2O$, and a sacrificial electron acceptor, such as $Na_2S_2O_8$. Scheme 1 (Chapter 1) shows the principle of photocatalytic water oxidation using these reagents, as summarized by Hara et al.[3] After photon absorption, the photo-excited Ru complex is rapidly oxidized by the electron acceptor, $S_2O_8^{2-}$, yielding SO_4^{2-}. The oxidized Ru complex activates the water oxidation catalyst by reduction to the original oxidation state, $[Ru(bpy)_3]^{2+}$. The activated water oxidation catalyst oxidizes water to produce O_2 and H^+. Hydrolysis of the oxidized Ru complex is an unwanted side reaction, rendering the complex inactive for completion of the catalytic cycle. The photo-excited Ru complex is reasonably stable at pH 5, and hydrolysis of the complex dominating at lower pH.

Using the above cycle, Hara et al. found a turnover frequency in water oxidation catalyzed by colloidal IrO_2 of c.a. 0.2 s^{-1} *per* photosensitizer molecule.[3] Although IrO_2 is quite effective in H_2O oxidation, iridium is scarce in nature, which inevitably restricts practical application on a large scale. Recently, Jiao et al. showed Co_3O_4 supported on mesoporous SBA-15 is also an efficient O_2-evolving catalyst.[4] A turnover frequency (TOF) of 0.01 s^{-1} per surface Co center was reported for SBA-15/Co_3O_4 (4 wt-%), compared to that of only 0.0006 s^{-1} for micrometer-sized unsupported Co_3O_4 particles. A follow-up study on nano-structured manganese oxide clusters supported on mesoporous silica KIT-6 showed a turnover frequency of 0.6 $s^{-1}nm^{-2}$.[5] The oxygen yield of this material is 26 times larger than observed for micrometer-sized Mn_2O_3 particles. Various parameters determining the performance of the above mentioned silica scaffold supported catalysts have not yet been systematically investigated, such as the particle size of the metal oxides, as well as the structure of the applied silica-based support.

Confining the growth of crystallites by controlling the pore structure of the support has been reported. Li et al. showed cobalt catalysts supported on silica with different pore sizes.[6] The crystallite size of the Co_3O_4 was found to decrease in the order of Co/SBA-15 > Co/Silica gel > Co/MCM-48. Sietsma et al. demonstrated that the addition of NO during thermal decomposition of nitrate precursors allowed the preparation of small Ni and Co oxide nanoparticles.[7] A recent report discusses small particle sizes and uniform dispersions of cobalt

oxides deposited on SBA-15 and MCM-41 via moderated nitrate decomposition under nitric oxide (NO/Ar) calcination.[8]

In this article, various catalysts were compared in the water oxidation reaction, in particular focusing on dispersed Co_3O_4 over porous silica. It will be demonstrated that these catalysts are indeed very effective for water oxidation, while down-sizing of the Co_3O_4 particle size has a positive effect on the performance. The nature of the silica supports also showed an effect on the O_2 production.

Experimental Section

Catalysts preparation. Degussa P25 TiO_2, ZnO, SiC and Co_3O_4 are commercially available, and were used as received from Sigma-Aldrich. CuO/TiO_2 and ZnO/TiO_2 were prepared starting from Titanium (IV) butoxide (TBOT, $Ti\text{-}(OC_4H_9)_4$) by sol-gel methodology and under hydrothermal conditions, as described in a previous study[9], with the exception of the addition of PolyEthylene Glycol (PEG). Use of PEG was avoided to reduce the extent of carbon residue left in the catalyst formulations. The used metal-salt precursors were $Cu(NO_3)_2$ and $ZnCl_2$, respectively. Solid catalysts were obtained by treatment at 80°C for 28 h, filtration, drying at 150°C for 3 h, and calcination at 500°C for 5 h. NiO/TiO_2 was obtained by incipient wetness impregnation of Degussa P25 with nickel nitrate ($Ni(NO_3)_2{\cdot}6H_2O$). After drying at 80°C overnight, the catalyst precursor was calcined at 500°C for 6 h. Based on elemental analysis (ICP), the metal loading of the above samples amounted to 1.0 wt-% Cu, 1.2 wt-% Zn, and 1.1 wt-% Ni, respectively.

Ti-SBA-15 was synthesized by dissolving 4 g of a surfactant, pluronic P123 ($EO_{20}PO_{70}EO_{20}$), in 20 mL $HCl_{(aq)}$ and 130 mL water. After mixing overnight, 9.14 mL TEOS (tetraethylorthosilicate) and 300 μL TBOT (titanium (IV) butoxide) were added under vigorous stirring, which was maintained for 7.5 h at 45°C. The solution was aged overnight at 80°C in an oil bath. After filtration, washing, drying and calcination at 550°C for 6 h (1°C/min), Ti-SBA-15 was obtained. Pure SBA-15 was also prepared, following the same synthesis procedure without the addition of TBOT.

Catalysts consisting of cobalt oxide embedded in SBA-15 and MCM-41 were synthesized as follows. SBA-15 was prepared according to the recipe reported by Zhao et al., using aging at 80°C.[10] MCM-41 was synthesized using $C_{19}H_{42}NBr$ as template, and aging at 100°C, following the procedure reported by Cheng et al.[11] Prior to impregnation, the SBA-15 and

MCM-41 supports were dried at 80°C in dynamic vacuum to remove water from the pores. Subsequently, the scaffolds were impregnated to incipient wetness with a 3 M $Co(NO_3)_2$ solution as reported by Wolters et al.[8] After impregnation, the catalyst precursors were dried at 60°C for 12 h in stagnant air, and calcined at 240°C in a flow of air, or 1 % (v/v) NO/N_2 for 2 h. Air or NO calcined Co_3O_4-SBA-15 and Co_3O_4-MCM-41 were thus obtained. The intended loading is 12 wt-% of Co for Co_3O_4-SBA-15 samples and 19.4 wt-% of Co for Co_3O_4-MCM-41 samples. Based on elemental analysis (ICP), the cobalt loading of the above samples is 11.9 wt-% for the air calcined Co_3O_4-SBA-15, 11.5 wt-% for NO calcined Co_3O_4-SBA-15, 14.4 wt-% for air calcined Co_3O_4-MCM-41, and 13.8 wt-% for NO calcined Co_3O_4-MCM-41.

Catalyst characterization. Transmission Electron Microscopy (TEM) was performed using a Tecnai 20 apparatus, operated at 200 keV. Powder X-ray diffraction (XRD) patterns were obtained at room temperature from 30 to 60° 2θ with a Bruker-AXS D8 Advance X-ray Diffractometer setup using $CoK_{\alpha 12}$ radiation (λ = 0.179 nm). The average crystallite size of Co_3O_4 was calculated from the most intense lines at 43.1° (3 1 1) 2θ. The cobalt content was determined by inductively coupled plasma - optical emission spectrometry (ICP-OES), using a PerkinElmer Optima 3000 dV apparatus. The solid samples were firstly dissolved in a mixture of 1.25 % H_2SO_4 and 1 % HF solution to allow analysis. N_2-physisorption measurements were performed at -196°C, using a Micromeretics Tristar 3000 apparatus. Prior to the measurement, the samples were degassed in a flow of nitrogen at 300°C for 12 h.

Catalytic evaluation. Liquid phase photocatalytic H_2O oxidation was performed in a custom-built combinatorial photoreactor system, consisting of an array of multiple batch photoreactors, a compact gas chromatograph, and a valve system controlled by a user interface in LabView. In the applied setup, 12 cylindrical reactors (inner volume 50 mL) shared the same loop for gas dosage and sampling. The compact gas chromatograph was equipped with a TCD detector, and a combination of a Molsieve 5A (5 m) and a capillary Porabond Q column (10 m) for the separation of H_2, O_2, N_2, CO, and CH_4, respectively. Due to the short column length, and absence of a ramping procedure, quantitative data representing each reactor were obtained within 80 seconds. The applied light source was a 120 Watt high pressure mercury lamp. The spectrum of this mercury lamp ranges from 280 to 650 nm. A

bundle consisting of 12 quartz light guides was used to introduce the light into the 12 reactors, yielding an identical and rather homogeneous irradiance profile, as described in Chapter 4.

The photocatalytic H_2O oxidation experiments were performed in the presence of the photosensitizer - $[Ru(bpy)_3]Cl_2 \cdot 6H_2O$, and a sacrificial electron acceptor - $Na_2S_2O_8$. 75 mg of the catalyst was suspended in a 15 mL buffer solution. The buffer solution contains 0.022 M of Na_2SiF_6, and 0.028 M of $NaHCO_3$, yielding an initial pH of 5.3. $[Ru(bpy)_3]Cl_2 \cdot 6H_2O$, $Na_2S_2O_8$, and Na_2SO_4 were added in the respective concentrations of 0.002 M, 0.014 M, and 0.069 M. Three evacuation-helium purge cycles were applied to remove O_2 from the solution. The initial He pressure was 1.03 bar. Sampling was achieved by removing 0.3 mL of gas from the headspace of the reactor, and inserting it into the sampling loop every 15 min , for a total illumination period of 2 hours. The volume of the headspace is 21.4 mL. The amount of O_2 in these individual samples of 0.3 mL was quantified by the TCD of the GC.

To confirm if any leaching of cobalt occurred during illumination, the solution was filtered, diluted 10 times with 0.5 M $HNO_{3(aq)}$, and the cobalt concentration (ppm) measured by ICP-OES using the PerkinElmer Optima 3000 dV apparatus.

Results

Screening of catalytic activity in H_2O oxidation. Figure 1 shows a comparison of the performance of various catalytic formulations in H_2O oxidation. All experiments were repeated three times, in order to confirm reproducibility. The tested materials can be separated into four groups: dense phase metal oxides and carbides (TiO_2, ZnO, Co_3O_4, SiC), metal oxide promoted titania catalysts (CuO/TiO_2, ZnO/TiO_2, NiO/TiO_2), dispersed titania in porous materials (Ti-SBA-15), and dispersed cobalt oxide embedded in porous silica materials (Co_3O_4-SBA-15, Co_3O_4-MCM-41). Co_3O_4 yielded a similar O_2 quantity as ZnO after 2 hours of illumination. Both samples are more active than TiO_2 in H_2O oxidation. SiC showed no activity for H_2O oxidation, considering the O_2 production was similar to the background level of 0.3 μmol. This was expected based on the hydrophobicity of SiC. For the metal oxide promoted titania catalysts, only NiO was beneficial to the performance of TiO_2, showing an increase in O_2 production (0.8 μmol, *vs* 0.5 μmol for un-promoted TiO_2). Ti-SBA-15 is barely active in producing O_2 by water oxidation.

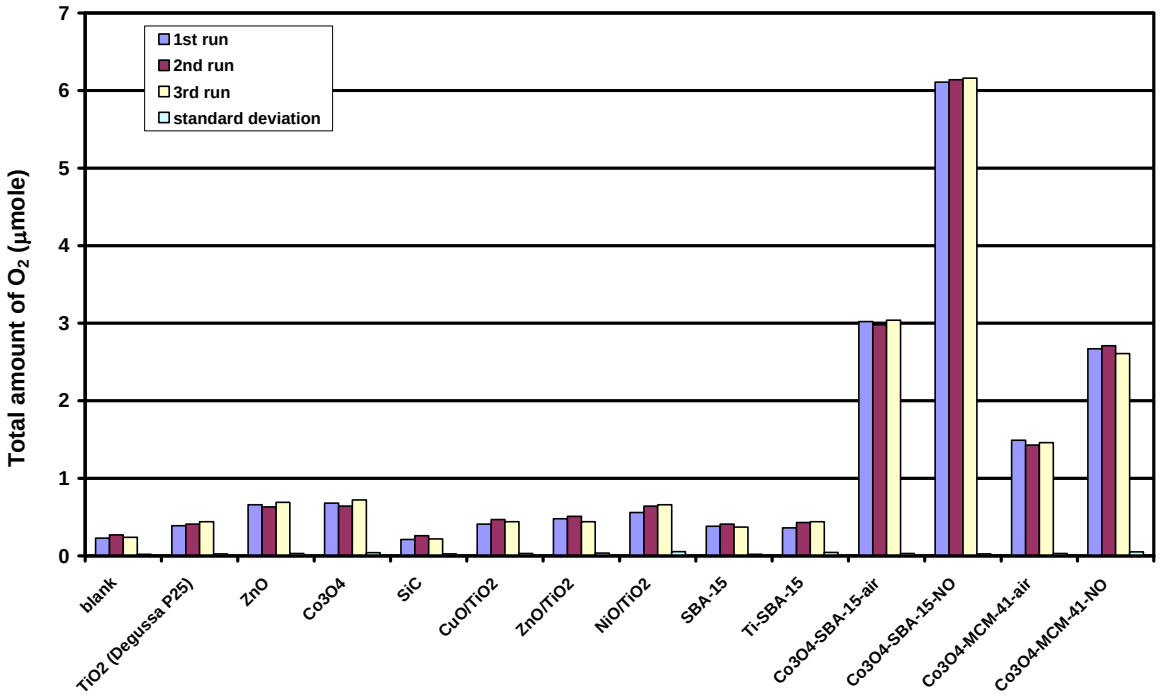

Figure 1. Total amount of O_2 present in the headspace of the reactor for various catalysts after 2 h of illumination. The measurements were performed for the suspended solution with the initial pH 5.3.

The catalysts based on dispersed cobalt oxide in porous silica materials, Co_3O_4-SBA-15 and Co_3O_4-MCM-41, show excellent performance in O_2 production, in particular compared to dense phase Co_3O_4. After 2 hours of illumination, an order in activity of Co_3O_4-SBA-15-$_{NO\ calcined}$ > Co_3O_4-SBA-15-$_{air\ calcined}$ > Co_3O_4-MCM-41-$_{NO\ calcined}$ > Co_3O_4-MCM-41-$_{air\ calcined}$ can be established. Among all these tested samples, dispersed Co_3O_4-SBA-15-$_{NO\ calcined}$ showed the highest O_2 production, 6.14 µmol after 2h of illumination. An increase of one order of magnitude in terms of O_2 production per Co_3O_4 site, as compared to dense phase Co_3O_4, can be calculated. In the following, a more detailed analysis of the activity of the Co-supported catalysts will be provided.

Dispersed cobalt oxide in SBA-15 or MCM-41. Figure 2 shows the time-profiled O_2 evolution curve of Co_3O_4-SBA-15 and Co_3O_4-MCM-41 calcined in air or 1%(v/v) NO/N_2, respectively. An amount of 3.7 µmol of O_2 was observed after 45 minutes of illumination for the Co_3O_4-SBA-15-air calcined sample. Continuing illumination for 2 hours, the O_2 quantity was slightly decreased to 3.0 µmol. The same O_2 production profile was observed for the

Co_3O_4-SBA-15-NO calcined sample. The evolution of O_2 reached 8.1 μmol after 45 minutes of illumination, and then decreased to 6.1 μmol after 2 hours of illumination. For the Co_3O_4-MCM-41-air calcined sample, 1.3 μmol of O_2 was produced after 40 minutes of illumination, leveling off to 1.5 μmol after 130 minutes. Finally, the Co_3O_4-MCM-41-NO calcined sample yielded a maximum of 3.1 μmol O_2 after 37 minutes of illumination decreasing to 2.7 μmol after 127 minutes. Overall, the NO calcined samples show higher O_2 production rates than the air calcined ones. Furthermore, SBA-15 appears the preferred support.

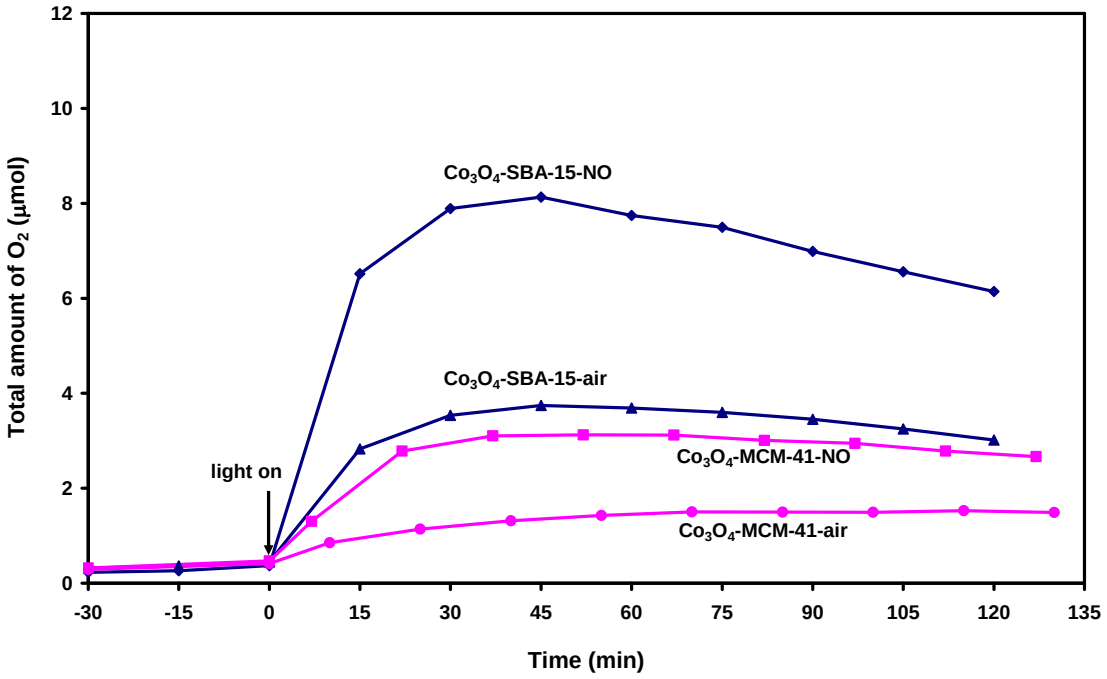

Figure 2. Total amount of O_2 in the headspace of the reactor as a function of time for Co_3O_4-SBA-15 and Co_3O_4-MCM-41 during illumination.

Leaching of dispersed Co_3O_4 during photoreaction. To establish the stability of the supported Co_3O_4 catalysts, the catalysts were filtered and added to a fresh buffer solution containing $Ru(bpy)_3Cl_2$ and $Na_2S_2O_8$, followed by a 2nd illumination period. Figure 3 compares the time-profiled O_2 production curves of the fresh and used Co_3O_4-SBA-15 samples. Comparable oxygen production curves were obtained for the fresh and used Co_3O_4-SBA-15-air calcined sample. However, a significant decrease in O_2 production rate was observed for the used Co_3O_4-SBA-15-NO calcined sample as compared to the fresh analogue. For the used catalyst, a maximum of 6.7 μmol O_2 was obtained after 45 min of illumination. The pH of the solution quickly decreased from 5.3 to 4.1 for the NO-calcined samples and 3.9

for the air-calcined samples after 45 min of photoreaction. Only slight decrease in pH occurred in the subsequent stages of the photoreaction, down to 3.9 and 3.8 for the NO- and air-calcined samples, respectively.

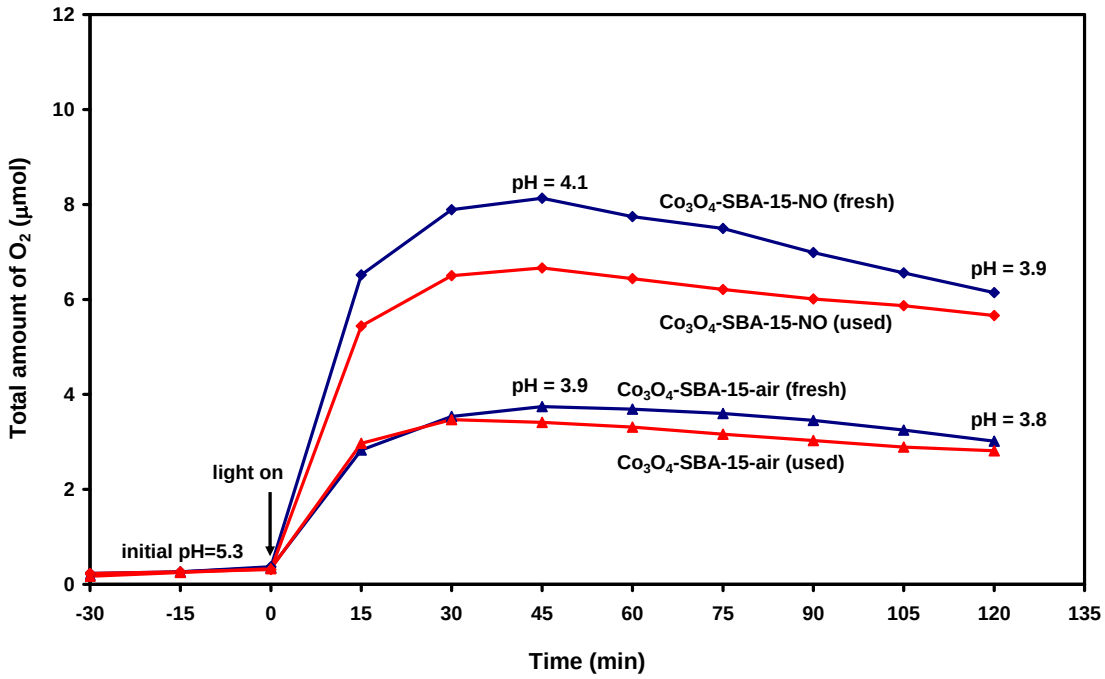

Figure 3. Total amount of O_2 in the headspace of the reactor as a function of time using Co_3O_4-SBA-15-NO or air calcined samples. The reaction was performed for used samples in order to evaluate the catalyst deactivation.

Elemental analysis of the filtered solutions after the first run, as well as analysis of the used catalysts, demonstrated significant Co-leaching of the Co_3O_4-SBA-15-NO calcined sample, with a decrease in Co-loading from 11.5 wt-% to 9.9 wt-%. Leaching was less severe for Co_3O_4-SBA-15-air calcined, as is indicated in Table 1. Leaching of Co_3O_4 was also observed for Co_3O_4–MCM-41 materials. The Co-loading of Co_3O_4-MCM-41-NO calcined sample decreased from 13.8 wt-% to 11.1 wt-%. Considering the acidic conditions in this system (pH 4~5), the most likely dissolution reaction for the Co_3O_4 is:

$$Co_3O_4 + 6H^+ \rightarrow 3Co^{2+} + H_2O + \frac{1}{2}O_2 \qquad (1)$$

Also Co^{3+} might be formed in solution, either by the direct dissolution of Co_3O_4 or by oxidation of Co^{2+} in solution by the persulfate or via the Ru dye. However, if Co^{3+} is formed

in solution at these pH values, it is thermodynamically unstable and expected to react with water, forming oxygen:

$$2Co^{3+} + H_2O \rightarrow 2Co^{2+} + 2H^+ + \frac{1}{2}O_2 \qquad (2)$$

Given the high initial oxygen evolution rate at pH values where reference experiments have shown the absence of O_2 evolution in the absence of the photosensitizer, the contribution to the total oxygen production of these leaching reactions is estimated to be small.

Table 1. Elemental analyses and textural properties of Co_3O_4-SBA-15 and Co_3O_4-MCM-41.

	cobalt loading (%)		cobalt (ppm)	crystalline size[c] Co_3O_4 (nm)		texture property		
sample	fresh	used[a]	filtrated solution[b]	fresh	used[a]	S_{BET} (m^2/g)	pore volume (mL/g)	pore diameter (nm)
SBA-15	-	-	-	-	-	603	0.7	8.2
Co_3O_4-SBA-15-air	11.9	11.7	19	7	8			
Co_3O_4-SBA-15-NO	11.5	9.85	73	4	5			
MCM-41	-	-	-	-	-	1092	1	3.7
Co_3O_4-MCM-41-air	14.4	13.0	20	4	4			
Co_3O_4-MCM-41-NO	13.8	11.1	77	3	3			

[a] The "used" sample denotes the one after 2 h photoreaction, filtration, and washing with 100 mL of de-ionized water.

[b] The filtrated solution was collected from the suspended solution after 2 h of photoreaction.

[c] The crystalline size of Co_3O_4 was determined by the most intense line in the XRD pattern at 43.1° (3 1 1).

Figure 4 shows TEM images of the fresh and used Co_3O_4-SBA-15 materials. For the fresh air calcined sample, Figure 4 (a), large particles deposited on the external surface and contained inside the pores of SBA-15 can be observed.[8] Different from the big clusters in the air calcined samples, NO calcined samples consist of a dark and strip-like morphology of Co-oxide along the pore of the supports, as shown in Figure 4 (b). For the used air calcined samples as shown in Figure 4 (c), the large and irregular deposition of Co_3O_4 clusters remained. Furthermore, the pore structure of SBA-15 appeared hardly affected. Also the morphology of the NO calcined catalyst was not affected by the water oxidation experiment.

The used NO calcined sample shows the strip-like pattern of small Co_3O_4 particles inside the pore structure of SBA-15, as demonstrated in Figure 4 (d). No distinguishable degrading of the support or particle size could be observed.

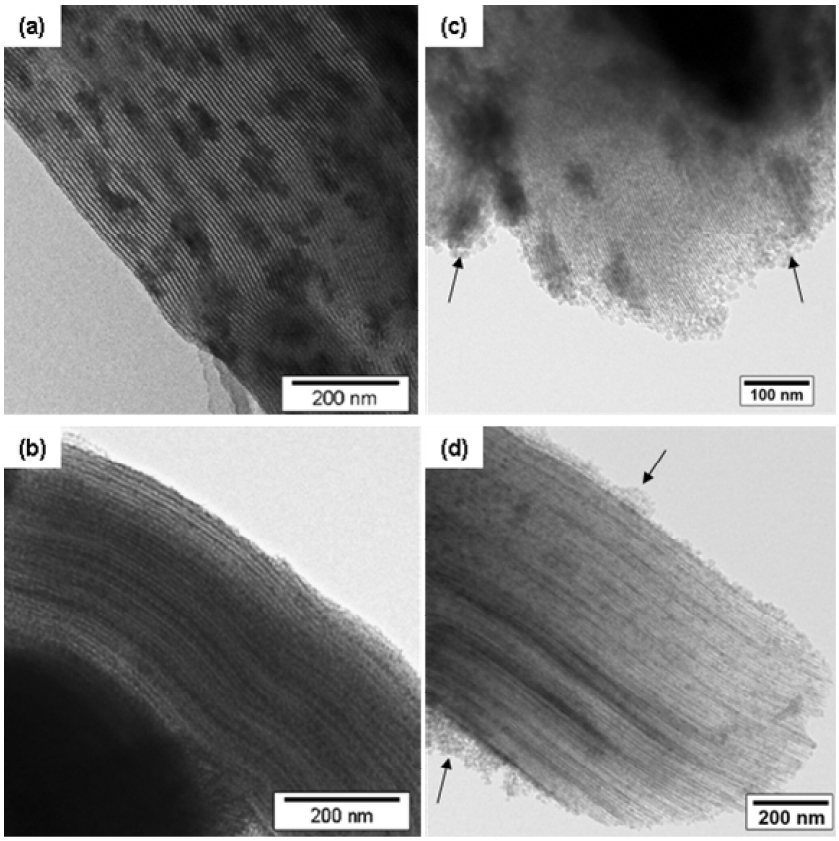

Figure 4. TEM images of the fresh Co_3O_4-SBA-15 (a) air and (b) NO calcined samples; compared with the used Co_3O_4-SBA-15 (c) air and (d) NO calcined samples.

However, some irregular deposits outside of SBA-15 were found for the samples after photoreaction, as the arrow indicates in Figure 4 (b) and 4 (d). This might be due to redeposition of cobalt species at the pore ending or outside of the SBA-15 particles during photoreaction. The crystalline sizes of Co_3O_4 were also calculated on the basis of respective XRD patterns, and included in Table 1. In general, the NO-calcined samples contain smaller crystalline sizes of Co_3O_4 than the air calcined samples. After photoreaction, there was no obvious change in XRD pattern, in agreement with the TEM data. The Co_3O_4 particle size observed in TEM images and the crystalline size determined by XRD demonstrate that the leaching for the NO calcined samples is more severe than for the air calcined samples. This is most likely due to the smaller particle size of Co_3O_4.

Further analysis of the effect of process conditions on performance. Although some leaching was observed for the applied Co-catalysts, this cannot account for the decreasing oxygen concentration observed in Figs. 2 and 3. Figure 5 summarizes experiments conducted to further establish the effect of variations in the applied catalyst evaluation procedure. It should be noted that the pH value of the solution decreased from 5.3 to 4.1 within the first 45 min of illumination (Figure 3). Due to the fact that the Ru complex is only stable at pH 5, the pH decrease causes significant hydrolysis of the Ru complex. A 0.4 M $NaOH_{(aq)}$ solution was therefore used to readjust the pH to 5.3. Adding subsequently fresh $Ru(bpy)_3Cl_2$ did not revive O_2 production. Simply adding $Na_2S_2O_8$ shows a slight increase in O_2 production to 2.5 µmol after 1 h illumination. The addition of both $Ru(bpy)_3Cl_2$ and $Na_2S_2O_8$ shows an only slightly stronger increase in O_2 evolution than addition of $Na_2S_2O_8$ alone. The fact that the performance of the system is not regained to the level of re-suspension of a filtered used catalyst in a fresh buffer solution (compare to Figure 3), is most likely the result of the much lower buffer capacity in a second use (after $NaOH_{(aq)}$ addition to readjust the pH to 5.3). The much more rapidly decreasing pH will limit the performance of the $Ru(bpy)_3Cl_2$.[3]

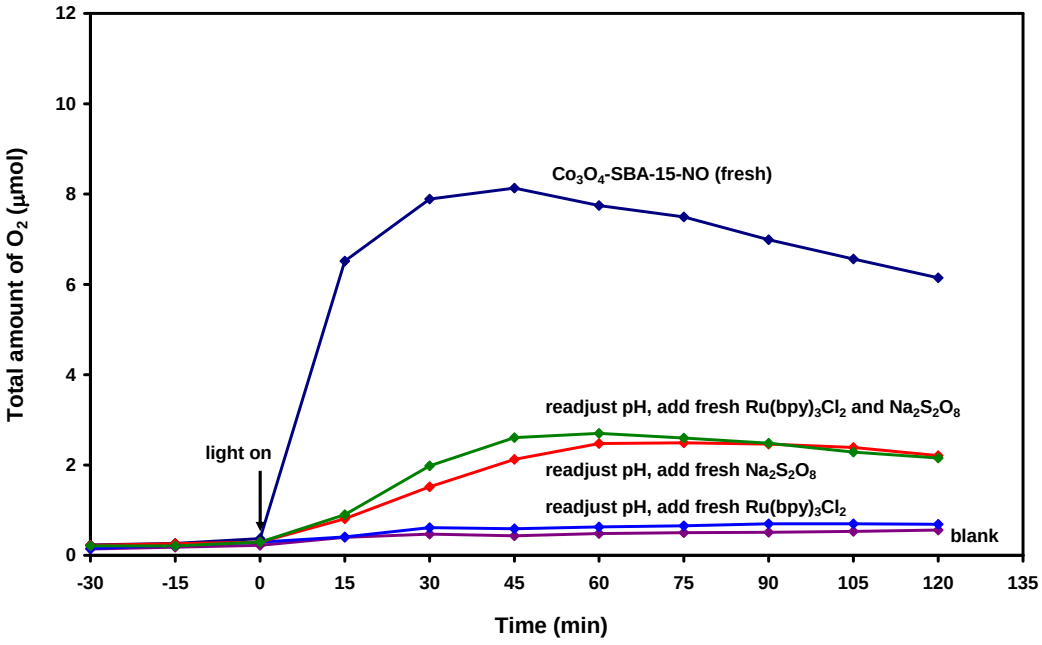

Figure 5. Total amount of O_2 in the headspace of the reactor as a function of time for the Co_3O_4-SBA-15-NO calcined sample. After the 1st photoreaction, the pH value was readjusted to 5.3 and fresh $Ru(bpy)_3Cl_2$, or $Na_2S_2O_8$, or both chemicals added, for initiating the 2nd photoreaction.

To further study the effect of process parameters on the rate of oxygen evolution, the amount of Co_3O_4-SBA-15-NO present in suspension was varied. Figure 6 (a) shows that 25 mg of catalyst in solution (containing 11.7 mg Co_3O_4), produced the highest O_2 amount of 12 µmol after 45 minutes of illumination. By increasing the suspension density of catalyst to 150 mg (containing 70.5 mg Co_3O_4), O_2 production significantly decreased to only 2 µmol after 45 min. Figure 6 (b) shows the trend in O_2 production obtained after 45 minutes (normalized by Co_3O_4 loading), as a function of Co_3O_4 loading. The more Co_3O_4 was loaded in the reaction mixture, the smaller the O_2 production.

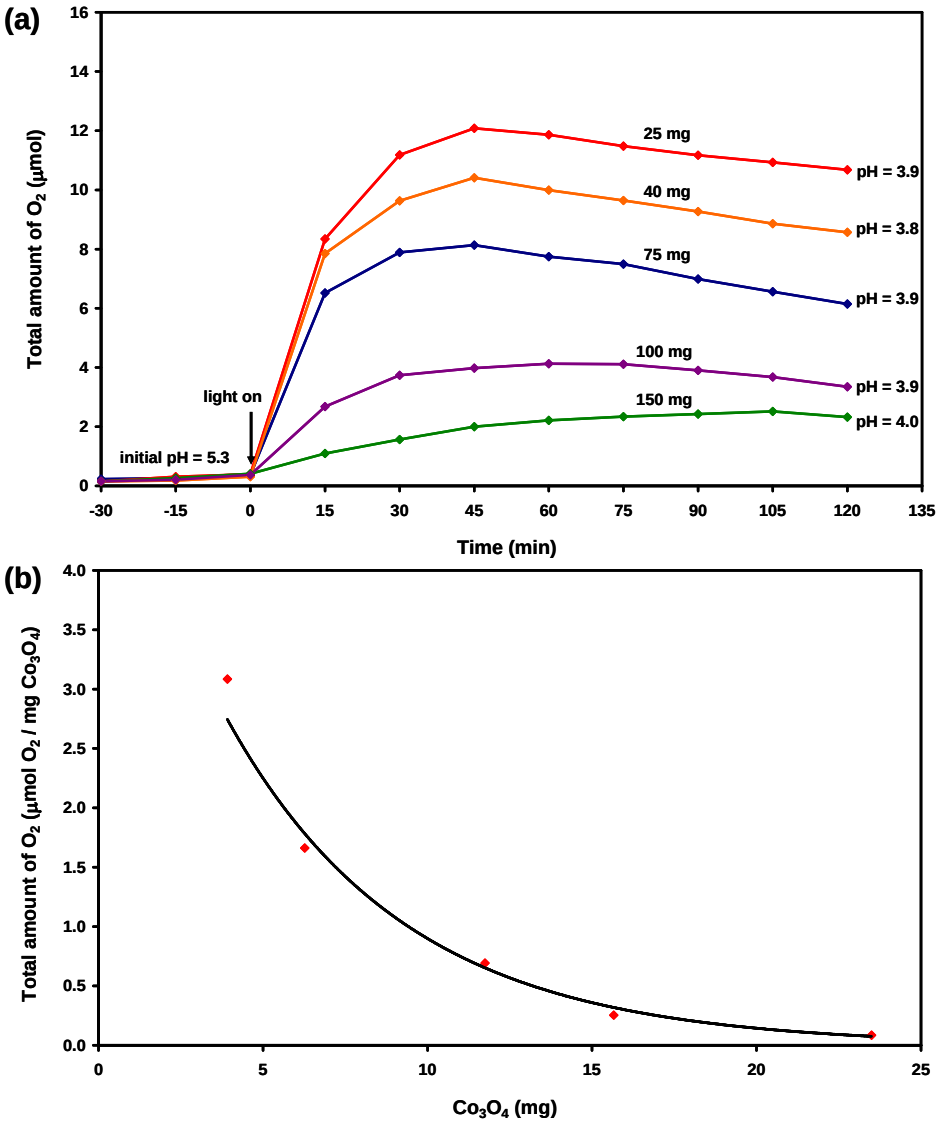

Figure 6. (a) Total amount of O_2 in the headspace of the reactor as a function of time for different amounts of Co_3O_4-SBA-15-NO. (b) The amount of O_2 produced after 45 min of illumination, normalized by Co_3O_4 loading, as a function of Co_3O_4 loading.

Both light distribution, and $[Ru(bpy)_3]^{2+}$ adsorption on the silica scaffold could explain this observation. To further evaluate this, the following experiment was performed and the results are shown in Figure 7. The reaction was conducted with the same amount of Co_3O_4-SBA-15-NO calcined catalyst as used in Figure 1, in the presence of a variable amount of (bare) SBA-15. Clearly, oxygen evolution significantly decreases as a function of increasing SBA-15 quantity, suggesting adsorption of the $[Ru(bpy)_3]^{2+}$ on the silica scaffold is affecting the performance. Indeed, SBA-15 obtained a light orange color, as observed after filtration.

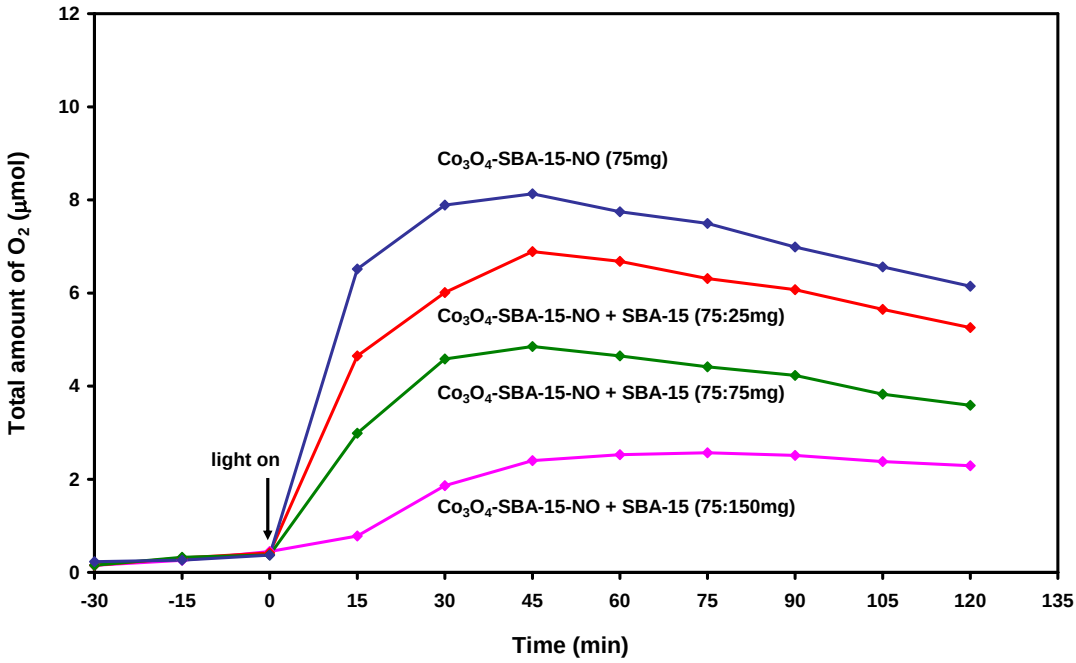

Figure 7. Total amount of O_2 in the headspace of the reactor as a function of time for Co_3O_4-SBA-15-NO, mixed with pure SBA-15 (75:25, 75:75, and 75:150 mg).

To further quantify the amount of adsorbed sensitizer, the used samples were analyzed after the photoreaction, filtration and washing with 100 mL of de-ionized water. The quantities are summarized in Table 2. After the photoreaction, each gram of pure SBA-15 contained 0.003 gram of Ru. Co_3O_4-SBA-15 contained 0.0023 g-Ru/g-catalyst for the air-treated samples, and 0.0025 g-Ru/g-catalyst for the NO-treated samples. Significantly higher quantities were obtained for the MCM-41 samples: Co_3O_4-MCM-41 showed 0.0068 g-Ru/g-catalyst for the air-treated sample, and 0.0073 g-Ru/g-catalyst for the NO-treated sample.

Table 2. Adsorption of the Ru complex on the (used) SBA-15, Co_3O_4-SBA-15 and Co_3O_4-MCM-41 samples.

sample[a]	Ru content (g per g-sample)
SBA-15	0.0030
Co_3O_4-SBA-15-air	0.0023
Co_3O_4-SBA-15-NO[b]	0.0025
Co_3O_4-MCM-41-air	0.0068
Co_3O_4-MCM-41-NO[b]	0.0073

[a] The used samples were dissolved in a mixture of 1.25 % H_2SO_4 and 1 % HF before ICP analysis.

[b] The fresh Co_3O_4-SBA-15-NO and Co_3O_4-MCM-41-NO samples showed a Ru content less than 0.0002 g/g-sample (below the detection limit of the ICP analysis).

Discussion

Comparison of screening results to literature reports. Screening of catalyst formulations clearly demonstrates that many unsupported metal oxides used in overall water splitting and/or CO_2 reduction are not very effective in catalyzing water oxidation. A few observations require further discussion. Addition of NiO enhanced activity of TiO_2 in water oxidation. NiO addition has been reported previously to promote the activity of TiO_2 in photocatalytic water decomposition.[12] Although the role of NiO as co-catalyst was predominantly assigned to promotion of H_2 evolution[13], we now demonstrate NiO also promotes water oxidation into O_2, albeit not very effectively.

Another result of interest is the low activity of the Ti-SBA-15 catalyst for water oxidation, although the UV induced photo-excited state is capable of reducing CO_2 in gas phase conditions.[14] It thus appears that the water oxidation step is limiting the performance of these catalysts, and linking this material to an efficient water oxidation catalyst should promote its performance. This has already been achieved by the group of Frei and coworkers[15], by linking photoactive systems to IrO_2 nano-particles. In view of the performance of the various investigated catalysts, the performance of the supported Co_3O_4 clusters is remarkable. Still, the best system in the present study, Co_3O_4-SBA-15-NO calcined, shows a 20 times lower O_2 evolution rate than reported for Co_3O_4-SBA-15 by Jiao.[4] The applied process conditions used in this study as compared to the study of Jiao et al. are summarized in Table 3. While it is

generally quite difficult to compare catalytic activity data obtained in different labs, various factors might determine the difference in performance. First, the calcination temperature of the catalysts was quite different. The NO/N_2 calcination procedure was performed at 240°C for 2 h, whereas the Co_3O_4-SBA-15 samples of Jiao were obtained by calcination at 500°C for 3 h in air.[4] As expected, the higher calcination temperature leads to a larger crystalline size of the Co_3O_4 particles (around 4 nm in our study, compared to spheroid-shaped clusters with diameters varying from 35 nm wide to 65 nm long in the reported results of Jiao[4]). The lower activity of our catalysts is thus quite remarkable, given the positive effect of a smaller particle size on improving water oxidation activity observed in Figure 1, and generally reported in the literature. For example, Mihai et al. have shown that smaller sizes of ZnO nanoparticles embedded in SBA-15 and MCM-41 yield higher rates in methylene blue photodegradation.[16]

Table 3. Comparison results with literature report on Co_3O_4-SBA-15 for water oxidation.

sample	Co_3O_4-SBA-15	Co_3O_4-SBA-15
source	Jiao et al.[4]	this study
sample weight (mg)	200	75
Co_3O_4 (mg)	8.4	11.7
suspension (mL)	40	15
Na_2SiF_6-$NaHCO_3$ (M)	0.022-0.028	0.022-0.028
$Na_2S_2O_8$ (M)	0.014	0.014
Na_2SO_4 (M)	0.069	0.069
$Ru(bpy)_3Cl_2$ (M)	0.002	0.002
light source	476 nm Ar ion laser	280-650 nm Hg lamp
irradiance (mW/cm^2)	93.75	151
initial pH (before illumination)	5.8	5.3
final pH (after illumination)	-	3.9
O_2 evolution after 45 min (μmole)	125	8.13
O_2 evolution after 2 h (μmole)	140	6.14

Further comparison shows that the Co_3O_4 content is different in both studies: effectively our suspension contained 11.7 mg of Co_3O_4, as compared to 8.4 mg Co_3O_4 in the reported data of Jiao.[4] Given the higher catalyst quantity, again one would assume a higher oxygen production rate in our experiment, which was not observed. It should be noted, however, that the Co_3O_4 catalysts are quite black. Light penetration into our reactor system might therefore have been less effective. Also given that the applied light source was different, this might at

least partly explain the data: in our study a 120 Watt high pressure Mercury lamp was used, with wavelengths ranging from 280 to 650 nm and a total irradiance of 151 mW/cm^2. The effective intensity between 400 and 500 nm, absorbed by the Ru-complex and inducing the desired metal-to-ligand charge transfer (MLCT)[17], amounted to 53 mW/cm^2. Jiao et al. used a 240 mW Argon ion laser, and a well defined emission at 476 nm. The beam of the light was expanded to 1.6 cm in diameter yielding an effective irradiance of 94 mW/cm^2. Reduced penetration of light into the suspension is also the most likely explanation for the reducing oxygen quantitity as a function of increasing catalyst density (Figure 6). The black supported Co_3O_4 particles strongly attenuate the light, leading to a very small effective reaction volume in the case of the highest catalyst loading (150 mg).

Both, $[Ru(bpy)_3]^{2+}$ adsorption and light penetration effects are evident from comparing the O_2 producing rates in experiments containing a total of 100 mg SBA-15 (Figs. 6 and 7): ~6.8 μmol is produced for 75 mg of the Co_3O_4-SBA-15-NO calcined catalyst combined with 25 mg bare SBA-15, as compared to only ~4 μmol for 100 mg of Co_3O_4-SBA-15-NO calcined. Light attenuation is, however, not the only factor determining the overall performance of the system. Another difference lies in the quantity of buffer solution. To maintain the same suspension composition when scaling down the total volume from 40 mL to 15 mL, the added amount of buffer solution was decreased, which leads to smaller capacity of the buffer to maintain the pH at ~5 during the photoreaction. As the results show in Figure 3, a quick decrease of pH occurred in the first 45 min of the photoreaction, corresponding to a leveling-off in O_2 concentration. When the pH of the solution deviates from 5, the Ru complex deactivates quickly, slowing down and eventually halting O_2 production. During each sampling, only 1.4 % of the head space volume (0.3 mL out of 21.4 mL) was introduced in the sampling loop and removed by evacuation, not sufficient to explain the observed decrease in O_2 production. It should be mentioned that CO was detected by TCD in the later stages of the photoreaction, in agreement with the study reported by Jiao[4]. The degradation of the Ru complex explains the formation of CO, which also accounts for the observed consumption of O_2. Concluding, the net result of O_2 production from H_2O oxidation, and O_2 consumption due to sampling and degradation of the Ru complex leads to a decrease in O_2 concentration after 45 min of the photoreaction, as shown in Figs. 2 to 6.

Particle size and silica support effect on O_2 production. As shown in Table 1, the NO calcined Co_3O_4-SBA-15 contains smaller crystalline Co_3O_4 particles (4 nm) than the air

calcined sample (7 nm). As the results show in Figure 2, the particle size affects O_2 evolution significantly. Smaller Co_3O_4 particles were obtained by NO pretreatment, leading to higher O_2 production. Also, for the MCM-41 supported catalysts, the smaller Co_3O_4 particles yielded improved performance. A positive effect of particle size on photocatalytic activity is generally observed in the literature. Anpo et al. reported the application of different sizes of anatase TiO_2 powder in photocatalytic hydrogenation of CH_3CCH.[18] Downsizing the particle size showed an increase in photocatalytic activity, especially for particles below 10 nm in size. Zhang and his coworkers prepared nanocrytalline TiO_2-based catalysts for photocatalytic decomposition of chloroform.[19] The results indicated an increase in activity when decreasing the particle size of the photocatalyst. The explanation for the particle size effects in photocatalysis is generally a decrease in chance of recombination of charge carriers in the interior of the crystals, and an increase in surface area leading to more efficient catalysis. The former explanation is not applicable here, since the photosensitizer is photo-activated, migrates to the active surface sites of Co_3O_4, and initiates the oxidation of water (as shown in Figure 1). Reducing the particle size and consequently increasing the surface area of Co_3O_4 thus facilitates the electron transfer between the photoexicited Ru complex and the Co_3O_4 surface and leads to a higher production of O_2.

However, particle size is not the only factor determining photocatalytic water oxidation activity. Other than the particle size effect, the silica support also showed an impact on O_2 evolution. The air-calcined Co_3O_4-SBA-15 sample possesses the same Co_3O_4 crystalline size as NO-calcined Co_3O_4-MCM-41 (4 nm). However, MCM-41 contains smaller pore sizes (3.7 nm) than SBA-15 (8.2 nm), resulting in a significantly higher surface area of MCM-41. The higher surface area of MCM-41 *vs* SBA-15 (~1000 m^2/g *vs* 600 m^2/g) will lead to a higher extent of the $[Ru(bpy)_3]^{2+}$ photosensitizer complex being adsorbed on the silica walls, which renders this inactive for Co_3O_4 oxidation. Table 2 summarizes the quantity of adsorbed Ru complex on the used samples after photoreaction, characterized by elemental analysis (ICP). The results clearly indicate a higher quantity of the Ru complex adsorbed on the MCM-41 support as compared to the SBA-15 support, which is likely diminishing the effectivity of the Co_3O_4-MCM-41 catalysts.

Finally, the accessibility of Co_3O_4 particles for the Ru complex is another factor affecting O_2 production. The bulky Ru complex needs to migrate into and inside the pores of the silica, where Co_3O_4 is located. Considering the diameter of Ru complex (1.3 nm[20]), it is more likely difficult for the complex to reach Co_3O_4 particles inside the smaller pores of MCM-41, than

the case for the bigger pores of SBA-15. In this regard, only part of the active sites – Co_3O_4 – can be efficiently used for water oxidation, resulting in lower O_2 production for the MCM-41 supported materials.

Conclusions

We demonstrate that Co_3O_4 supported on silica scaffolds is very active in photocatalytic water oxidation. Reducing the size of the Co_3O_4 nano-particles enhances the performance. The initial activity in O_2 production is influenced by the particle size and the amount of photosensitizer near Co_3O_4. However, deactivation of the photosensitizer is almost immediate due to lowering of the pH and consequent degradation of the Ru complex. This deactivation might also affect the quantification of O_2 in the later stages of the photoreaction, and hence activity comparison should be evaluated with care. Compared to Co-MCM-41, Co-SBA-15 shows a higher rate in O_2 production at comparable particle size, likely the result of better accessibility of the pores and the lower surface area of SBA-15, and consequently less severe immobilization of the $[Ru(bpy)^3]^{2+}$ complex, which renders this inactive for H_2O oxidation. Leaching of Co_3O_4 was also observed during photoreaction, leading to diminishing rates in O_2 production. Maintaining the solution at pH above 5 is thus not only crucial for the stability of the $[Ru(bpy)^3]^{2+}$ complex, but also to prevent leaching of Co^{2+}.

Acknowledgements

This work was supported by ACTS (NWO, the Netherlands), in the framework of an NSC-NWO project (Project Number NSC-97-2911-I-002-002). The author kindly acknowledges Tamara M. Eggenhuisen, Mariska Wolters, Petra E. de Jongh and Krijn P. de Jong at Utrecht University (UU) for the collaboration and fruitful discussions on the dispersed cobalt oxide materials, and Jarian Vernimmen at University of Antwerp and Yi-Hui Yu at National Taiwan University for providing photocatalysts. The author kindly thanks Hans Meeldijk and Cor van der Spek (UU) for the STEM and TEM analysis. Ruben Lubkemann at University of Twente is gratefully acknowledged for technical support.

References

1. **J. Kiwi and M. Gratzel, *Angew. Chem. Int. Ed.*, 1978, 17, 860-861.**
2. **A. Harriman, I. J. Pickering, J. M. Thomas and P. A. Christensen, *J. Chem. Soc., Faraday Trans. 1*, 1988, 84, 2795-2806.**
3. **M. Hara, C. C. Waraksa, J. T. Lean, B. A. Lewis and T. E. Mallouk, *J. Phys. Chem. A*, 2000, 104, 5275-5280.**
4. **F. Jiao and H. Frei, *Angew. Chem. Int. Ed.*, 2009, 48, 1841-1844.**
5. **F. Jiao and H. Frei, *Chem. Commun.*, 2010, 46, 2920-2922.**
6. **H. L. Li, J. L. Li, H. K. Ni and D. C. Song, *Catal. Lett.*, 2006, 110, 71-76.**
7. **J. R. A. Sietsma, J. D. Meeldijk, J. P. den Breejen, M. Versluijs-Helder, A. J. van Dillen, P. E. de Jongh and K. P. de Jong, *Angew. Chem. Int. Ed.*, 2007, 46, 4547-4549.**
8. **M. Wolters, L. J. W. van Grotel, T. M. Eggenhuisen, J. R. A. Sietsma, K. P. de Jong and P. E. de Jongh, *Catal. Today*, 2011, 163, 27-32.**
9. **C. C. Yang, Y. H. Yu, B. van der Linden, J. C. S. Wu and G. Mul, *J. Am. Chem. Soc.*, 2010, 132, 8398-8406.**
10. **D. Y. Zhao, J. L. Feng, Q. S. Huo, N. Melosh, G. H. Fredrickson, B. F. Chmelka and G. D. Stucky, *Science*, 1998, 279, 548-552.**
11. **C. F. Cheng, D. H. Park and J. Klinowski, *J. Chem. Soc., Faraday Trans.*, 1997, 93, 193-197.**
12. **K. Sayama and H. Arakawa, *J. Photochem. Photobiol., A*, 1994, 77, 243-247.**
13. **A. Kudo, *Catal. Surv. Asia*, 2003, 7, 31-38.**
14. **J. S. Hwang, J. S. Chang, S. E. Park, K. Ikeue and M. Anpo, *Top. Catal.*, 2005, 35, 311-319.**
15. **H. X. Han and H. Frei, *J. Phys. Chem. C*, 2008, 112, 16156-16159.**
16. **G. D. Mihai, V. Meynen, M. Mertens, N. Bilba, P. Cool and E. F. Vansant, *J. Mater. Sci.*, 2010, 45, 5786-5794.**
17. **S. Campagna, F. Puntoriero, F. Nastasi, G. Bergamini and V. Balzani, in *Photochemistry and Photophysics of Coordination Compounds I*, Springer-Verlag Berlin, Berlin, 2007, vol. 280, pp. 117-214.**
18. **M. Anpo, T. Shima, S. Kodama and Y. Kubokawa, *J. Phys. Chem.*, 1987, 91, 4305-4310.**

19. Z. B. Zhang, C. C. Wang, R. Zakaria and J. Y. Ying, *J. Phys. Chem. B*, 1998, 102, 10871-10878.

20. C. V. Kumar and Z. J. Williams, *J. Phys. Chem.*, 1995, 99, 17632-17639.

Chapter 7

Summary and Prospect for Photocatalytic CO_2 Activation

Summary

Photocatalytic activation of CO_2 and water has potential for producing fuels by conversion of photon energy. However, the low productivity still limits practical application. In this study, the goal was to gain more fundamental insight in CO_2 activation, and to provide guidelines for rational design of improved photocatalytic systems.

In **Chapter 2**, in-situ IR spectroscopy (DRIFTS) was used to explore the surface chemistry in converting CO_2 and H_2O of a Cu(I)/TiO_2 catalyst, reported quite effective for CO_2 conversion in the literature. When filled with $^{13}CO_2$, both ^{13}CO and ^{12}CO were observed during illumination on the copper-loaded titania, Cu(I)/TiO_2. The former is clear evidence of CO_2 reduction. The latter, ^{12}CO, originates from the carbon residue left from the synthesis procedure. Apparently carbon residue is not completely removed by calcination, even though weight loss from the material is no longer observed in thermal gravimetric analysis (TGA) in oxidative environment. ^{12}CO evolution was found to be significantly reduced by omission of polyethylene glycol (PEG) from the synthesis procedure, or pretreatment of the catalyst by prolonged exposure to illumination in the presence of moist air. The thus produced hydroxyl radicals are more effective to remove carbon residue, as compared to high temperature calcination. It is demonstrated that gas phase $^{13}CO_2$ reduction into ^{13}CO can occur over titania-based catalysts, where Cu(I) not only acts as co-catalysts as proposed in the literature[1-5], but also provides for an excellent probe to detect CO in infrared experiments.

TiO_2 surfaces show a rich carbonate/bicarbonate/carboxylate chemistry, when exposed to CO_2. Surface carbonate species were found to be more stable than bicarbonate and carboxylate species, when a preloaded CO_2 sample was flushed with He, as demonstrated in **Chapter 3.** Furthermore, it was demonstrated that pretreatment of TiO_2 surfaces by carbonate (Na_2CO_3) impregnation, resulted in evolution of CO when illuminated in inert environment, Helium. Carbonate decomposition leads to CO formation. Increasing the surface content of carbonate, by changing the concentration of the Na_2CO_3 solution used for impregnation, showed increasing ^{12}CO quantities, further evidence for a role of carbonates in CO formation over TiO_2 based catalysts. When $^{13}CO_2$ was introduced to Na_2CO_3-impregnated samples, more ^{13}CO and ^{12}CO evolved in comparison to pure Cu(I)/TiO_2. This result suggests a route of surface carbonate enhanced photocatalytic CO_2 reduction.

In **Chapter 4**, a parallel photoreactor system is presented, applied in gas phase photocatalytic CO_2 reduction. Due to the diversity in catalytic systems reported in the

literature, as well as the reaction conditions, the apparatus was designed as a platform for the comparison of photocatalytic activity under identical conditions. A homogeneous irradiance and temperature profile was established as a necessary basis. Fully automated gas sampling and quick analysis by a compact gas chromatograph allows a high throughput analysis for 12 samples at a time. The catalyst screening results showed that dispersed titania in a porous silica support, Ti-SBA-15, is the most active catalyst in CH_4 production. Ti-SBA-15 was therefore used as reference sample to further evaluate the parallel photoreactor system. An optimized catalyst loading in the reactor was found to be 0.2 g. Higher quantities negatively influence the light distribution, resulting in lower CH_4 production. The apparent quantum yield (AQY), which is generally considered as the index of photon-into-chemical conversion to evaluate the performance of a sample, can be easily calculated in this system. However, the ambiguity of the apparent quantum yield was discussed. Ti-SBA-15, for example, has an extremely small absorption cross section in the UV range (200-250 nm), which leads to a very low AQY, 6.7×10^{-5} %, when considering the whole incident spectrum of the light source (280-650 nm). Certainly improving the light absorption properties of Ti-SBA-15 is necessary to further enhance the AQY and solar to fuel productivity.

A mechanistic study of photocatalytic CO_2 reduction over Ti-SBA-15 is reported in **Chapter 5**. Different gas mixtures containing CO, CO_2, H_2O or H_2 were exposed to illumination in the presence of Ti-SBA-15, in order to clarify the route to hydrocarbons in photocatalytic CO_2 reduction over this photocatalyst. A mixture of CO and H_2O led to the highest quantities of CH_4, C_2H_4, and C_2H_6 after 7 hours of reaction, whereas a mixture of CO_2 and H_2 lead to the lowest production rate of these products. H_2O is thus more efficient in activation of CO and CO_2 than H_2. CH_3OH was not detected as significant product, and when fed to the catalyst, did not yield extensive product formation. Formaldehyde was found very reactive over the catalytic system, yielding a product distribution (C_1-C_3) of similar nature as obtained by CO activation. Finally, the backward reaction, hydrocarbon oxidation into CO or CO_2, was found significant over this catalyst system. Based on the experimental activity profiles, results indicated above, and available literature, a mechanism for photocatalytic CO_2 reduction is proposed involving formation of CO in the initial stages, followed by consecutive formation of formaldehyde, which converts to CH_4, C_2H_4, and C_2H_6, presumably by reaction with photo-activated H_2O (OH radicals). Photo-induced Ti(III)-O(I) sites initiate CO_2 and H_2O splitting into CO, as proposed in the literature[6]. Also peroxide species are likely involved as intermediates in the reaction.[7]

The half reaction of water oxidation was also investigated. **Chapter 6** is focused on the study of materials active in photocatalytic water oxidation. Screening results showed dispersed cobalt oxide in porous silica (Co_3O_4-SBA-15) as most active in O_2 evolution during illumination. The particle size of cobalt oxide, Co_3O_4, was controlled by tuning the calcinations environment, NO/Ar or air.[8] Smaller Co_3O_4 particles were obtained by NO/Ar treatment. Water oxidation over highly dispersed cobalt oxide particles in porous silica was studied, applying photo-activation of the $Ru(bpy)_3^{2+}$ photosensitizer complex and a sacrificial electron acceptor ($S_2O_8^{2-}$). Co_3O_4 particles of 4 nm dispersed in SBA-15, obtained by calcination of impregnated $Co(NO_3)_2$ in an NO/Ar atmosphere, showed higher O_2 evolution rates than 7 nm Co_3O_4 particles, obtained by air calcination of the same catalyst precursor. A similar trend was observed for Co_3O_4 embedded in MCM-41, while MCM-41 catalysts showed lower O_2 production rates than SBA-15 catalysts of comparable Co_3O_4 sizes. The effect of the scaffold was demonstrated to be the consequence of the higher surface area of MCM-41 *vs* SBA-15 (~1000 m^2/g *vs* 600 m^2/g) and the consequently higher content of the $[Ru(bpy)_3]^{2+}$ photosensitizer complex adsorbed on the silica walls, which renders this inactive for Co_3O_4 oxidation. Furthermore, deactivation of the investigated Co_3O_4 catalysts was observed, assigned to leaching of Co^{2+} in solution as the result of acidic pH conditions.

Prospect

To mimic photosynthesis by activating CO_2 with H_2O, two half reactions – CO_2 reduction and H_2O oxidation – were studied and described in this dissertation. The screening results show that dispersed titania and cobalt oxide in porous silica SBA-15 are active in photocatalytic CO_2 reduction and H_2O oxidation, respectively. The prospect is to link these two catalysts together and achieve higher conversion of CO_2 into hydrocarbons. Figure 1 shows the idea of combining CO_2 reduction and H_2O oxidation in a system containing the photosensitizer, $[Ru(bpy)_3]^{2+}$. The band position of Ti-SBA-15 and Co_3O_4-SBA-15 is still imaginary. The objective is to make use of the visible light sensitivity of the photosensitizer to drive these two reactions, without any addition of electron donors or acceptors. When the photosensitizer $[Ru(bpy)_3]^{2+}$ is excited by visible light, the excited Ru complex will be oxidized by electron injection into Ti-SBA-15, leading to CO_2 reduction. Meanwhile, the catalytic cycle of the Ru complex will be completed by collecting electrons from Co_3O_4-SBA-15, which were generated by water oxidation. Assembly of the system in a nano-scaled silica

wall has the advantages, not only to obtain a small crystallite size, but also because it transmits protons fast on the time scale of catalytic turnover, but yet is impermeable to small molecules like O_2.[9] The material may act as a membrane for separating reduction and oxidation sites.

The challenge of this catalytic system lies in establishing efficient charge transfer between reduction catalyst (Ti-SBA-15), oxidation catalyst (Co_3O_4-SBA-15) and photosensitizer. Slow charge transfer will lead to charge accumulation, and eventually eliminate the reaction. This requires extensive knowledge on the band position of the dispersed metal oxides in porous silica materials.

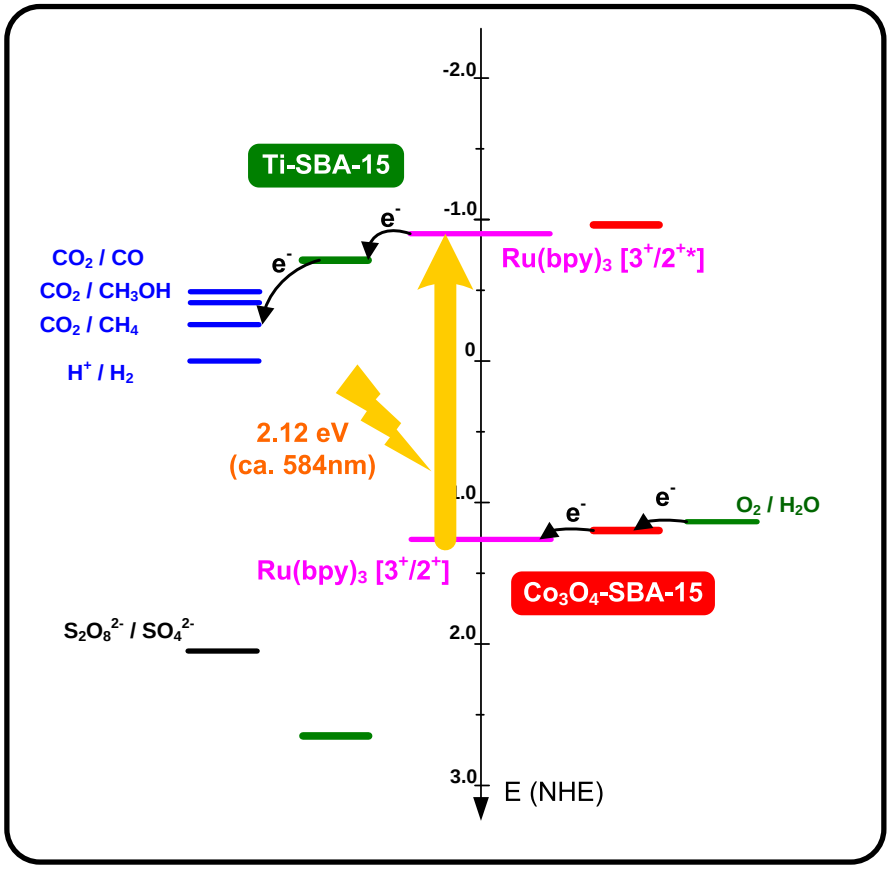

Figure 1. Schematic illustration of artificial photosynthesis with aid of the $[Ru(bpy)_3]^{2+}$ - catalyst system.

References

1. **O. Ishitani, C. Inoue, Y. Suzuki and T. Ibusuki, *J. Photochem. Photobiol., A*, 1993, 72, 269-271.**
2. **I. H. Tseng, W. C. Chang and J. C. S. Wu, *Appl. Catal., B*, 2002, 37, 37-48.**
3. **I. H. Tseng, J. C. S. Wu and H. Y. Chou, *J. Catal.*, 2004, 221, 432-440.**
4. **O. K. Varghese, M. Paulose, T. J. LaTempa and C. A. Grimes, *Nano Lett.*, 2009, 9, 731-737.**
5. **H. C. Yang, H. Y. Lin, Y. S. Chien, J. C. S. Wu and H. H. Wu, *Catal. Lett.*, 2009, 131, 381-387.**
6. **M. Anpo, H. Yamashita, Y. Ichihashi and S. Ehara, *J. Electroanal. Chem.*, 1995, 396, 21-26.**
7. **W. Y. Lin, H. X. Han and H. Frei, *J. Phys. Chem. B*, 2004, 108, 18269-18273.**
8. **M. Wolters, L. J. W. van Grotel, T. M. Eggenhuisen, J. R. A. Sietsma, K. P. de Jong and P. E. de Jongh, *Catal. Today*, 2010.**
9. **H. Frei, *Chimia*, 2009, 63, 721-730.**

Chapter 8

Nederlandse Samenvatting

Samenvatting en toekomst perspectief voor fotokatalytische CO_2 activering

Samenvatting

De fotokatalytische activering van CO_2 en water biedt mogelijkheden om brandstoffen te produceren door omzetting van de in fotonen beschikbare energie. De praktische toepassing wordt echter gelimiteerd door de lage productiviteit van de fotokatalysatoren. Het doel van deze studie is daarom om meer inzicht te krijgen in de fundamentele aspecten van CO_2 activering en om daarnaast richtlijnen te verschaffen voor het systematisch ontwerpen van betere fotokatalytische systemen.

In **Hoofdstuk 2** is in-situ IR spectroscopy (DRIFTS) gebruikt om de oppervlakte chemie te verkennen voor de omzetting van CO_2 en H_2O op een Cu(I)/TiO_2 katalysator, die in literatuur beschreven staat als een goede katalysator voor CO_2 omzetting. Wanneer $^{13}CO_2$ gas was gebruikt, werd gedurende de belichting van de Cu(I)/TIO_2 katalysator zowel ^{13}CO als ^{12}CO waargenomen. De vorming van ^{13}CO is een duidelijk bewijs van CO_2 reductie. Aan de andere kant vindt ^{12}CO zijn oorsprong in de resten koolstof die zijn achtergebleven na de katalysator synthese. Blijkbaar worden de koolstofresten dus niet volledig verwijderd door het calcineren, zelfs als er geen gewichtsafname van het materiaal meer waarneembaar is bij een thermo-gravimetrische analyse (TGA) in een oxidatieve omgeving. De vorming van ^{12}CO bleek flink af te nemen wanneer de synthese zonder polyethyleen glycol (PEG) werd uitgevoerd of wanneer bij de voorbehandeling de katalysator langdurig werd belicht in de aanwezigheid van vochtige lucht. De gevormde hydroxyl radicalen zijn dus veel effectiever in het verwijderen van de koolstof resten dan dat het calcineren bij hoge temperaturen is. Het is dus aangetoond dat gas fase ^{13}CO reductie naar ^{13}CO kan plaats vinden op een titania gebaseerde katalysator. Hierbij functioneert Cu(I) niet alleen als cokatalysator, zoals beweerd in de literatuur, maar ook als een uitstekende sensor om CO waar te nemen in infrarood experimenten.

Op het oppervlak van TiO_2, wanneer bloot gesteld aan CO_2, wordt een grote verscheidenheid aan carbonaten, bicarbonaten en carboxylaten waargenomen. In **Hoofdstuk 3** wordt aangetoond dat carbonaten, gevormd ten gevolge van CO_2 adsorptie, op het TiO_2 oppervlak stabieler zijn dan bicarbonaten en carboxylaten. Daarnaast is ook aangetoond dat indien een TiO_2 oppervlak is geïmpregneerd met carbonaat (Na_2CO_3), er bij belichting in een inerte omgeving van helium, CO vrijkomt. Blijkbaar veroorzaakt het uiteenvallen van het carbonaat de vorming van CO. Wanneer de hoeveelheid carbonaat op het oppervlak werd

vergroot door het gebruik van hogere concentraties Na_2CO_3 in de impregnatie oplossing, werden grotere hoeveelheden CO waargenomen. Dit versterkt het bewijs dat de carbonaten een rol spelen bij de vorming van CO op een TiO_2 gebaseerde katalysator. Wanneer een met Na_2CO_3 geïmpregneerde Cu(I)/TiO_2 katalysator wordt vergeleken met een schone Cu(I)/TiO_2 katalysator, blijkt dat indien $^{13}CO_2$ wordt gebruikt, zowel meer ^{13}CO als ^{12}CO vrijkomt. Deze resultaten doen vermoeden dat de carbonaten aan het oppervlak de fotokatalytische CO_2 reductie bevorderen.

In **Hoofdstuk 4** wordt een parallel fotoreactor systeem gepresenteerd, dat gebruik wordt voor evaluatie van fotokatalytische CO_2 reductie in de gas fase. Door de verscheidenheid van katalytische systemen beschreven in literatuur, almede door de verscheidenheid in reactiecondities, is dit fotokatalytisch reactor systeem ontwikkeld om een vergelijking van de activiteit van verschillende fotokatalysatoren onder gelijke omstandigheden mogelijk te maken. Een hiervoor noodzakelijke homogene belichting en temperatuursprofiel zijn bewerkstelligd. Door een volledig geautomatiseerd gas monstername systeem en een snelle analyse met een compacte gaschromatograaf is het mogelijk 12 monsters simultaan te evalueren. Uit de resultaten van de katalysator evaluatie bleek dat titania gedispergeerd in een poreuze silica drager, Ti-SBA-15, de meest actieve katalysator is voor de productie van CH_4 vanuit CO_2 en H_2O. Ti-SBA-15 is daarom geselecteerd als referentie voor de verdere evaluatie van het fotoreactor systeem. Een optimale hoeveelheid katalysator in de reactor blijkt 0.2 gram te zijn. Grotere hoeveelheden hebben een negatieve invloed op de verdeling van het licht, hetgeen een lagere CH_4 productie tot gevolg heeft. Voor dit systeem kan de zichbare quantum opbrengst (AQY) gemakkelijk berekend worden. De AQY wordt beschouwd als de methode om de omzetting van fotonen naar chemicaliën te evalueren, alsmede de prestatie van de katalysator. De berekening van de zichtbare quatum opbrengst geeft ook aanleiding tot discussie. Zo geeft Ti-SBA- 15 bijvoorbeeld aanleiding tot absorptie in een klein UV-gebied (200-250 nm), wat een zeer laag AQY van $6.5x10^{-5}$ opleverd, indien als referentie het hele spectrum van de lichtbron (280-650 nm) wordt gebruikt. Het is echter duidelijk dat het verbeteren van de licht absorptie door Ti-SBA-15 noodzakelijk is om de AQY en de productie van zonne-brandstoffen te verbeteren.

In **Hoofdstuk 5** is een studie uitgevoerd naar de mechanismen van de fotokatalytische CO_2 reductie op Ti-SBA-15. Met als doel om bij fotokatalytische CO_2 reductie over Ti-SBA-15 de routes naar koolwaterstoffen in kaart te brengen zijn een aantal verschillende gasmengsels belicht in de aanwezigheid van Ti-SBA-15. De gasmengels bevatten CO, CO_2, H_2O en H_2. De

combinatie van CO en H_2O gaf de grootste hoeveelheden CH_4, C_2H_4 en C_2H_6, na 7 uur reactie tijd. De combinatie van CO_2 en H_2 aan de andere kant gaf de laagste productie van deze koolwaterstoffen. Voor de activatie van CO_2 en CO is water dus effectiever dan H_2. CH_3OH is niet als noemswaardig product gevonden. Indien methanol als voeding voor de katalysator werd gebruikt, was er geen grote opbrengst van methaan of andere producten, waarmee dit als intermediair voor de productie van methaan kan worden uitgesloten. Formaldehyde bleek zeer reactief over deze katalysator en er werden producten (C1-C3) gevonden, die vergelijkbaar waren met die gevonden bij CO activatie. Tot slot bleek dat de terug reactie van koolwaterstoffen naar CO en CO_2 over dit katalytische systeem ook aanzienlijk is. Een mechanisme voor de fotokatalytische CO_2 reductie is voorgesteld, gebaseerd op de experimentele activiteits profielen, de hierboven beschreven resultaten en de beschikbare literatuur. Dit mechanisme behelst de formatie van CO in het begin stadium, opgevolgd door omzetting naar formaldehyde dat waarschijnlijk door een reactie met fotokatalytisch geactiveerd H_2O (OH-radicalen) omgezet wordt naar CH_4, C_2H_4 en C_2H_6. De door licht geactiveerde Ti(III)-O(I) entiteit initieert waarschijnlijk, zoals beschreven in de literatuur, de reactie van CO_2 en H_2O naar CO. Het is daarnaast ook waarschijnlijk dat verschillende peroxides betrokken zijn als tussenproducten in de reactie.

De half reactie van de water oxidatie is ook onderzocht. In **Hoofdstuk 6** wordt een studie gedaan naar de materialen die actief zijn voor de fotokatalytische water oxidatie. De resultaten van de screening laten zien dat voor de prodcutie van O_2 onder belichting, kobaltoxide gedispergeerd in poreus silica (Co_3O_4-SBA-15) het meest actief is. De grootte van de kobaltoxidedeeltjes, Co_3O_4, werd gecontroleerd door de keuze van de calcineerings omgeving, NO/Ar of lucht. Kleinere deeltjes werden verkregen indien NO/Ar werd gebruikt. De studie naar de water oxidatie met zeer goed gedispergeerde kobaltoxide deeltjes in poreus silica als katalysator systeem werd gedaan met de toepassing van licht activatie van een zogenaamd $Ru(bpy)_3^{2+}$ complex en door het gebruik van een electronen acceptor ($S_2O_8^{2-}$). Co_3O_4 deeltjes, gedispergeerd in SBA-15 met een grootte van 4 nm, verkregen door calcinering van geimpregneerd $Co(NO_3)_2$ in de aanwezigheid van NO/Ar gas, bleken meer zuurstof te produceren dan 7 nm deeltjes, die verkregen werden door calcinatie in lucht van hetzelfde materiaal. Een vergelijkbare trend was zichtbaar voor Co_3O_4 in MCM-41, echter de O_2 productie in MCM-41 was lager dan in SBA-15 voor vergelijkbare deeltjes grootte van Co_3O_4. Het effect van deze drager blijkt het gevolg te zijn van het oppervlak van MCM-41 dat groter is dan van SBA-15 (~1000 m^2/g tegen 600 m^2/g). Hierdoor is de hoeveelheid van het

$[Ru(bpy)_3]^{2+}$ complex, dat op het silica oppervlak wordt geadsorbeerd, groter. Dit heeft als effect dat het $[Ru(bpy)_3]^{2+}$ complex niet beschikbaar is voor activatie van Co_3O_4. Verder blijkt dat de deactivatie van het onderzochte Co_3O_4 toe te schrijven is aan oplossen van Co_3O_4 tot Co^{2+}, als gevolg van de zure pH omstandigheden.

Toekomst perspectief

Om de fotosynthese te kunnen nabootsen met de activatie van CO_2 en H_2O, zijn twee half reacties –CO_2 reductie en H_2O oxidatie – bestudeerd en beschreven in dit proefschrift. De resultaten van katalysator screening laten zien dat gedispergeerd titania en kobaltoxide in poreus silica SBA-15 actief is voor respectievelijk fotokatalytische CO_2 reductie en H_2O oxidatie. Het vooruitzicht is om deze twee katalysatoren te combineren en zo doende hogere conversies van CO_2 in koolwaterstoffen te bereiken. Fig. 1 (Hoofdstuk 7) toont het idee van een gecombineerde CO_2 reductie en H_2O oxidatie in een systeem dat het complex $[Ru(bpy)_3]^{2+}$ bevat. De band posities van Ti-SBA-15 en Co_3O_4-SBA-15 zijn denkbeeldig. Wanneer de photosensitizer $[Ru(bpy)_3]^{2+}$ wordt geëxciteerd door zichtbaar licht, wordt het Ru-complex geoxideerd door de injectie van electronen in Ti-SBA-15 en zal dit CO_2 reductie tot gevolg hebben. Ondertussen zal de katalytische cyclus van het Ru-complex voltooid worden door electronen op te nemen van Co_3O_4-SBA-15, waardoor oxidatie van water mogelijk wordt. Het in elkaar zetten van het systeem op een nano-schaal silica oppervlakte biedt het voordeel dat niet alleen kleine kristallen verkregen worden, maar ook dat het aan de ene kant protonen snel overdraagt op de schaal van katalytische reactiesnelheden en aan de andere kant, dat het impermeabel is voor kleine moleculen zoals zuurstof. Het materiaal functioneert dus als een membraan voor de scheiding van de reductie en oxidatie reacties.

De uitdaging van dit katalytische systeem zit hem in het verkrijgen van een efficiente ladingsoverdracht tussen de reductie katalysator (Ti-SBA-15), de oxidatie katalysator (Co_3O_4-SBA-15) en de photosensitizer. Een trage ladings overdracht zal tot ophoping van lading leiden en mogelijk to de eliminatie van de reactie. Hiervoor is dus zeer goed begrip van de band posities van de gedispergeerde metaal oxiden in de poreuze silica materialen nodig.

List of Publications and Presentations

Publications

How Gold Deposition Affects Anatase Performance in the Photo-catalytic Oxidation of Cyclohexane
J. T. Carneiro, **C.-C. Yang**, J. A. Moma, J. A. Moulijn, G. Mul
Catalysis Letter, 129, 12-19, 2009.

Artificial photosynthesis over crystalline TiO_2-based Catalysts: Fact or Fiction?
C.-C. Yang, Y.-H. Yu, B. v.d. Linden, J. C.S. Wu, G. Mul
Journal of the American Chemical Society, 132, 8398-8406, 2010.

Effect of Carbonates on Promoting Photocatalytic CO_2 Reduction over Cu-TiO_2-based Catalyst
C.-C. Yang, B. v.d. Linden, J. C.S. Wu, G. Mul
Physical Chemistry Chemical Physics (submitted)

A Parallel Screening Device for Photocatalytic Activity Evaluation in Gas Phase CO_2 Reduction
C.-C. Yang, B. v.d. Linden, G. Mul
Applied Catalysis B: Environmental (submitted)

Mechanistic Study of Hydrocarbon Formation in Photocatalytic CO_2 Reduction over Ti-SBA-15
C.-C. Yang, J. Vernimmen, V. Meynen, P. Cool, G. Mul
Journal of Catalysis (submitted)

Effect of Particle Size and Silica Scaffold on H_2O Oxidation Activity of Dispersed Cobalt Oxide
C.-C. Yang, T. M. Eggenhuisen, M. Wolters, B. v.d. Linden, P. E. de Jongh, K. P. de Jong, G. Mul
Energy & Environmental Science (submitted)

Oral Presentations

Catalyst-Screening System Design and Mechanism Exploration for Photocatalytic CO_2 Reduction
C.-C. Yang, B. v.d. Linden, G. Mul
Symposium of Catalysis for NWO/NSC Collaborating Projects, Taipei, Taiwan,
12 – 13 January, 2009.

Combinatorial Reactors for Screening of Photocatalysts in CO_2 Reduction and H_2O Oxidation
C.-C. Yang, B. v.d. Linden, G. Mul
239th American Chemical Society Meeting (ACS), San Francisco, USA,
21 – 25 March, 2010.

Photocatalytic CO_2 Reduction over TiO_2-Based Catalysts: Fact or Fiction?
C.-C. Yang, Y.-H. Yu, B. v.d. Linden, J. C.S. Wu, G. Mul
3rd International Conference on Semiconductor Photochemistry (SP3), Glasgow, Scotland,
12 – 16 April, 2010.

Photocatalytic CO_2 Activation into CH_4 over Titania Dispersed Materials – Catalyst Screening and Mechanism Exploration
C.-C. Yang, J. Vernimmen, Bart v.d. Linden, V. Meynen, P. Cool, G. Mul
12th Netherlands' Catalysis and Chemistry Conference (NCCC), Noordwijkerhout, the Netherlands, 28 February – 2 March, 2011.

Poster Presentations

Operando DRIFTS Characterization of Photocatalytic CO_2 Reduction
C.-C. Yang, G. Mul
9th Netherlands' Catalysis and Chemistry Conference (NCCC), Noordwijkerhout, the Netherlands, 3 – 5 March, 2008.

Photocatalytic CO_2 Reduction over Ti-Siliceous Materials
C.-C. Yang, J. Vernimmen, V. Meynen, P. Cool, F. Kapteijn, G. Mul
1st International workshop on Nanoporous Materials in energy and Environment (NAPEN), Chania, Greece, 12 – 15 October, 2008.

Direct Evidence of CO Formation during Photocatalytic CO_2 Reduction over Cu/TiO_2
C.-C. Yang, Y.-H. Yu, B. v.d. Linden, J. C.S. Wu, F. Kapteijn, G. Mul
10th Netherlands' Catalysis and Chemistry Conference (NCCC), Noordwijkerhout, the Netherlands, 2 – 4 March, 2009.

Application of Ti-activated Bimodal Siliceous Materials for the Photocatalytic Reduction of CO_2
J. Vernimmen, C.-C. Yang, G. Mul, F. Kapteijn, V. Meynen, P. Cool
10th Netherlands' Catalysis and Chemistry Conference (NCCC), Noordwijkerhout, the Netherlands, 2 – 4 March, 2009.

Origin of CO Formation over CuO/TiO_2 in Photocatalytic CO_2 Reduction
C.-C. Yang, Y.-H. Yu, B. v.d. Linden, J. C.S. Wu, F. Kapteijn, G. Mul
11th Netherlands' Catalysis and Chemistry Conference (NCCC), Noordwijkerhout, the Netherlands, 1 – 3 March, 2009.

Photocatalytic CO_2 Reduction over TiO_2-Based Catalysts: Fact or Fiction?
C.-C. Yang, Y.-H. Yu, B. v.d. Linden, J. C.S. Wu, G. Mul
3rd International Conference on Semiconductor Photochemistry (SP3), Glasgow, Scotland, 12 – 16 April, 2010.

Acknowledgements

In addition to show my deep gratitude to everyone who helped me through this period, the acknowledgments, I consider, should also be a reflection of my four-year life in the Netherlands. So maybe ten years after, when I open this book again, I can still remember the interactions with all the people I met during my life of Ph.D.

The first person I want to thank is my supervisor/promoter. Guido, you are the key to open the door of Ph.D. for me. When I recall how we started the e-mails about a Ph.D. position till we met in Taiwan, I consider myself very lucky to contact the right person at the right timing. The whole story would have been completely different, if you found another person or said "NO" to me for this position. Starting from a bit lost in the research by your guidance, but afterward I find the way to interact with you. Thank you for giving me lots of freedom to work on the study in my own way, and being open for discussion when I have doubts – no matter what they are. In the end, you were in an irreplaceable position to guide me through my Ph.D. I value your way of looking at the positive side when tackling difficult problems. You always know what you are aiming for, have a clear mind going for it, and try not to be messed up by the others. I am still learning this from you. Thank you, Guido. I truly wish you all the best and success for your future career.

Joana, you are the second person who came to my Dutch life and became a kindred spirit of mine. You welcomed me with your open-arms when I just arrived to this country. We shared lots of good and bad time in both work and life. (I always remember that we sang together, while I played the X'mas songs at our office.) You are the one who told me the truth, no matter it was sweet, bitter, or sugar-coated. I appreciate your good heart and directness, which despite sometimes put you into troubles. I want to say thank you, Joana, for being a strong shoulder to me in my Ph.D. life. Joana, I have no doubts that you will make your life as what you expect to be. Alex, you are the one who got bored sometimes while Joana and I were talking about work when we went out. Thank you for all the time being there when we need you, and fading out as the background when we are so into the serious discussion. Joana and Alex, I cherish our friendship and deeply wish you (including Aurora, Gizmo, and Maxwell) a happy life in the future.

Bart (van der Linden), I consider you as my 2nd supervisor during my Ph.D. Besides your all-time instant help, your passion and interest in my work was a good support to me,

especially in the low period of my study. I will never forget your exciting face, when I told you I detected hydrogen out of water splitting; even it is just 1 %. Thank you for doing so much more than what a colleague does. You recognition on my work means a lot to me.

I began my Ph.D. study at CE (Catalysis Engineering) group in TU-Delft. Els and Elly, thank you for being so kind and patiently helping me through the administration paper work. I like your smiles and always greetings when I was back from holidays or conferences. Harrie, Kevin, and Willy, thank you for taking care of the technical work to ensure the lab-activities done properly. (Especially thanks to Harrie for transporting my equipments from Delft to Twente.) Johan (Groen), some conversations with you in the Spectroscopy Lab gave me confidence to keep working on my research. Thank you for cheering me up with your delightful humor. Freek, though we had only a very short period of interaction and you thought I am from Korea when we met at the Kröller-Müller Museum, your comments on my work pushed me forward to complete my Ph.D. Michiel, you gave me a tough start-up of my lab-work on the safety report, but I learned that is an important step to be entitled to work in the lab afterwards. Later on, I notice your trust on my way of experimenting, by saying nothing to me sometimes working after 18:00. I also learned from you that the first impression on a person is not always right. Thank you for being critical but still leaving space for me to work on my plans. Patricia (Kooyman), I appreciate your efforts to create a fair working environment to everyone in the group. Besides, thanks for the helps, together with Valerie and Ugo, in TEM characterization. Jorge, you not only offered some helps to my work but also introduced me into Spanish community. I also learned how determined one needs to be, to reach a position where you are. Dirk, some discussions with you are very instructive, and you always offer your help to the others. I feel really warm when you told me that I am always very welcome to drop by if I go back to Delft. Christian, you are the one who introduced me into the volleyball club, and I had great time in Kratos. I also appreciate your help in learning Dutch, by lending me your comic book, Donald Duck and Suske en Wiske. It is a great pleasure to know you. Xiaoding, I am glad to have a mentor like you, telling me sometimes your experience related to work, volleyball, and Dutch life. Mul's group members – Rita, Sander and Christa, thank you for sharing your experience while working together. Other group members - Bandar, Jasper, Inge, Daniel, Nathalie, Johan (van den Bergh), Malles, Pita, Rob (Berger), meeting you in CE was very pleasant. Thank you for making my stay so joyful. Your words before I left TU-Delft for U. Twente were definitely a motivation to help me finish my study. Nico (Alberts) and Bart (Boshuizen), your technical

contributions to the combinatorial photoreactors are very crucial to my research. Thank you for being so thoughtful of putting my work into your tight schedule, every time that I asked for help.

Yongqi and Qingxiang, you were the core of linking the Chinese community together. You always organized and invited us for very nice and delicious meals. The trip to Italy with you is unforgettable in my life. The same thing to Qingping and Meimei, you took over the dinner-organizing job, after Yongqi and Qingxiang leaving for USA. I enjoy so much the moments we shared while staying in Delft. Jianrong, you always put other people's request in front of yours, and offer your help when people need you. Too polite to say "No" is not always good, but that is the thoughtful Jianrong. (I am glad that you did not say "NO", when I need some paper-searching.) Thank you all for creating such a pleasant environment in Delft. Some words to the Spanish community, Asun, Pedro, Sonia, and Loli. We spent some good time together. There was a period that I knew more Spanish than Dutch. Meeting various people is an important experience to me in these four years. You showed me a different way of leading your lives. Patricia (Lopez), I always remember what you told me before my 1st X'mas in Europe. You are a considerate person. Thank you for being so delightful and looking after me like an elder sister.

A smooth transition from Delft to Twente achieved in my last year of Ph.D. was thanks to Leon and the whole CPM (Catalytic Process and Materials) group's host and help. It would have been a lot more difficult for me to continue my study in Twente without your accommodation. Thanks to Bert, Karin, Tom, and especially Ruben, for your help in reconstructing my setup and hospitality, while I was working in the CPM lab. Ruben was very patiently helping me to upgrade the setup in a nicer operating way. Other group members - Seshan, Barbara, Arie, Sergio, Marijana, Dennis, Yingnan, Masoud, Yejun, Joline, Kamila, all made my short-stay cheerful. Thank you for hosting me as a fresh group member. Arturo and Shilpa, I enjoyed very much the time we spent together in Enschede, especially when we went for the movies. Thank you for introducing me into your network. I like you both for your unique personalities, which transmits happiness to people surrounding you. Can, another volleyball-lover, who helped me during my last period of running crucial experiments. Thank you for being so generous to offer your help. I hope I could have some chance to help you back, and maybe to share some more time in volleyball.

I would also like to thank all the people from PCS (PhotoCatalytic Synthesis) group. We started the group with three people, and Guido managed to grow it up in short time. Rob

(French), we firstly met during your interview at Delft, and then you were the only group member when I just moved to Twente. You have some very different attitudes toward life from mine, which somehow changed a bit my way of evaluating things. Thank you for being a good company, and always answering me what the right English word is when I was stuck in writing. Engin, thank you for trying to cheering me up, when I was sometimes grumpy during the writing. Vic and Bindikt, thanks for your efforts of dragging me into coffee breaks during some of my horrible writing periods. I enjoyed a lot during coffee breaks, lunch and some self-organized group dinners. And thanks to Bindikt for the excellent English-to-Dutch translation of the summary. Lidy and Nienke (Timmer), thank you for helping out with all the documentations during my last period of Ph.D. Robert (Meijer), thank you for making things so much organized in PCS. One-year stay in PCS with all your company was very delightful for me. I am very much honored to work together with you and very proud of being the first Ph.D. in PCS.

Without the collaboration work, half of the dissertation would not be presented like the way it is. I want to thank Jarian, for the catalysts-supply and your from-time-to-time encouragement. You are not only a collaborator, but also a good listener with your wisdom. I always feel comfortable to share my thoughts with you about my work and life. Vera and Pegie also made their great contribution to the work, with their amazing in-time paper revision and comments. Enlightened by Krijn and Guido, my dissertation was completed with the chapter about water oxidation. Tamara and Mariska, thank you for your input on the catalysts syntheses and detailed characterizations. Those prompt feedbacks from Tamara were what I can never ask for more. Petra and Krijn provided some perspective insights, which benefit a lot the work. I am glad to see all the collaborations leading to fruitful discussions and results. NWO-NSC project is the financial funding that brought me from Taiwan to the Netherlands. Yi-Hui (議輝) and Prof. Wu (吳老師) from NTU were directly involved in the research about CO_2 reduction. Thank you for bridging the cooperation so successfully, leading to good results out of it.

Jelmer, Nico (Janssen), Dorette, Nienke (Firet) and Arjen, it was great pleasure to work together with you on your LO or bachelor project at Delft. You showed the initiative to the assigned topics I proposed, and completed them with your comprehension toward the research. Thank you for making your vital contribution to my work. Even more, I made friends with some of you afterwards. Jelmer, you are a lot younger than me but have very rational thought, which teaches me a lot in various prospects. I am lucky to have a friend like you. (though you

were not satisfied with my Dutch pronunciation.) Nico, I believe people know you all have the same opinion as mine that you are a sincere person, which is the part I value you the most as a friend. (And I love your home-made brownies, which is the best I have ever tasted so far.) Dorette, your occasional greeting mails always made my day. You are a cheerful person trying to spread your joy to the others. Meeting you all adds so many flavors into my Dutch life. Playing volleyball was part of my life in these four years. I love this sport for a long time but never dare to play it. Thanks to volleyball, it helped me to release so much pressure from work and life. I met many people in the clubs, Kratos and Harambee. Frank is a good friend I made during my volleyball-life. I like cheering for the points we made during the game. It is a great memory for me playing volleyball and hanging out with you sometimes on weekends.

Prof. Wan (萬老師), Prof. Cheng (鄭老師) and 吳煒老師 - my previous master supervisor and mentors, thank you for the occasional mails caring about my progress in work and life. You are never stingy with compliments and giving me confidence, so that I can overcome the tough part in my life. My deep gratitude goes to your generous inspiration and supports. My best friends since high school, Yu-Yuan (宇淵) and Zhi-Wei (志偉), though I spent very few time in Taiwan in the past four years, you always welcome me when I am back to Taiwan. Che-Wei (哲維), always keep me in your thought though you are far way in USA. Thank you all for being there as always, when I need someone to talk to.

The last but the most important acknowledgment is to my family in Taiwan. My deep regret is that I was not there when my dog, Money, passed away (Aug. 29, 2008) in his 18 year-old. Thank you, Money, for bring so much happiness to me with you faithful company. May you be happy in the other world.

Father, you've backed me up in different way. Thank you for doing whatever you can.

Li-Ling and Mom, I probably lost my words to describe how great and important you are in my life, but you have been the strongest supports to me. You tolerate my bad temper. When I was down, you were the ones listening to my annoying complains. Even if I am on the other side of the earth, you still clearly let me know that you are there for me. Thank you for always being the same to me. I love you, and I will always be there for you too.

非常感謝四年多來,在臺灣一直支持,關心我的師長,親戚,朋友與家人們!!

將我這一刻的喜悅與你們一起分享!! 願你們身體健康,平安,快樂!!

Chieh-Chao Yang

Enschede, May 2011

About the Author

Chieh-Chao Yang (楊捷超) was born in Tainan, Taiwan, on September 7th, 1980. In September 1998, he started with a bachelor study in Chemical Engineering at National Taiwan University in Taipei and received the bachelor degree in June, 2002. He continued the master study in Chemical Engineering Department of National Taiwan University and graduated in June, 2004. His master thesis is the study on "Study of Gold Effects on Photocatalytic Water Decomposition." From July 2004 to December 2005, he took the military service as a Lieutenant Officer at Artillery Army in Taiwan. From June 2006 to April 2007, he worked as a research assistant in Chemistry Department of National Taiwan University. The topic is "Selective Oxidation of Carbon Monoxide in Rich Hydrogen Environment on Transition Metal Loaded Ceria Materials." In May 2007, he started his PhD research in the Catalysis Engineering group, Delft University of Technology, under the supervision of Dr. G. Mul. In April 2010, he moved to PhotoCatalytic Synthesis group initiated by Prof. dr. G. Mul and continued his PhD research at University of Twente. The results obtained during this period are described in this dissertation and were presented at several (inter)national conferences. During the 4-year PhD research, he collaborated with Catalysis and Reaction Engineering group at National Taiwan University, Adsorption and Catalysis group at University of Antwerp, and Inorganic Chemistry and Catalysis group at Utrecht University.